NOAA Technical Memorandum ERL PMEL-74

OBSERVATIONS OF CURRENTS, SURFACE WINDS AND BOTTOM PRESSURE IN SHELIKOF STRAIT, AUTUMN 1984

A. T. Roach
J. D. Schumacher
P. Stabeno

Pacific Marine Environmental Laboratory
Seattle, Washington
July 1987

UNITED STATES DEPARTMENT OF COMMERCE

Malcolm Baldrige, Secretary

NATIONAL OCEANIC AND ATMOSPHERIC ADMINISTRATION

Anthony J. Calio, Administrator

Environmental Research Laboratories

Vernon E. Derr, Director

NOTICE

Mention of a commercial company or product does not constitute an endorsement by NOAA/ERL. Use of information from this publication concerning proprietary products or the tests of such products for publicity or advertising purposes is not authorized.

Contribution No. 925 from NOAA/Pacific Marine Environmental Laboratory

For sale by the National Technical Information Service, 5285 Port Royal Road
Springfield, VA 22161

CONTENTS

OBSERVATIONS OF CURRENTS, SURFACE WINDS AND BOTTOM PRESSURE IN SHELIKOF STRAIT, AUTUMN 1984

A.T. Roach
J.D. Schumacher
P. Stabeno

ABSTRACT. An extensive array of current meters and bottom pressure gauges was deployed in Shelikof Strait, Alaska, during 1984/85 as part of the Fisheries Oceanography Coordinated Investigations (FOCI). FOCI is aimed at understanding the physical and biological environment surrounding the early life stages of the Pacific pollock (*theragra chalcogramma*). These data, as well as calculated surface wind time series, were analyzed to investigate the influence of the Alaska Coastal Current (ACC) in this region. The ACC induced a strong mean flow (15 to 25 cm/s) during this season concentrated along the Alaska Peninsula on the northern side of the Strait. Outside the influence of the ACC, mean currents were weak (5-8 cm/s). This highly variable flow bifurcated in the vicinity of the Semidi Islands, with 75% of the ACC volume flux flowing seaward out of a deep (200+m) sea valley which meets the shelf break at a sill southwest of Kodiak Island. This strong outflow can induce an estuarine type circulation through entrainment of bottom water causing a mean inflow at depth. The remainder of the flow continues along the Alaska Peninsula. The currents were generally well correlated in the vertical at each mooring, while the horizontal correlations were weak, indicating the horizontal spatial scales of coherence were less than the 8 to 15 km mooring separation. Surface winds from a location near the Barren Islands (200 km north of the Strait) showed the strongest relation to currents and transport. There was an indication that the winds drove the pressure differences and thereby the currents, as there was a significant correlation between bottom pressure differences and currents.

1. INTRODUCTION

Fisheries-Oceanography Coordinated Investigations (FOCI) is a multi-year study of the physical and biological environments surrounding the early life stages of the Alaska Pollock (*theragra chalcogramma*) in Shelikof Strait, Alaska. FOCI is conducted jointly by scientists at Pacific Marine Environmental Laboratory and the Northwest and Alaska Fisheries Center in Seattle, Washington. This memo presents analysis of current, bottom pressure and surface wind time series from the winter of 1984/85.

Shelikof Strait is a region of complex topography (Fig. 1). The dominant bathymetric feature is a deep sea valley which starts at the north end of Kodiak Island and follows the axis of the Strait until it turns sharply seaward east of the Semidi Islands, becoming orthogonal to the shelf break. The sea valley ends at a 200 meter sill southwest of Kodiak Island. Shelikof Strait is bounded by the mountainous Alaska Peninsula to the north and the rugged Kodiak Island plateau to the south, both of which can have effects on the local winds. The regional winds are strong and variable due to intense cyclones crossing the North Pacific into the Gulf of Alaska. Large scale low pressure systems lying southwest of Kodiak Island can cause regions of strong convergence through the interaction of low-level, down gradient winds in the Strait with the onshore geostrophic flow southwest of Kodiak Island (Macklin, 1984). The high variability of the wind field precludes areas of consistent coastal convergence or divergence such as exist farther to the northeast or southwest, respectively (Schumacher and Reed, 1986).

The Alaskan Coastal Current (ACC) enters Shelikof Strait primarily through Kennedy Entrance south of Cook Inlet (Reed *et al.*, 1980). The ACC provides a source of low salinity water resulting from the large (23,000 m^3/s) line source of freshwater input around the perimeter of the Gulf of Alaska (Royer, 1979, 1982). This westward flowing current entrains slope water, which is warmer in winter than the ACC water, before entering the Strait (Schumacher *et al.*, 1979). Flow bifurcates near the Semidi Islands, with one branch continuing westward along the Alaska Peninsula and the other seaward through the sea valley (Schumacher and Reed, 1986).

Deep slope water is the source of saline water at the southern end of the sea valley, leading Reed *et al.* (1986) to use an estuarine-like model of circulation to characterize this area. The warm, relatively fresh upper layer flowing steadily southwestward overlies a cold and salty lower layer that periodically reverses. Mysak *et al.* (1981) presented a seasonal analysis of

the variance for three current meter records from Shelikof Strait in the fall and winter of 1976/77. They argued that the 2.5- to 5-day component of the fluctuating flow was due to the baroclinic instability of the mean southwestward flow.

This report describes the oceanographic conditions in and around Shelikof Strait, Alaska during the fall of 1984. The basic statistics and time series plots, as well as kinetic energy spectra, of all variables for the 34 current meter, 4 surface wind, and 6 bottom pressure records are presented. In addition, graphic representations of harmonic analyses for tidal currents and of the distribution of variance by frequency band are discussed. Time series relations are shown through correlation matrices and schematic diagrams of the coherence squared of currents across transport sections. In the summary, the major features of the circulation and volume transport through the Strait are listed and questions for further study are posed.

2. DATA AND METHODS

We present a statistical analysis of the current meter records, bottom pressure gauge records and surface winds spanning the period 25 Aug 1984 to 12 Jan 1985 (Table 1). The 34 current meters deployed were organized into 3 cross-sectional lines or sections (Figs. 1 and 2). Section #1 spanned the Strait between Cape Kekurnoi and Kodiak Island (Moorings 1, 2, and 3), Section #2 contained the meters from moorings 4, 5, and 6 between Sutwick Island and the Semidi Islands on the shallow continental shelf, while Section #3 (Moorings 7, 8, and 9) spanned the sea valley from the Semidis to Chirikof Island (Figs. 3-5). These sections measure volume transport through Shelikof Strait; beginning at Section #1 where the highest concentrations of pollock eggs are found, then downstream either along the Alaska Peninsula (Section #2) or seaward out of the sea valley (Section #3).

The current meters were Aanderaa RCM-4 instruments deployed on taut-wire moorings. Six of these moorings (1, 3, 4, 6, 7, 9), located on the sides of the transport sections, had Aanderaa bottom pressure gauges. All the instruments were recovered and provided a raw time series of hourly samples, except for the 26 m record from Mooring #2 which had faulty velocity data. Data were smoothed using a 35-hour Lanczos filter with a 10% cosine squared taper, and resampled at 6 hourly intervals. This filter passes more than 99% of the amplitude at periods of greater than 55 hours, 50% at 35 hours and less than 0.5% at 25 hours, effectively removing the tides. The pressure gauge records were similarly filtered. Time series of the observed variables are shown in Figs. 6-41. Detrended pressure gauge series were used to create series representing the pressure differences both along and across the continental shelf by subtracting one series from another. Figures 42 and 43 show the alongshelf and cross shelf pressure difference series respectively. Other series of importance to this report are the surface and bottom transport series. The low-pass filtered, principal axis speed components for all the records from 56 meters and above in each of the sections were multiplied by a representative area and summed to provide an estimate of the volume transport in the surface layer (Figs. 44-46). Similarly, the bottom records yielded a lower layer transport estimate. Note that the upper layer is approximately half way between the 56 m record and the one immediately below it (Fig. 2).

Tables 2, 3, and 4 present the vector mean flow, RMS error, principal axes, variance and variance ellipse statistics for current meter records from Sections 1, 2, and 3, respectively. The nomenclature used in referencing instruments is the mooring number followed by the instruments' sequential number from the surface and depth. Thus, the instrument on Section 1 with faulty velocity data was 2_1/26. Table 5 presents similar statistics for the surface winds, bottom and surface transports, and bottom pressure gauge records.

Spectra were computed by removing the mean from each record, using a 10% cosine taper and then dividing the variances by 0.875 to preserve the variance lost by that taper. The Fourier Transform of each time series was boxcar averaged to produce a spectrum such that the sum of the variances over all frequencies equaled the total variance (Pearson, 1981). The band averaged spectral energy for all nine moorings was also computed to get an overall picture of the frequency distribution which would have been difficult to ascertain from the spectra themselves. The bands used are detailed in Table 17.

Four time series of gradient winds (Fig. 47) were generated from surface atmospheric pressure fields using the METLIB package of programs. Surface winds were generated from gradient winds using a rotation of the wind direction by 15 degrees to the left and a 30% reduction in magnitude (Overland *et al.*, 1980). Synthetic winds may not replicate the small scale spatial variability of the actual winds (Royer, 1981; Luick, Royer and Johnson, 1987). The wind series near the Barren Islands (northeast of Kodiak Island) is designated as "BA", Shelikof Strait is "SH" and "SE" denotes the wind series near the Semidi Islands. There are no observed wind time series available.

3. CIRCULATION

A. Mean Conditions

Mean flow was in the along-channel direction at all three sections, with the exceptions of Mooring #5 and some of the deeper records with weak currents. Sections 1 and 3 were qualitatively similar with strong mean outflow on the right hand side (RHS) of the Section (looking downstream along the major axis) and weak and variable or reversing currents at depth on the left hand side. The alongshore mean speeds at moorings 1 and 2 exceeded 20 cm/s alongshore in the surface layer, and were reduced to less than 6 cm/s

at a nominal depth of 200 meters (Fig. 48). Most of the current variance was contained in the alongshore direction for Mooring 1, while the variance ellipse was nearly circular for Mooring 2. Similar mean speeds were present in the surface records at Moorings 7 and 8 on the RHS of Section 3 (Fig. 50). Currents at moorings 3 and 9 had weak and variable surface flow overlying a mean inflow of 7 and 3 cm/s below 150 m, respectively.

The mean currents at Section 2 (Fig. 49) were weaker (8-10 cm/s) above 56 m than those at the sections across the sea valley. There was no significant flow at 6_3/75 in the lower water column. All records on Section 2 were nearly circularly polarized and there was a consistent decrease of variance with depth at all locations.

The transport means suggested 70 to 80% of the water which flowed through Shelikof Strait (Section 1) exited through the sea valley (Section 3). The estimated mean transport through Section 1 was 0.82 Sverdrups (1 Sv = 10^6 m^3/s), while 0.26 Sv flowed through Section 2 and 0.68 Sv through Section 3. The transports balance to within 15%. The imbalance may be due to inaccuracies in the transport calculation or failure of these sections to include all significant flows in this region. In particular, a moderate 8 to 10 cm/s flow over the shallow shelf region southwest of Kodiak Island and east of Mooring 9 could add about 0.1 Sv to the balance. Satellite tracked drifters have gone between the Semidi Islands, indicating that area as one of possible importance to the regional flow. A strong (>25 cm/s) flow through the Islands, however, would contribute less than 0.05 Sv to the transport balance. Most of the volume transport was concentrated in the surface layers; 65% at Section 1, 92% at Section 2 and 75% at Section 3.

Bottom pressure recorders were placed on either side of the Strait to examine the mesoscale dynamics. Since the mean pressures are only indicative of the instruments' depth, the statistic of most interest is the variance of each record. The two series with the highest variances were on Section 2

(Moorings 4 and 6), while the least variable bottom pressure series was on Mooring 9 (Table 5 and Fig. 41). Even though the mean flow through Section 3 was double that of Section 2, variability was four times greater in the coastal region than over the sea valley.

The mean speeds for the along-channel surface winds showed a transition from winds favoring coastal convergence near the Barren Islands and in Shelikof Strait to statistically insignificant winds near the Semidi Islands (Table 5). This transition results from the location of cyclone trajectories in the Gulf of Alaska (Schumacher and Reed, 1986). These surface winds do not reflect the orographic effects of the local winds, which can be accelerated along the Strait and through gaps in the coastal mountains (Macklin, 1984).

B. Current Characteristics

Tidal currents contain a significant amount of kinetic energy in Shelikof Strait. Selected tidal constituents were estimated from eight 29-day tidal harmonic analyses of hourly current time series and are shown in Figs. 51-53. The tidal currents were mostly semi-diurnal with M2 speeds averaging 15 cm/s at Moorings 1 and 2, reaching 20 cm/s at Mooring 3. The same constituent had speeds of about 30 cm/s at Moorings 7 and 8 and 35 cm/s at Mooring 9. Thus, both sections showed the strongest tidal currents on the left hand side of the sea valley. There was less variability at Section 2, with average M2 speeds of 20 cm/s. Moorings 6, 7 and 9 showed subsurface maximums, which may be associated with an internal tide.

In Section 1, upper layer subtidal currents seldom reversed at Moorings 1 and 2. Reversals of up to nine days with speeds over 50 cm/s were common at Mooring 3. Lower layer currents showed similar differences with mean outflow at Moorings 1 and 2 and inflow on the Kodiak Island side of the Strait. Currents on the sides of the Strait were predominantly along the major axis, while currents at the center mooring (2) had significant rotary energy.

Upper layer currents at Section 3 were qualitatively similar to Section 1. The flow was rectilinear on both sides of the sea valley and the strong outflow which seldom reversed was on the right side of the Section (Moorings 7 and 8). There were fewer reversals in the surface layers at Mooring 9 than Mooring 3, but there was significant inflow in the lower layers of Section 3. The autumn baroclinic spinup (Royer, 1982; Reed and Schumacher, 1981) was most apparent in current and salinity observations from Mooring 7. The outflowing currents doubled in speed and salinity decreased by 1 ppt during September through mid-October.

The mean current was generally weaker at Section 2 than at the Sections across the sea valley. At Moorings 5 and 6 there was an autumn spin up with increased alongshelf speeds and reduced salinity which occurred simultaneously with the transition at Mooring 7. Currents at Mooring 4 showed little effect from the transition, remaining primarily alongshore, while currents at Moorings 5 and 6 were directed offshore. This divergence was present after the transition and may be a persistent feature.

4. TIME SERIES SPECTRA

A. Currents

The variance preserving spectra for all 34 current meters, 4 surface wind and 6 pressure gauge records are presented in Figs. 54-65. In general, fluctuations of the along-channel current were significantly larger than the across-channel component at the edges of the sea valley (Moorings 1, 3, 7, 9). Current fluctuations were most energetic at the surface, with the notable exception of Mooring 3. At that location (and to a lesser extent, at Mooring 8), the variance increased in the deepest layer (Fig. 67). Comparison with the band averaged frequency distribution shows this increase in variance at depth was in the diurnal and two- to five-day bands (Fig. 68). There was a 60% decrease in total variance between the 26-m and 56-m records at Mooring 6.

Spectra from Section 1 show the majority of kinetic energy at Moorings 1 and 3 to be along the major axis. There was a shift from low frequency energy at the surface to higher frequencies at the bottom for both locations. There was a surface intensification of the high frequency signal at Mooring 1, while mid-frequency energy (five to ten days) increased till mid-depth then decreased. There was, however, a consistent eight-day signal at all depths at that location. The cross-channel component at Mooring 3 showed a uniform distribution over the low frequencies separated from a significant mid-frequency band of five to eight days. The spectra from Mooring 2 showed the division of variance between the 220°T and 310°T components to be nearly equal. There was a concentration of energy in a cross-channel peak at three days, whereas the energy centered at eight days contained an equal amount of variance in both components.

Spectral peaks for the along- and across-channel components for Section 2 (250°T and 340°T, respectively) were usually well separated. Often a strong signal in one component meant less energy in the orthogonal component (e.g. the twelve day peak at 5_1/26, Fig. 58). There was more along-channel energy at low frequencies, especially at Mooring 6 (Fig. 59).

Along sea valley energy dominated all records from Section 3, except in the surface layer of Mooring 8. The currents on the sides of the sea valley had strong low frequency signals with a subsidiary peak at eight days. Mooring 8_4/205 (Fig. 61) showed a four-day peak which may be associated with inflow events. Section 3 had a lower percentage of its variance at higher frequencies than Section 1, even though their spectral structures were similar (Figs. 68, 70).

At the moorings in the center of each section, the currents are best described using rotary spectra (Fig. 66). At periods greater than five days, the current energy at Mooring 2 was equally divided between clockwise and counterclockwise components. At shorter periods, there was significantly more

counterclockwise energy in the upper layer and more clockwise energy in the lower layer. Current behavior at Mooring 8 was similar to Mooring 2 at depth, but had significantly more counterclockwise energy over most periods near the surface. Mooring 5 had no consistent pattern of rotational energy.

B. Wind and Bottom Pressure Spectra

The onshore/offshore component of the surface winds was consistently more energetic than the alongshore component, except at a period of eight days (Fig. 63). There was a significant alongshelf peak at that period in each of the four wind series. There was a consistent low frequency signal (centered at 17 days) in the cross-shelf component at all locations. The bottom pressure gauges had a bimodal structure with the primary peak at twenty days, which held most of the energy, and a secondary peak at five to six days (Fig. 65).

5. TIME SERIES RELATIONS

A. Currents

Tables 6 to 16 present correlation matrices for current and transport series versus surface winds, bottom pressures, and bottom pressure differences. In general, correlations were greatest in the vertical, but weak or insignificant across a section. For example, currents were correlated within Mooring 2, but virtually no correlation existed across the strait (Table 6). At Mooring 1 there was a tendency for the surface current to be decoupled from the bottom current. The decoupling was more complete at Mooring 3, where the currents above 106 m were well related to each other, as were those below 165 m. Those two groups, however, were not significantly correlated with each other (95% level). This surface-to-bottom difference was also suggested in the time scale estimates (Fig. 71) (Allen and Kundu, 1978).

Correlations between the currents in Section 2 (Table 7) were generally weaker than those in Section 1. The highest correlations in the vertical existed at Mooring 6, but may have been due to less vertical separation of the meters.

The greatest cross-channel correlations were found between Moorings 7 and 8 in Section 3 (Table 8). The correlations between currents in the upper layer at Mooring 7 and 9 were negative, while currents in the bottom layers of 7 and 9 were positively correlated. This relation is interesting since correlations were not significant between Moorings 8 and 9. The negative correlations suggest the presence of eddy-like features (such as those found in satellite imagery), while the positive correlations and time scale differences imply such features are restricted to the upper water column. Most of the time scales are comparable at about 100 hours, except those at the bottom of Mooring 9, which dropped to half that value (Fig. 71).

At most frequencies, coherence squared estimates showed similar results to those seen in the correlations; strong coherence in the vertical, weak or non-existent coherence in the horizontal (Figs. 72-74). At Section 1, the strongest coherences in the vertical were at the shortest periods. At longer periods, the bottom flow decoupled from the surface, especially at the sides of the channel. Diagrams combining Sections 2 and 3 showed more structure (Figs. 75-77). Coherence was weak at the shortest period and, similar to results from Section 1, the bottom current decoupled from the surface at the longest period. There was coherence in the horizontal current structure in the upper 106 m from mooring 6 to 8, particularly at about 17 days.

Correlations between transports are given in Table 9. At each section, the surface and bottom transports were well correlated. We note that transports were more highly correlated than currents because transport is mass flux, a conservative property. Section 2 was best correlated with the transport estimated upstream at Section 1. The lack of correlation between

Sections 2 and 3 may have resulted from the combined (baroclinic and barotropic) current components at Section 1 becoming separated downstream. That is, the barotropic component may have followed the sea valley, while surface intensified baroclinic flow continued through Section 2.

Ten-day averages of surface, bottom and total transport for each section are shown in Fig. 78. In the surface layer, transport was comparable at Sections 1 and 3 with concurrent maxima. The maxima at Section 2 lagged those at the other two sections. Bottom transport was greatest at Section 1 except for a short period in November. Since the depth at which upper and lower layers were divided was not exactly the same at each section, comparison of surface or bottom transport between sections is more difficult than examining total transport. There were three periods, separated by weak flow, when total transport at Section 1 or 3 exceeded 1 Sv. Transport at Section 1 exceeded combined flow at 2 and 3 for only three of the 10-day averages. During two 20-day periods outflow at 3 alone exceeded flow at 1. Total transport at Section 2 increased slowly to its maximum and lagged rapid increases in transport at Sections 1 and 3.

B. Current vs. Surface Wind

Major axis currents showed their highest correlation with the Barren Islands surface wind series, several hundred kilometers to the north. Table 10 shows the maximum correlations and associated lags between each of these time series. Their relationships varied strongly as a function of wind angle, but stayed constant for 20-30° around the axis of maximum correlation. For most of the current series, the wind component for maximum correlation lay in the along channel/onshore quadrant. It appeared that local winds played a minor role in current fluctuations during this study, but that larger scale atmospheric circulation had an important effect.

The highest correlation of the surface winds at each mooring was with the bottom currents, except at Mooring 1. The amount of variance explained by the wind in the deep currents was 40%. The corresponding relationship with the more energetic surface currents was weak. The highest correlations were between the onshore component of the wind and Moorings 7 and 8.

Transports were better correlated with winds than were currents, with Section 3 yielding the best results (Table 11). Like the currents, the strongest correlations were with the onshore component of the wind. We found the strongest correlation with the winds rotated 40° clockwise from the orographic axis, which is in agreement with recent findings from comparisons of measured winds and gradient winds in the Northern Gulf of Alaska (Luick *et al.*, 1987).

C. Currents vs. Bottom Pressure

Correlations between currents versus along- and across-channel pressure differences are presented in Tables 12 to 14. The correlations between the pressure difference series themselves are in Table 15. In the sea valley, the largest correlations were with currents on the right side, while there was little or no correlation with currents on the left side. The pressure differences which incorporated the pressure series from Mooring 1 were negatively correlated with all current series except at Mooring 9. These relations were strongest at Mooring 6, 7, and 8, although Mooring 2 showed some relation to PG1-PG4. The best overall correlation was with the cross-shelf difference of PG6-PG9, which had high coefficients with all records except currents at Moorings 3, 5, and 9. That cross-shelf pressure difference accounted for up to 60% of the variance in the bottom currents on the right hand side of Section 3. Section 1 current was best correlated with the pressure differences measured at Section 3, while currents at the other two sections were best correlated with the pressure differences measured locally.

Transport versus bottom pressure differences (Table 16) echo the results above. Transports through Section 2 and 3 were best correlated with local across-shelf differences, while transport at Section 1 was only weakly correlated with its local pressure. All along-channel pressure differences had negative correlation to transport, except at the bottom layer of Section 3.

6. SUMMARY

Analysis of current, bottom pressure and surface wind time series from 25 August 1984 to 12 January 1985 resulted in the following observations:

1) The non-locally forced Alaska Coastal Current (ACC) induced a strong mean flow. Currents in the upper 100 m on the northern side of Shelikof Strait (Section 1) were 15 to 25 cm/s toward the southwest; on the northern side of the section between Sutwick and the Semidi Islands (Section 2) they were 7 to 12 cm/s directed along the Alaska Peninsula; and on the western side of the sea valley between Semidi and Chirikof Islands (Section 3) they were 10 to 25 cm/s seaward. Outside the direct influence of the ACC, mean currents were weak. On the southern side of Shelikof Strait, mean currents in the upper water column did not differ significantly from zero. On the southern side of Section 2 flow was 1 to 6 cm/s, and on the eastern side of Section 3, a 4- to 6-cm/s current flowed seaward. Entrainment of bottom water into the ACC may have been responsible for the statistically significant mean estuarine-like flow (Reed *et al.*, 1986) into the sea valley, which was about 3 cm/s on the eastern side of Section 3 and 5 to 7 cm/s on the southern side of the Strait proper. The current observations support earlier studies (Schumacher and Reed, 1986) which suggest the ACC is bifurcated in the vicinity of the Semidi Islands, one branch flowing seawards and the other along the Peninsula.

2) The mean transports were 0.68 Sv and 0.26 Sv, flowing seaward and along the peninsula, respectively. Using these transport values, we estimate approximately 75% of the ACC volume flux flows seaward through the sea valley. Autumn baroclinic spin up was evident in transport and salinity time series.

3) Fluctuations in currents were generally well correlated in the vertical, particularly in the upper 106 m, while in the horizontal, they were either weakly or insignificantly correlated. Scales of horizontal correlation and coherence were less than the 8- to 15-km mooring separation. An exception to the low coherences in the horizontal was observed between currents at moorings 6 and 7, near the Semidi Islands, where coherence squared estimates of about 0.60 existed at several frequencies.

4) Although a significant part of current and transport fluctuations could be accounted for by surface winds, the nature of this relation is unclear. The best relations between surface winds and currents were with a wind 200 kilometers northeast and rotated 20° to 60° clockwise from its orographic axis.

5) There was a significant correlation between the across channel pressure difference and the currents (or transports). There was an indication that the winds drove the pressure differences and thereby the currents. The cross-channel pressure difference at Section 3 was the series that was best correlated with the wind fluctuations along 245°T.

The 10-day averages of transport opened up many areas for further investigation. First, there were three main peaks in the averages. The complete record (340 days) at Section 3 will be examined to see if this pattern continued, and if it was due to convergence and divergence of the ACC by winds or by other mechanisms. A more careful examination of the apparent lag of the transport at Section 2 is necessary to determine whether it was significant and if so what caused it. The combined outflow through Section 2

and 3 exceeded the flow through Section 1 for most of the 10-day periods. When transport through Section 1 exceeded that through 2 and 3 there followed shortly thereafter a large excess through 2 and 3. Is the transport through Sections 2 and 3 consistently larger than that through 1, except for short periods where there is a piling up of water due to atmospheric conditions followed by a relaxation?

7. ACKNOWLEDGMENTS

We wish to thank the many people who assisted in the field operations, data processing and discussions. In particular, we thank the complements of the NOAA ships FAIRWEATHER and DISCOVERER and the USCG ship FIREBUSH. Special thanks to T. Jackson and W. Parker who prepared, deployed and recovered all the equipment. L. Long and P. Proctor processed the time series with great care and patience. Discussions with R. Reed, L. Incze, and R. Romea were extremely helpful. This publication is a contribution to the Fisheries Oceanography Coordinated Investigations (FOCI) of NOAA.

8. REFERENCES

Allen, J.S. and P.K. Kundu, 1978: On the momentum, vorticity, and mass balance in the oregon shelf, *J. Phys. Ocean., Jan 78*, pp. 13-27.

Luick, J.L., T.C. Royer, and W.P. Johnson, 1987: Coastal atmospheric forcing in the northern Gulf of Alaska. *J. Geophys. Res., 92*(C4), 3841-3848.

Macklin,S.A., J.E. Overland, and J.P. Walker, 1984: Low-level gap winds in Shelikof Strait. 3rd Technical Conference on Meteorology of the Coastal Zone. Amer. Meteor Soc. 9-13 January, 1984, Miami FL. Paper JC-7.4.

Muench,R.D., H.O. Mofjeld, and R.L. Charnell, 1978: Oceanographic conditions in lower Cook Inlet; spring and summer 1973. *J. Geophys. Res., 83*, 5090-5098.

Muench, R.D., J.D. Schumacher, 1980: Physical oceanographic and meteorological conditions in the northwest Gulf of Alaska. NOAA Tech. Memo. ERL-PMEL-22, 147 pp.

Mysak L., R.D. Muench, and J.D. Schumacher, 1981: Baroclinic instability in a downstream varying channel: Shelikof Strait, Alaska. *J. Phys. Oceanogr., 11*(7), 950-969.

Overland, J.E., R.A. Brown and C.D. Mobley, 1980: METLIB--A program library for calculating and plotting marine boundary layer wind fields. NOAA Tech. Memo. ERL-PMEL-20, 82 pp.

Pearson, C.A., 1981: Guide to R2D2-Rapid retrieval data display. NOAA Tech. Memo. ERL-PMEL-29, 144 pp.

Reed, R.K., R.D. Muench and J.D. Schumacher, 1980: On baroclinic transport of the Alaskan Stream near Kodiak Island. *Deep-Sea Res., 27*, 509-523.

Reed, R. K. and J.D.Schumacher, 1981: Sea level variations in relation to coastal flow around the Gulf of Alaska. *J. Geophys. Res., 86*(7), 6543-6546.

Reed, R.K., J.D. Schumacher, and L.S. Incze, 1986: Water properties and circulation in Shelikof Strait, Alaska during 1985. NOAA Tech. Memo. ERL-PMEL-68, 35 pp.

Royer, T.C., 1979: On the effect of precipitation and runoff on coastal circulation in the Gulf of Alaska. *J. Phys. Oceanogr., 9*, 555-563.

Royer, T.C., 1981: Baroclinic transport in the Gulf of Alaska. 1. Seasonal variations of the Alaska Current. *J. Mar. Res., 39*(2), 239-250.

Royer, T.C. , 1982: Coastal fresh water discharge in the northeast Pacific. *J. Geophys. Res., 87*, 2017-2021.

Schumacher, J.D. and R.K. Reed, 1986: On the Alaska Coastal Current in the Western Gulf of Alaska, *J. Geophys. Res. 91, C8*, pp. 9655-9661.

Schumacher, J.D., R.K. Reed, M. Grigsby, and D. Dreves, 1979: Circulation and hydrography near Kodiak Island, September to November, 1977. NOAA Tech. Memo. ERL PMEL-13, pp. 49.

FIGURES

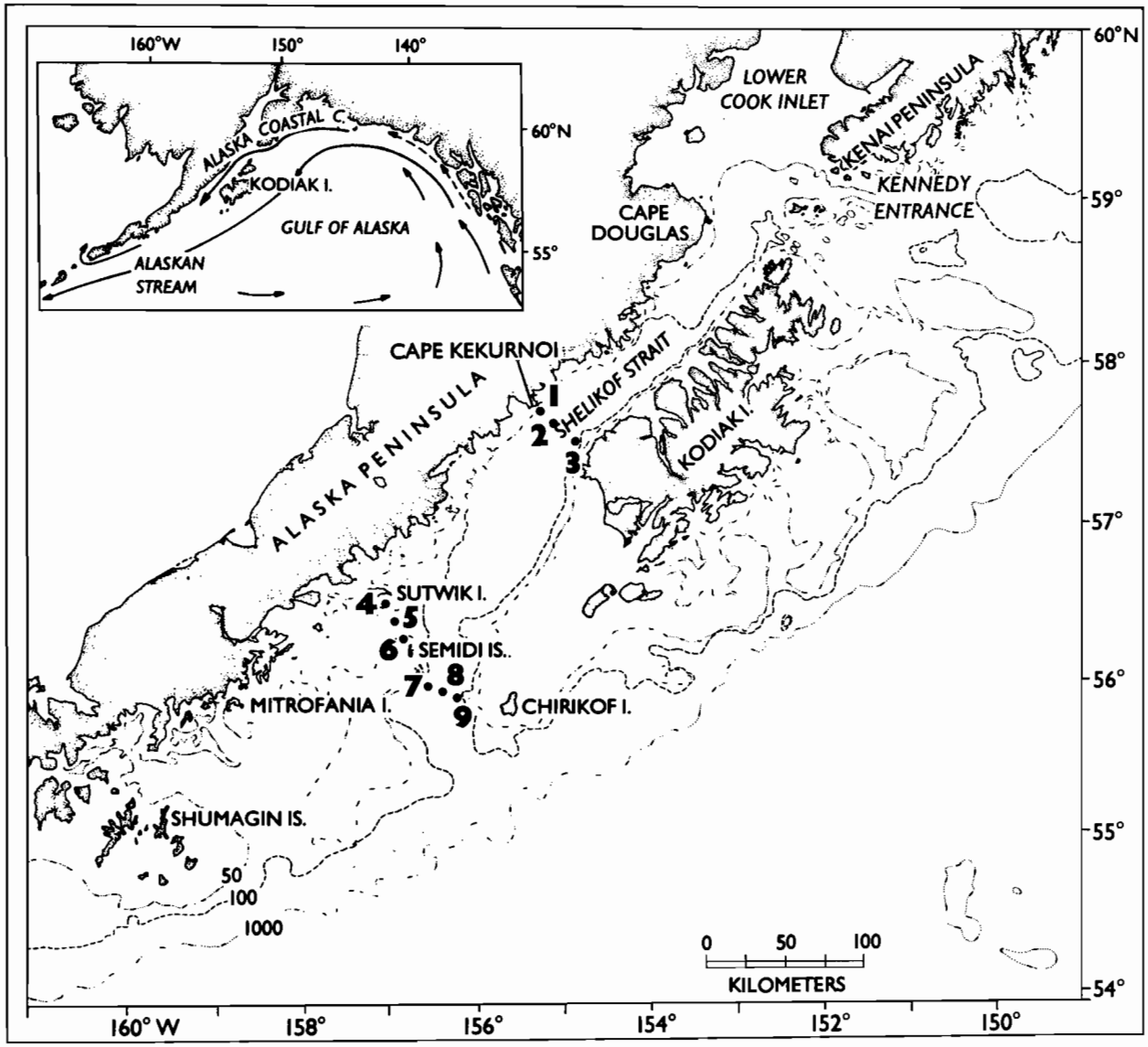

Figure 1.--Location figure showing the study region, location of the current meter moorings and geographical place names.

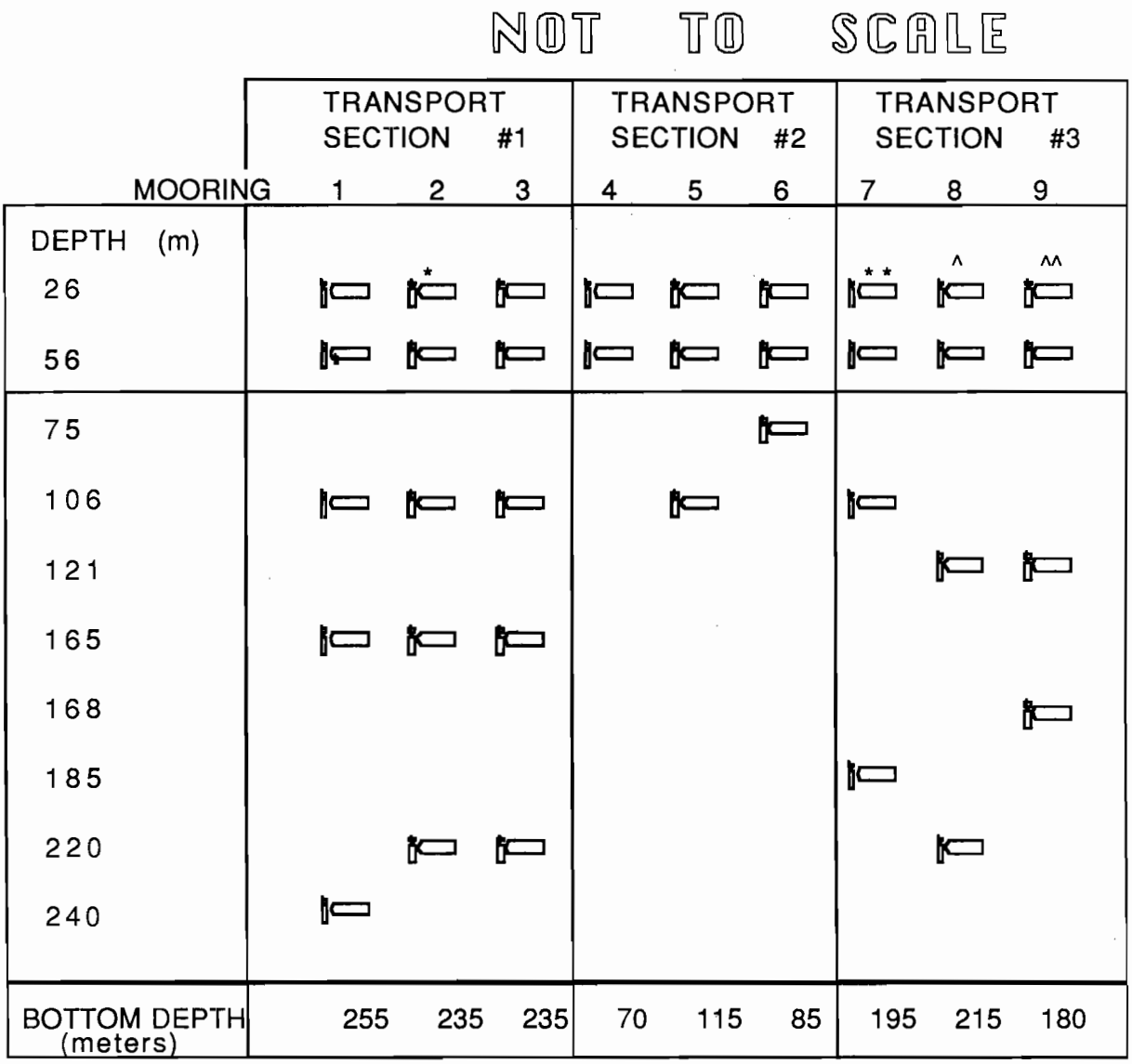

Figure 2.--Schematic of the location of the current meters for each of the moorings, showing the division into transport sections and the coverage of the water column. Note that this figure is not to scale.

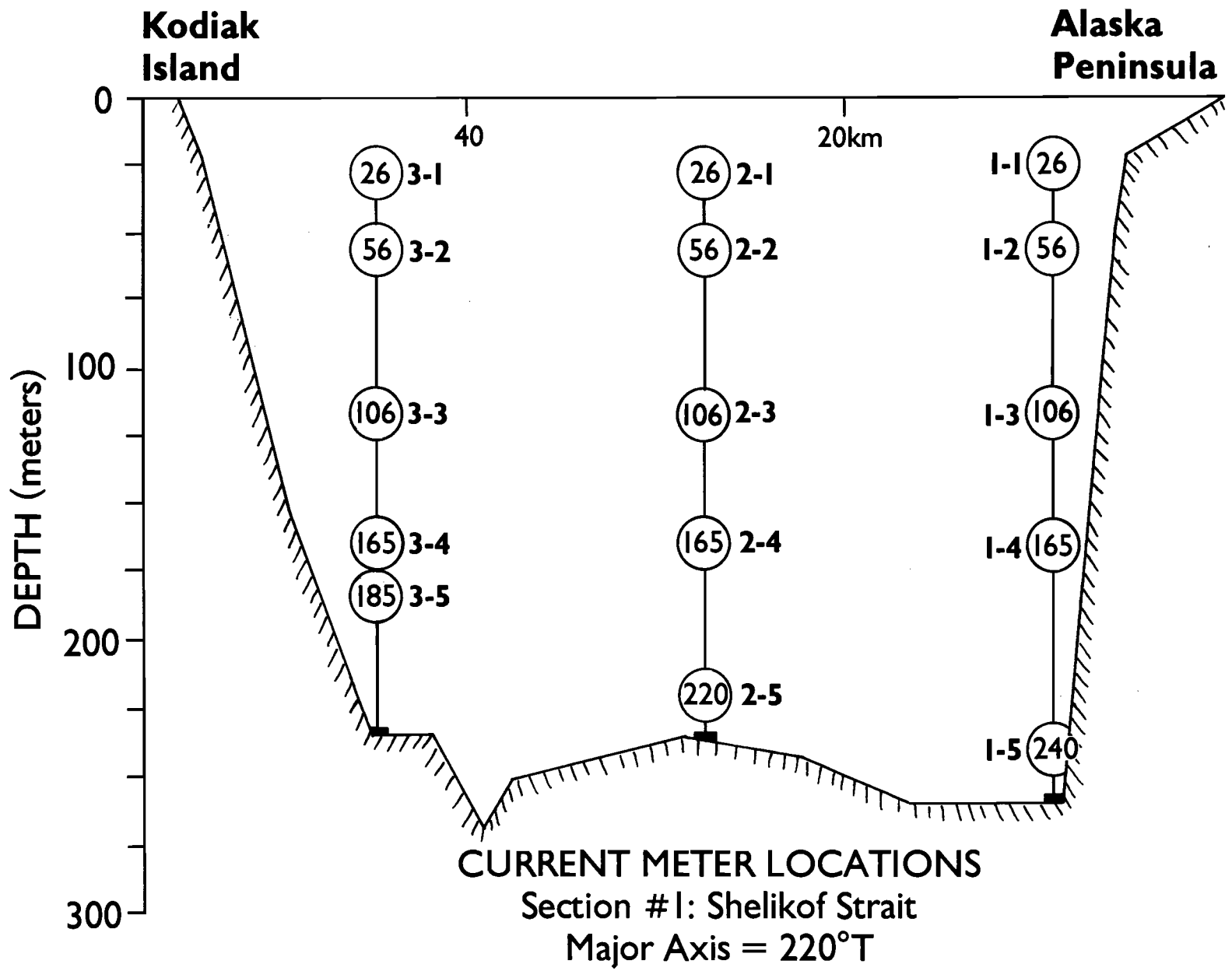

Figure 3.--Cross-section of Section #1 showing the placement of the instruments in relation to the actual bottom depth. The separation of the instruments in both horizontal and vertical directions is to scale. The view is facing in the direction of the principal axis of 220 T.

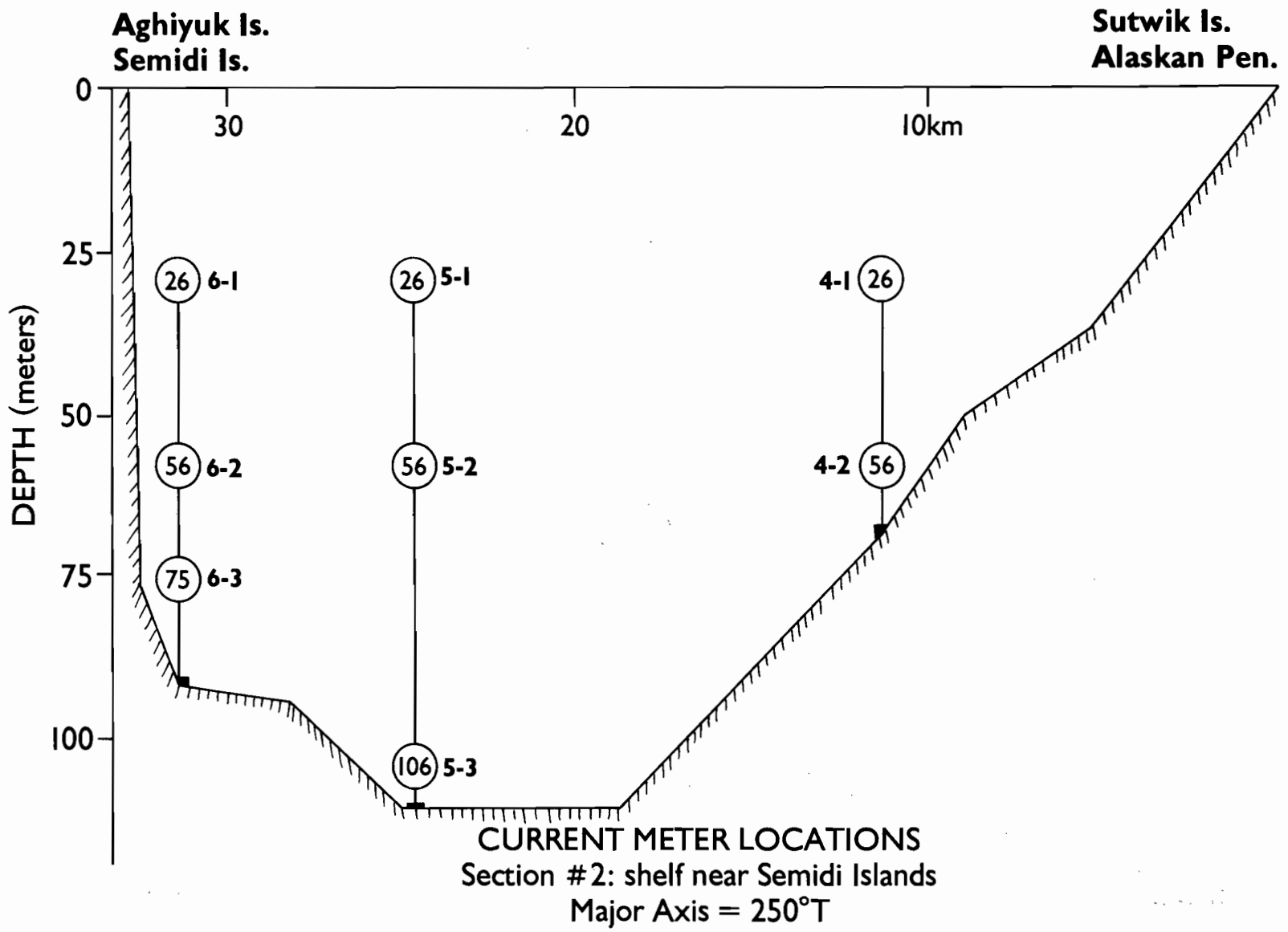

Figure 4.--Same as Figure 3, except for Section #2 along 250 T.

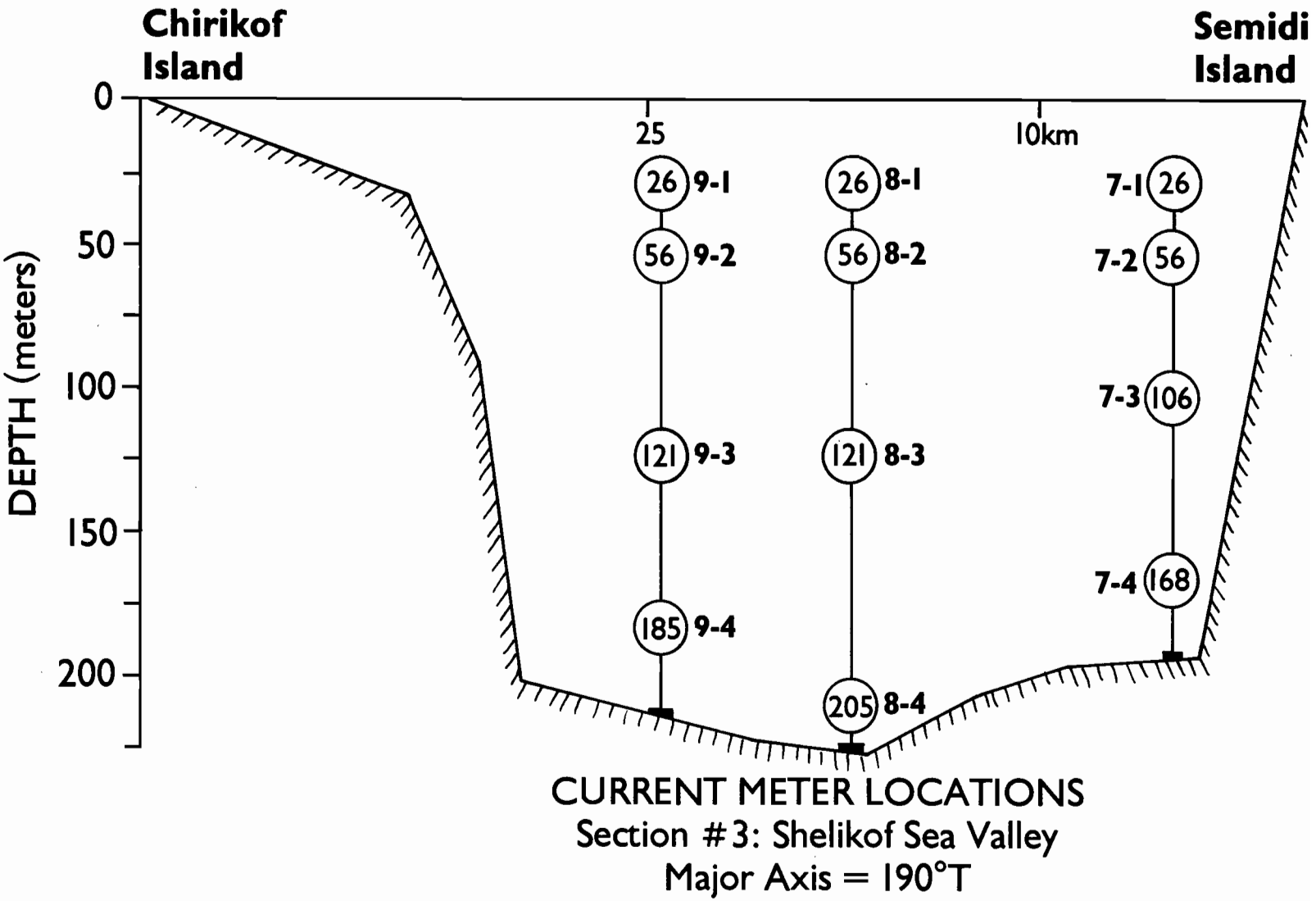

Figure 5.--Same as Figure 3, except for Section #3 along 190 T.

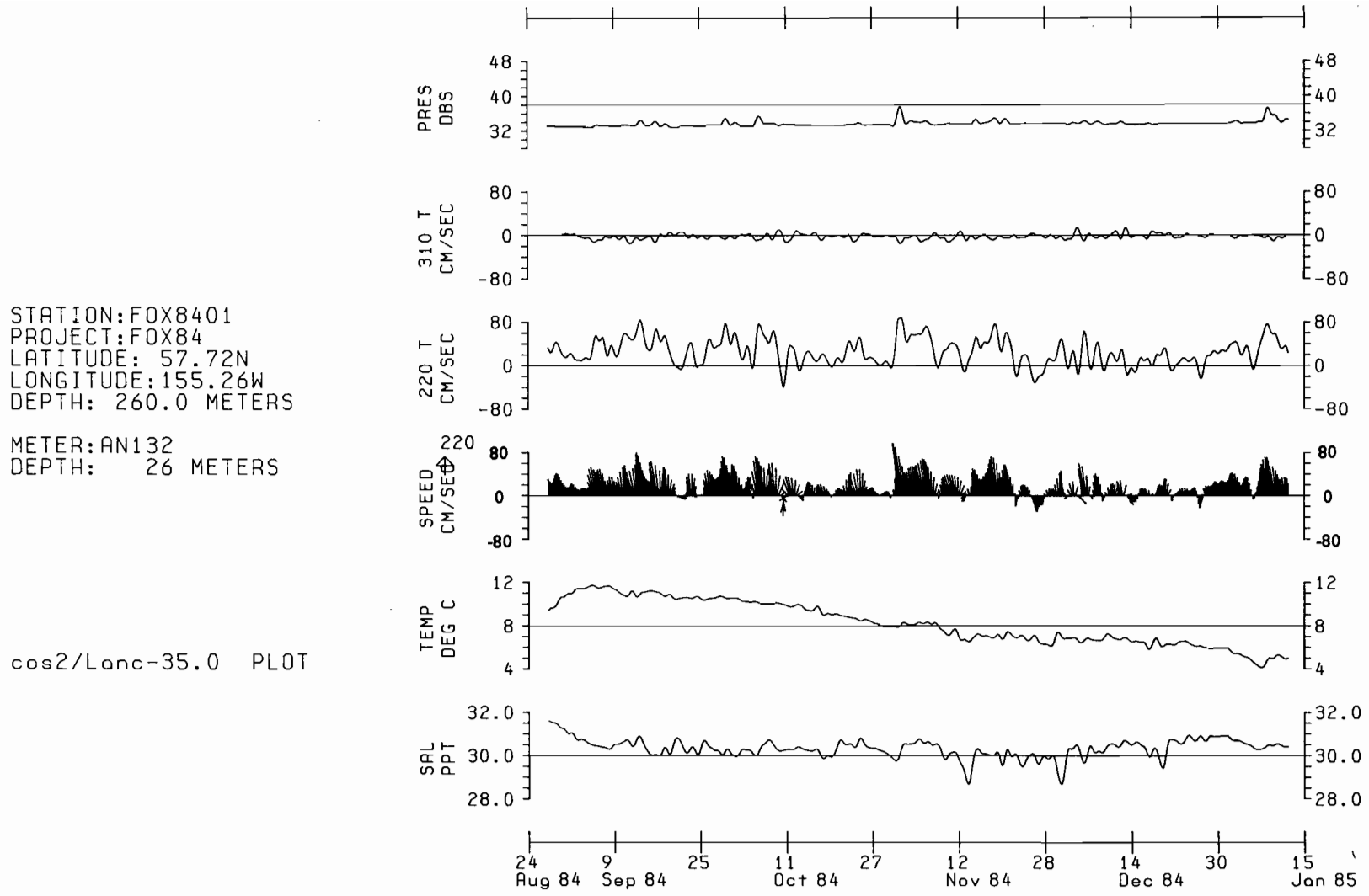

Figure 6.--Plot of all observed, low-pass filtered parameters for the current meter record from instrument 1_1 at 26 meters.

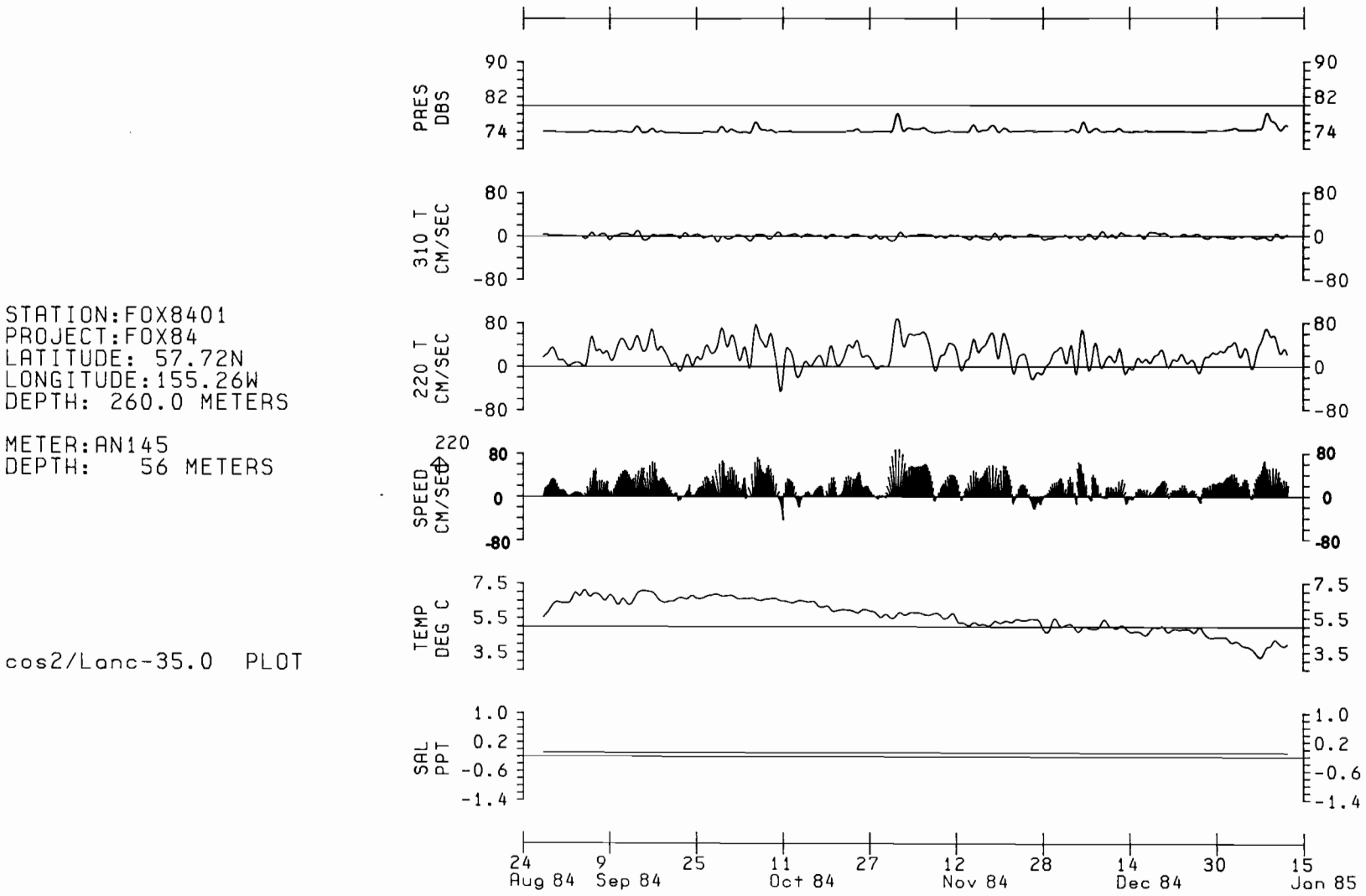

Figure 7.--Same as Figure 6, except for 1_2 at 56 meters.

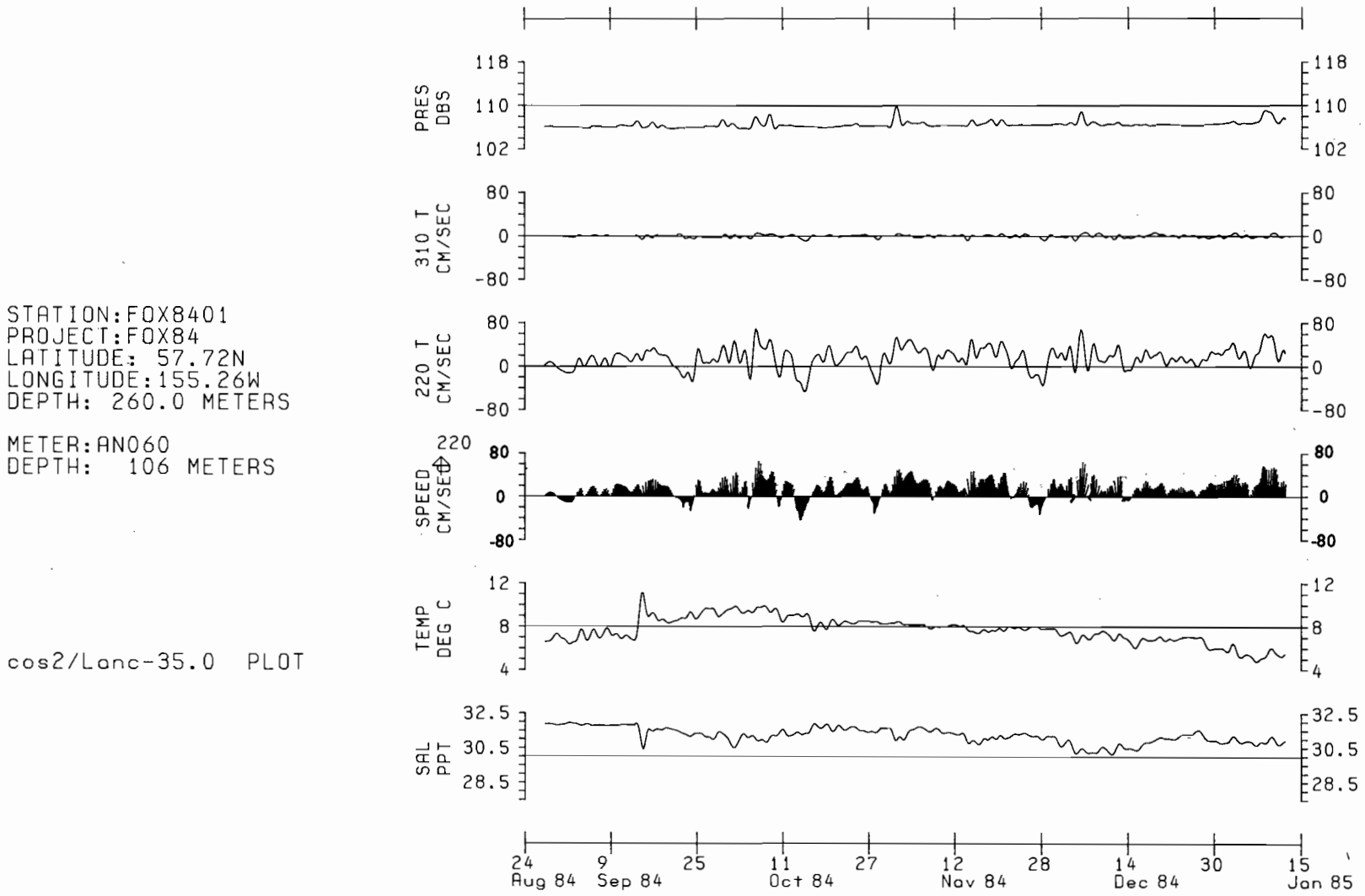

Figure 8.--Same as Figure 6, except for 1_3 at 106 meters.

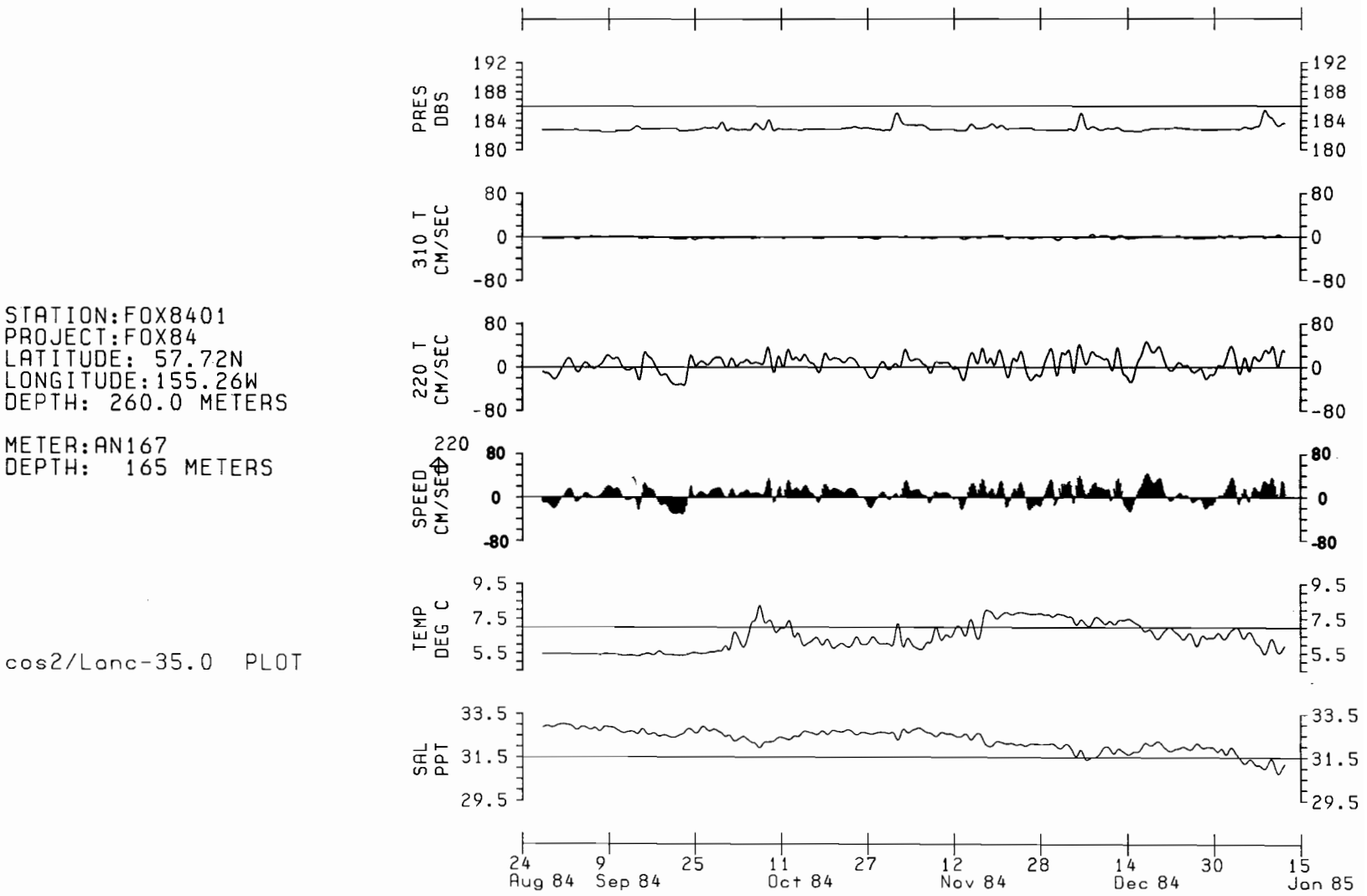

Figure 9.--Same as Figure 6, except for 1_4 at 165 meters.

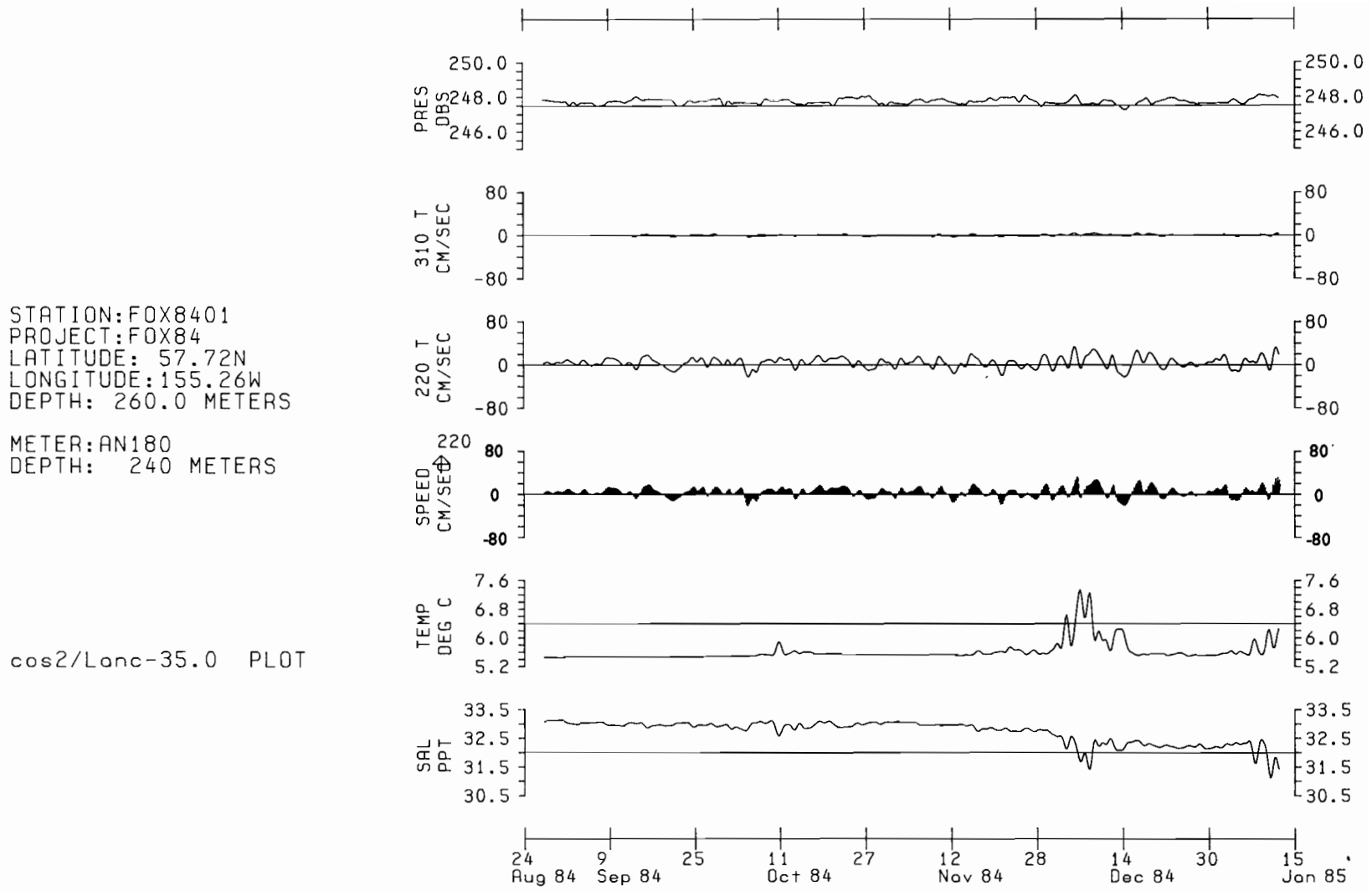

Figure 10.--Same as Figure 6, except for 1_5 at 240 meters.

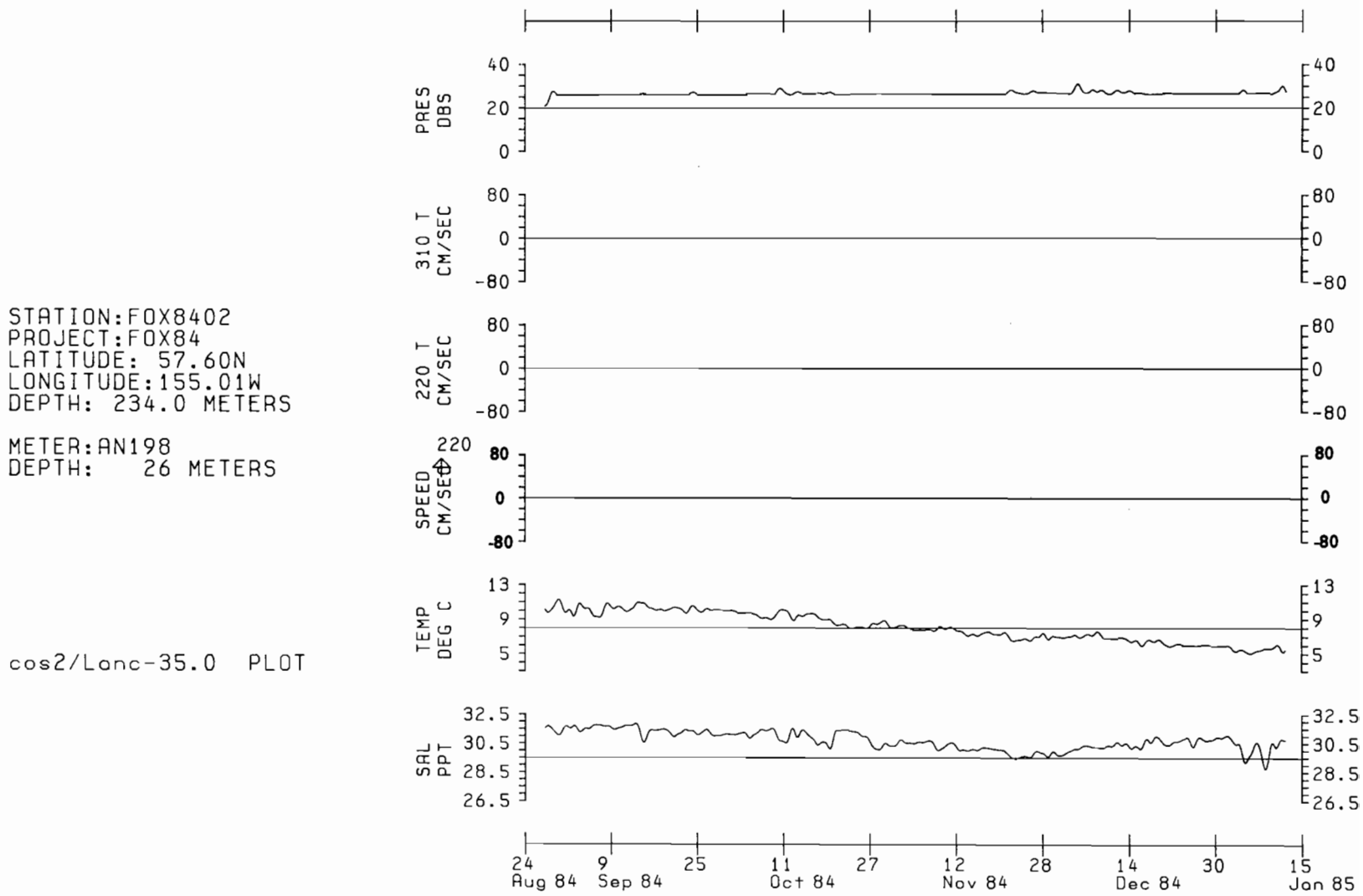

Figure 11.--Same as Figure 6, except for 2_1 at 26 meters.

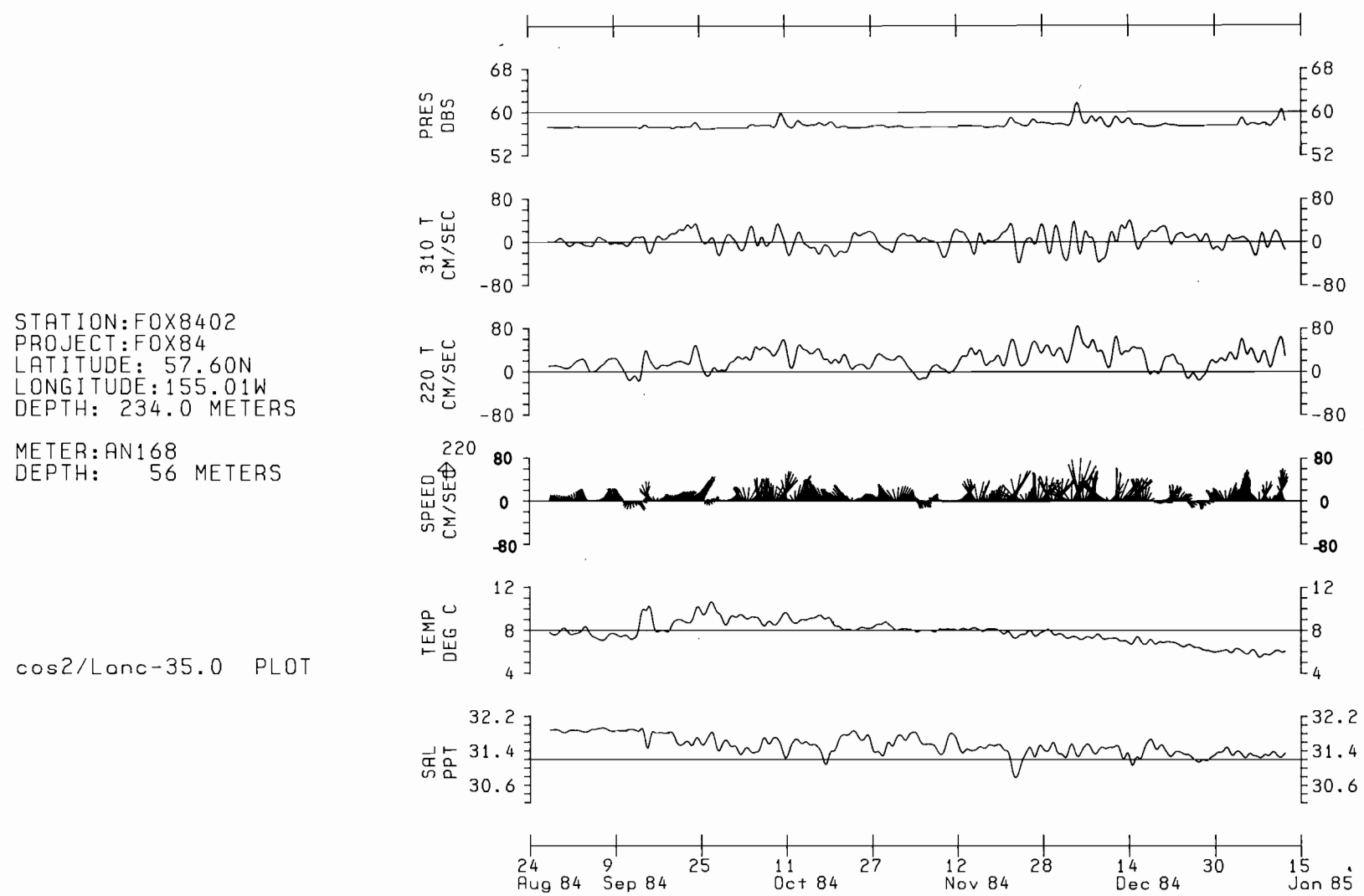

Figure 12.--Same as Figure 6, except for 2_2 at 56 meters.

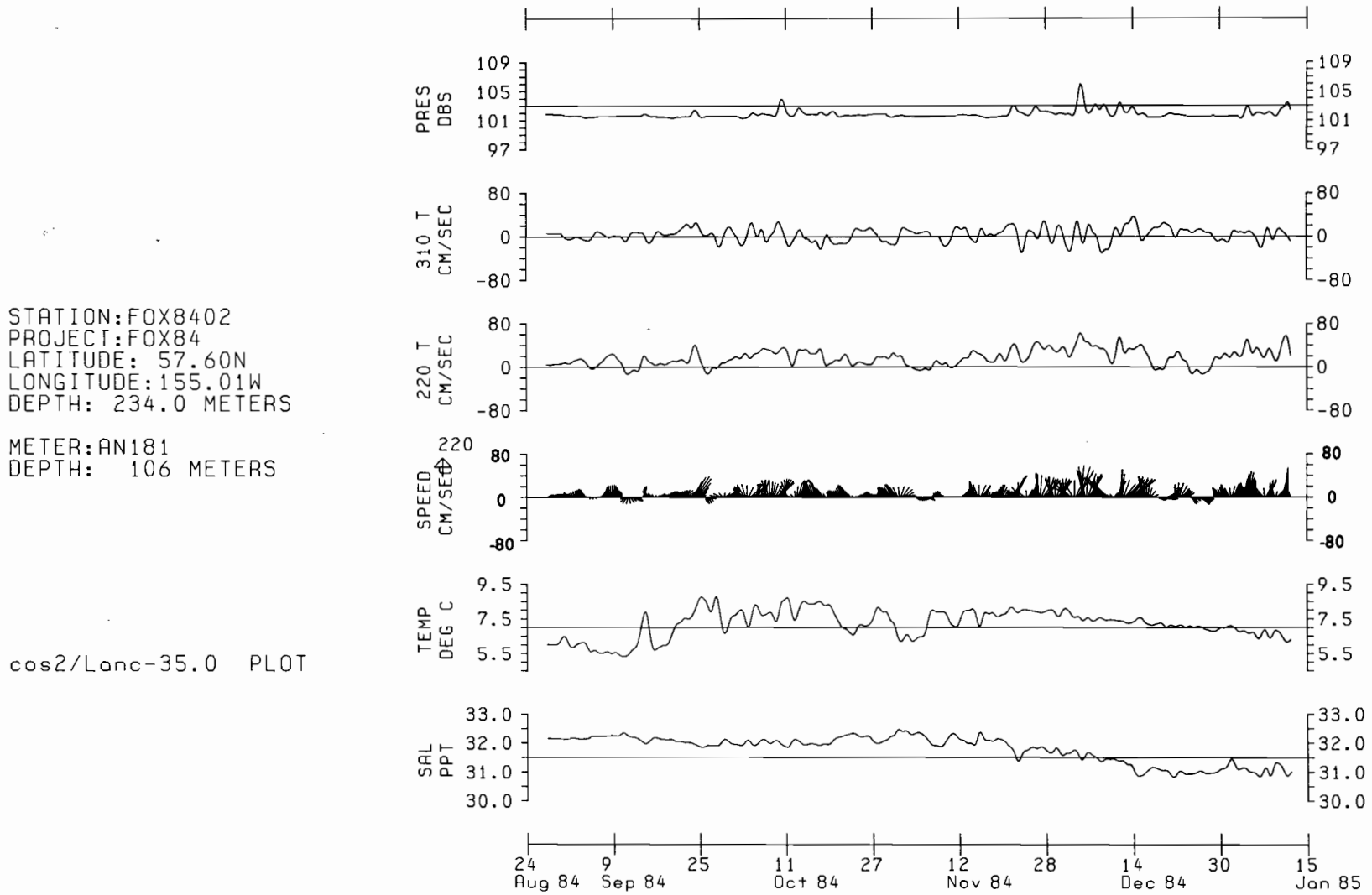

Figure 13.--Same as Figure 6, except for 2_3 at 106 meters.

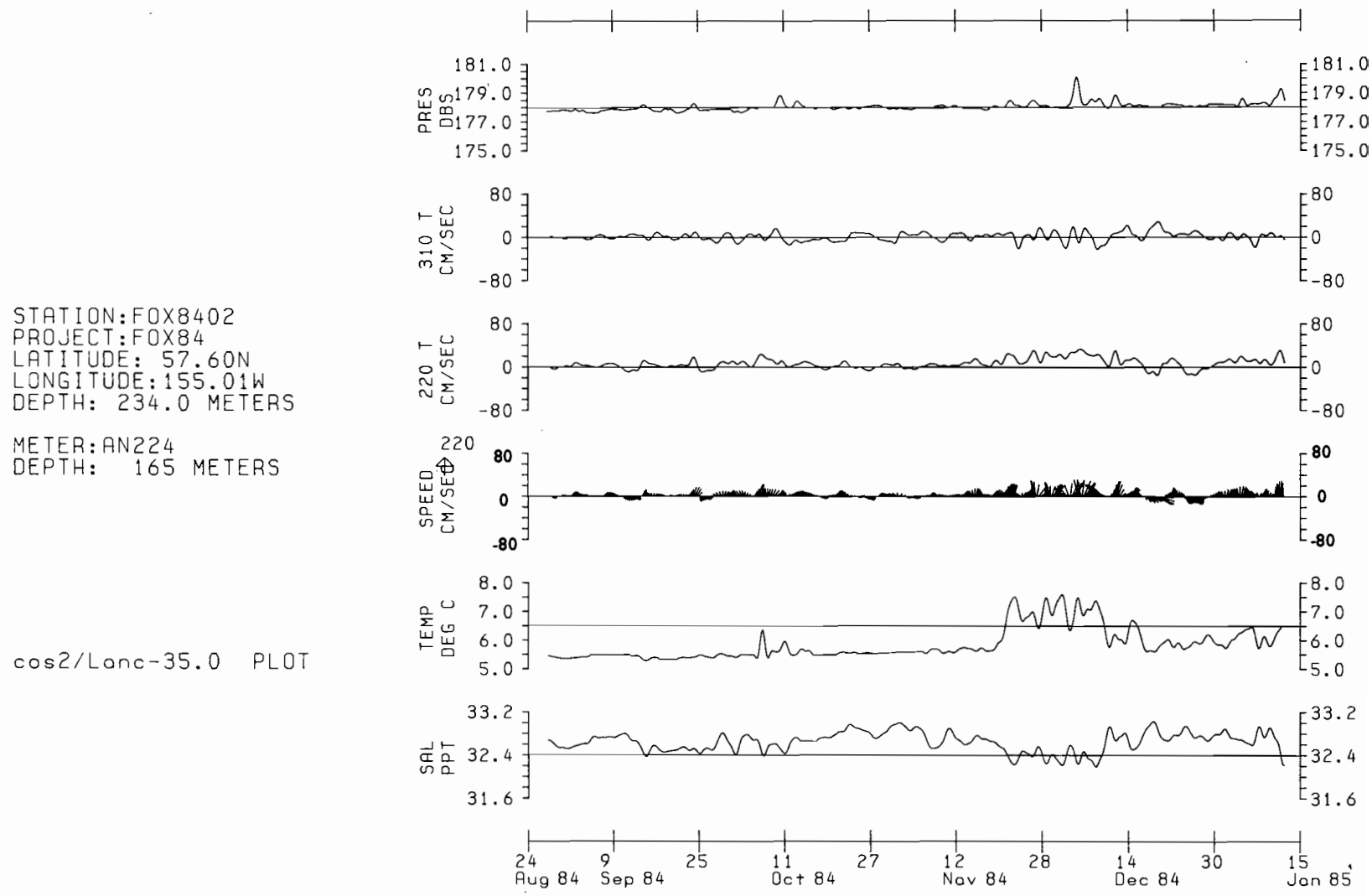

Figure 14.--Same as Figure 6, except for 2_4 at 165 meters.

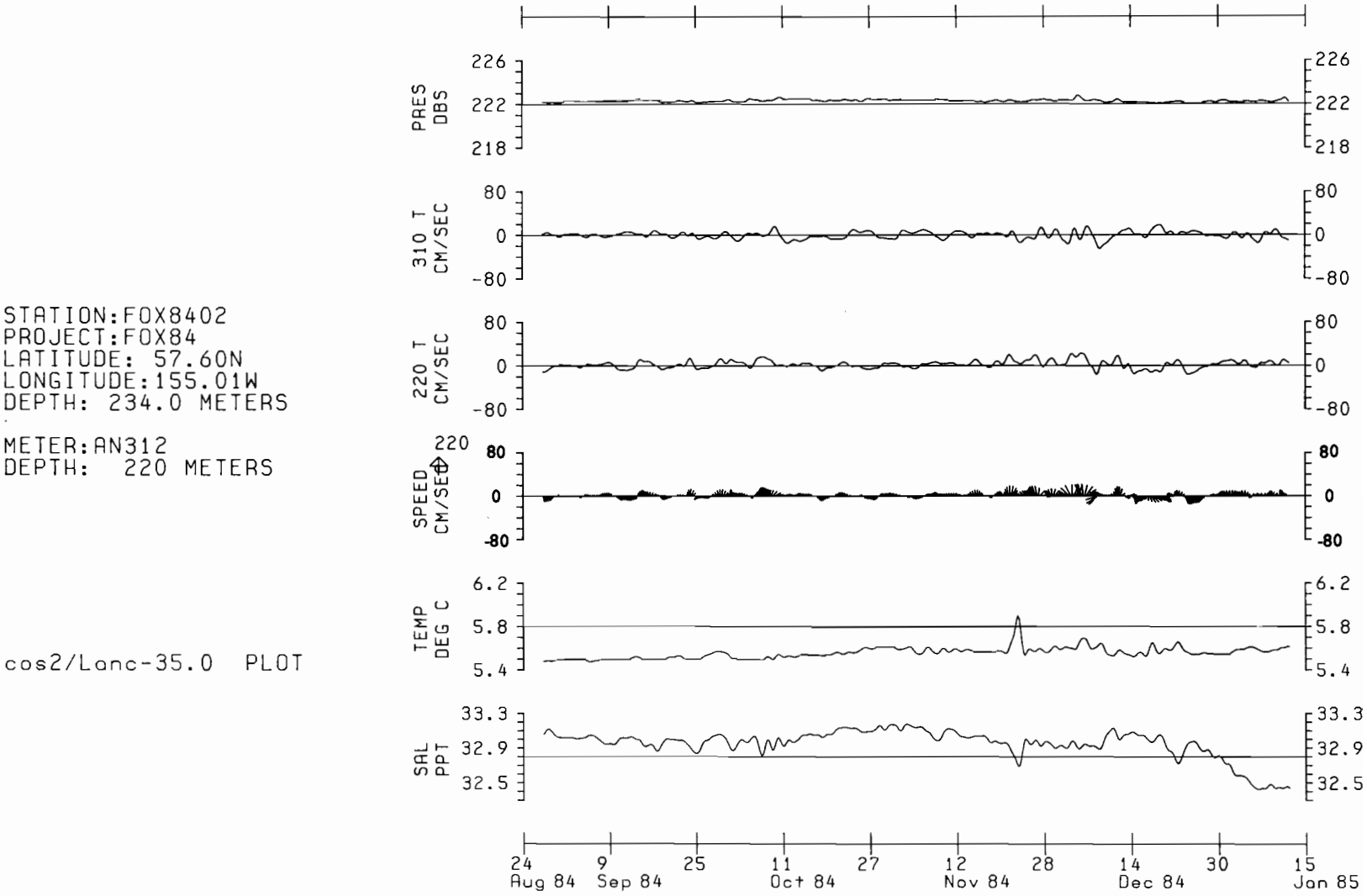

Figure 15.--Same as Figure 6, except for 2_5 at 220 meters.

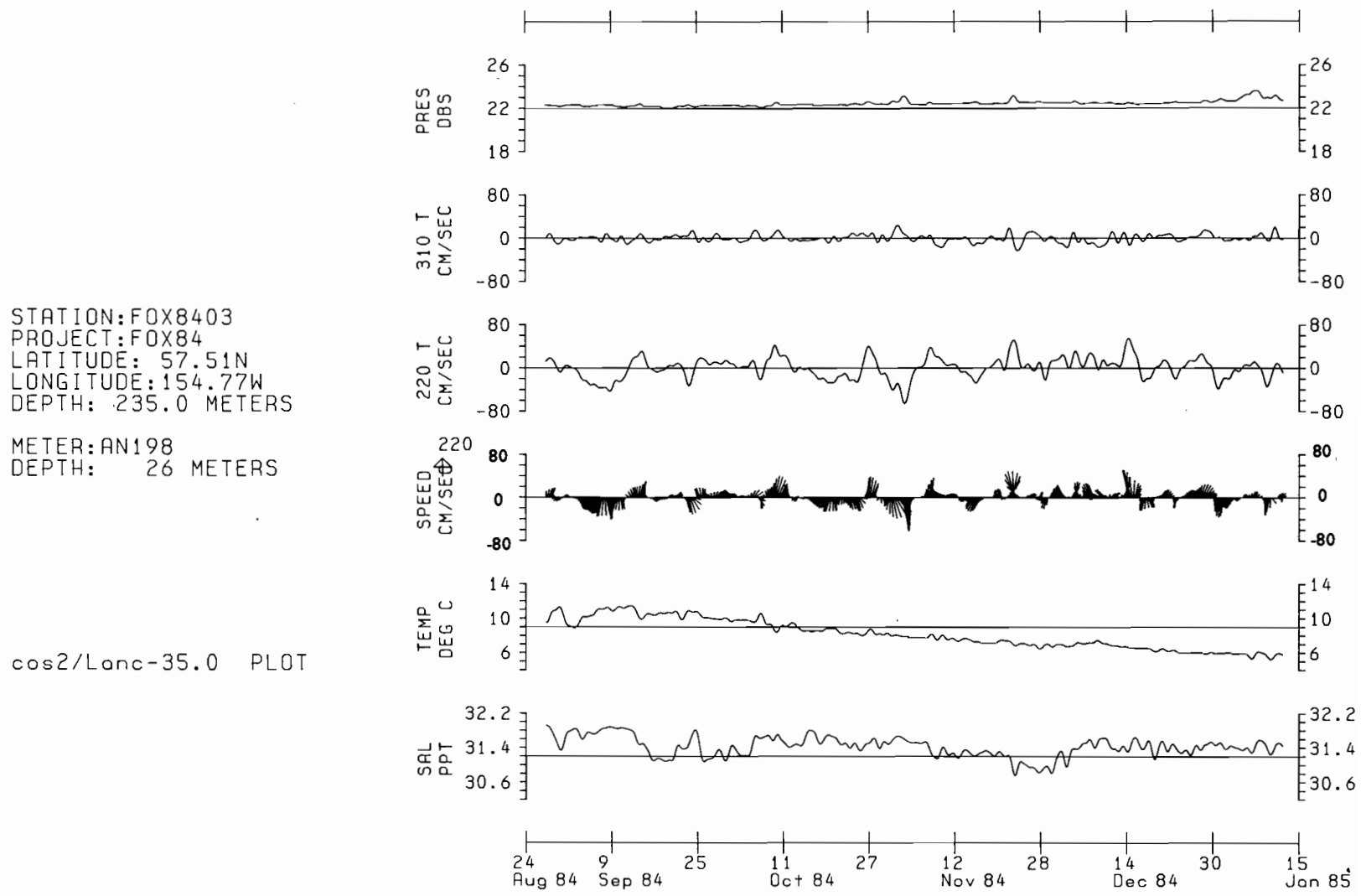

Figure 16.--Same as Figure 6, except for 3_1 at 26 meters.

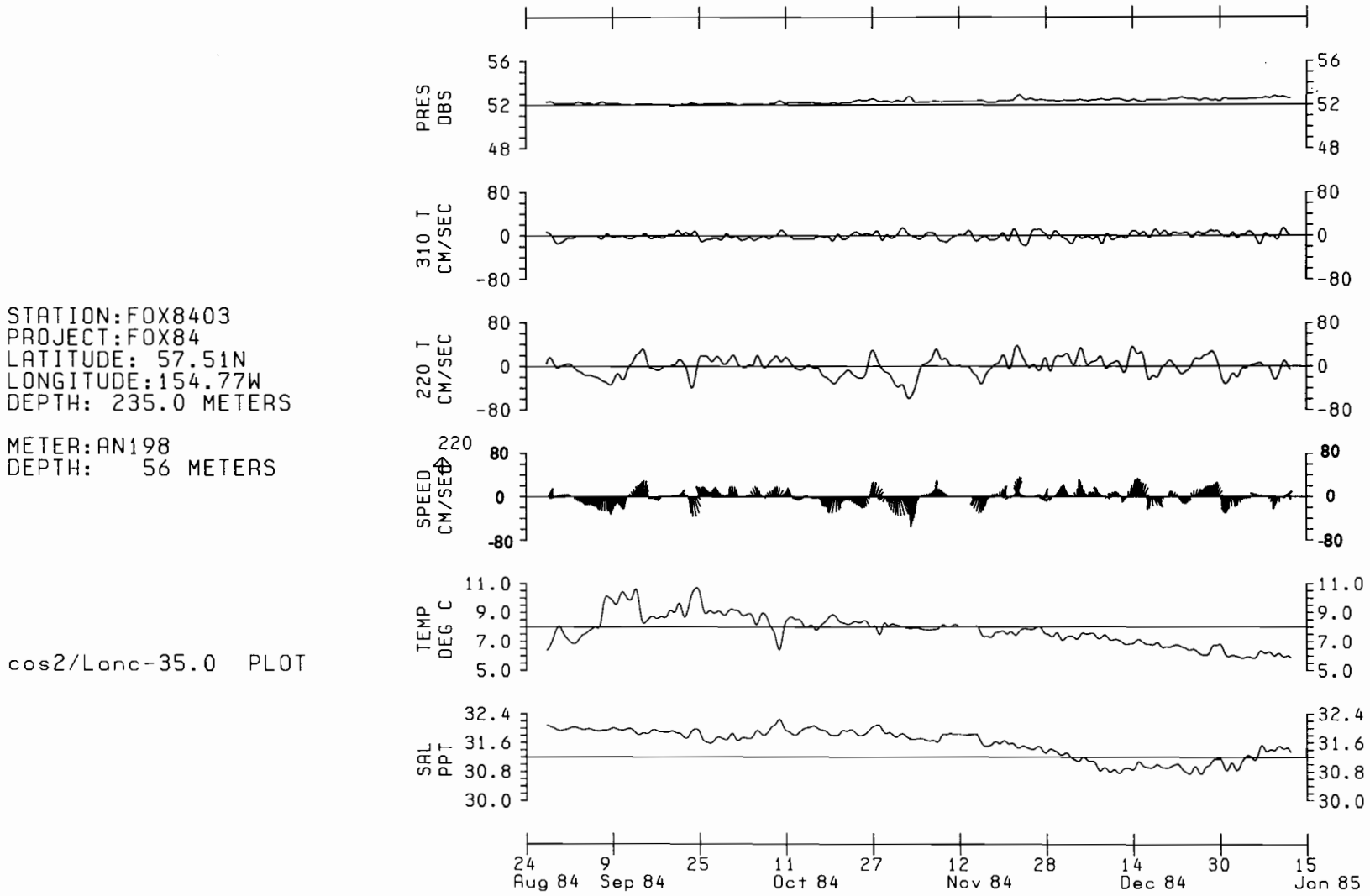

Figure 17.--Same as Figure 6, except for 3_2 at 56 meters.

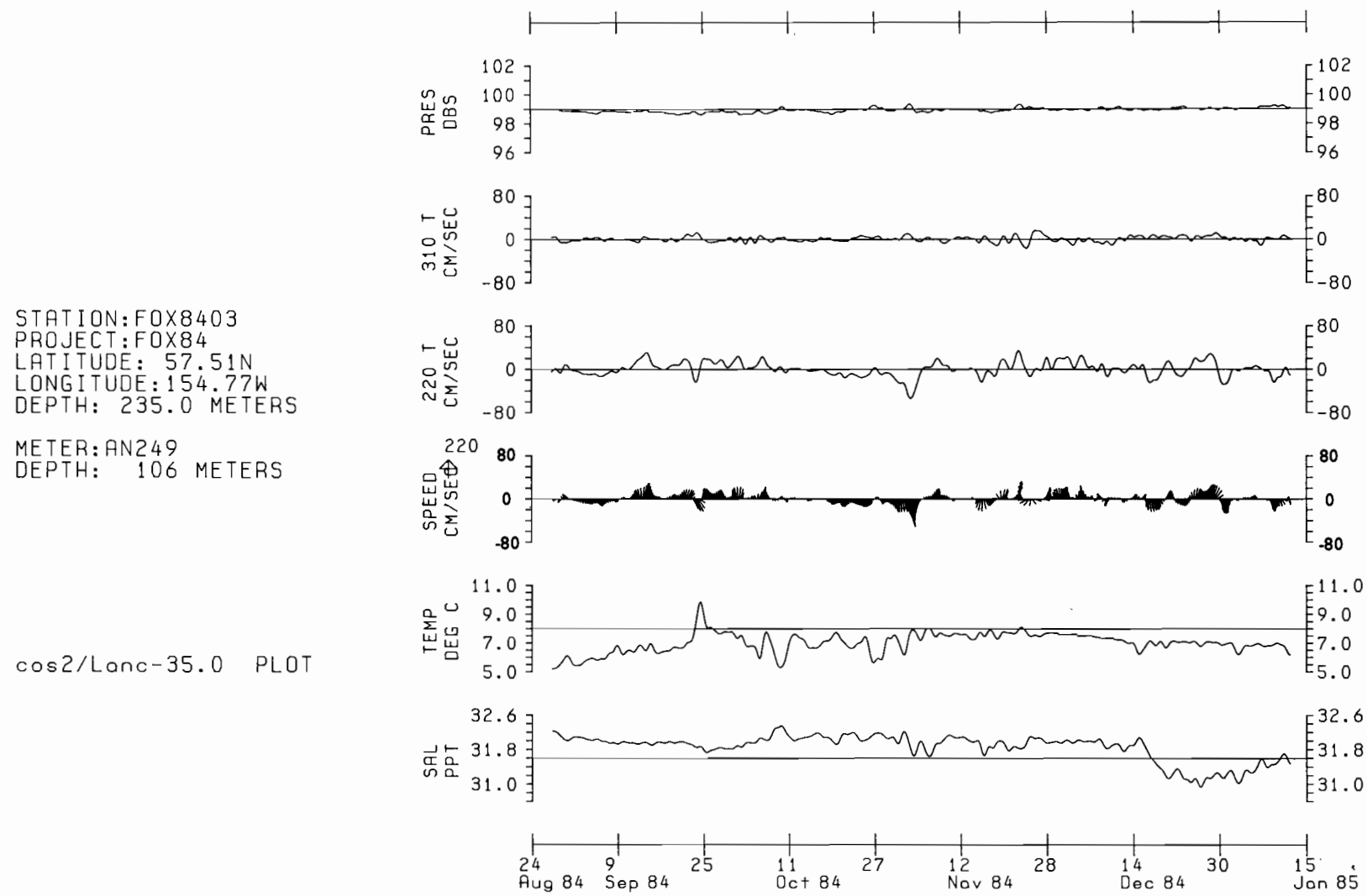

Figure 18.--Same as Figure 6, except for 3_3 at 106 meters.

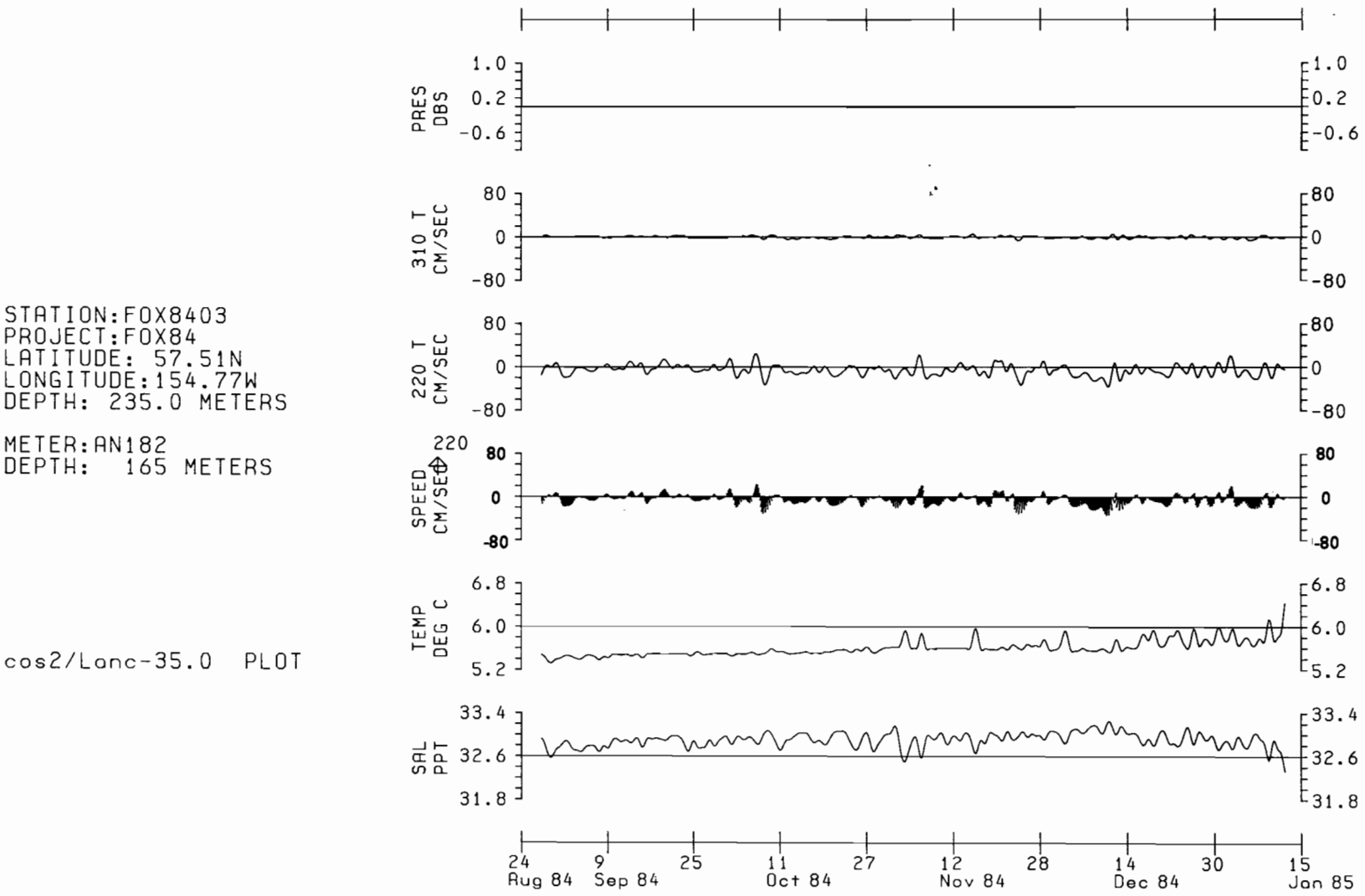

Figure 19.--Same as Figure 6, except for 3_4 at 165 meters.

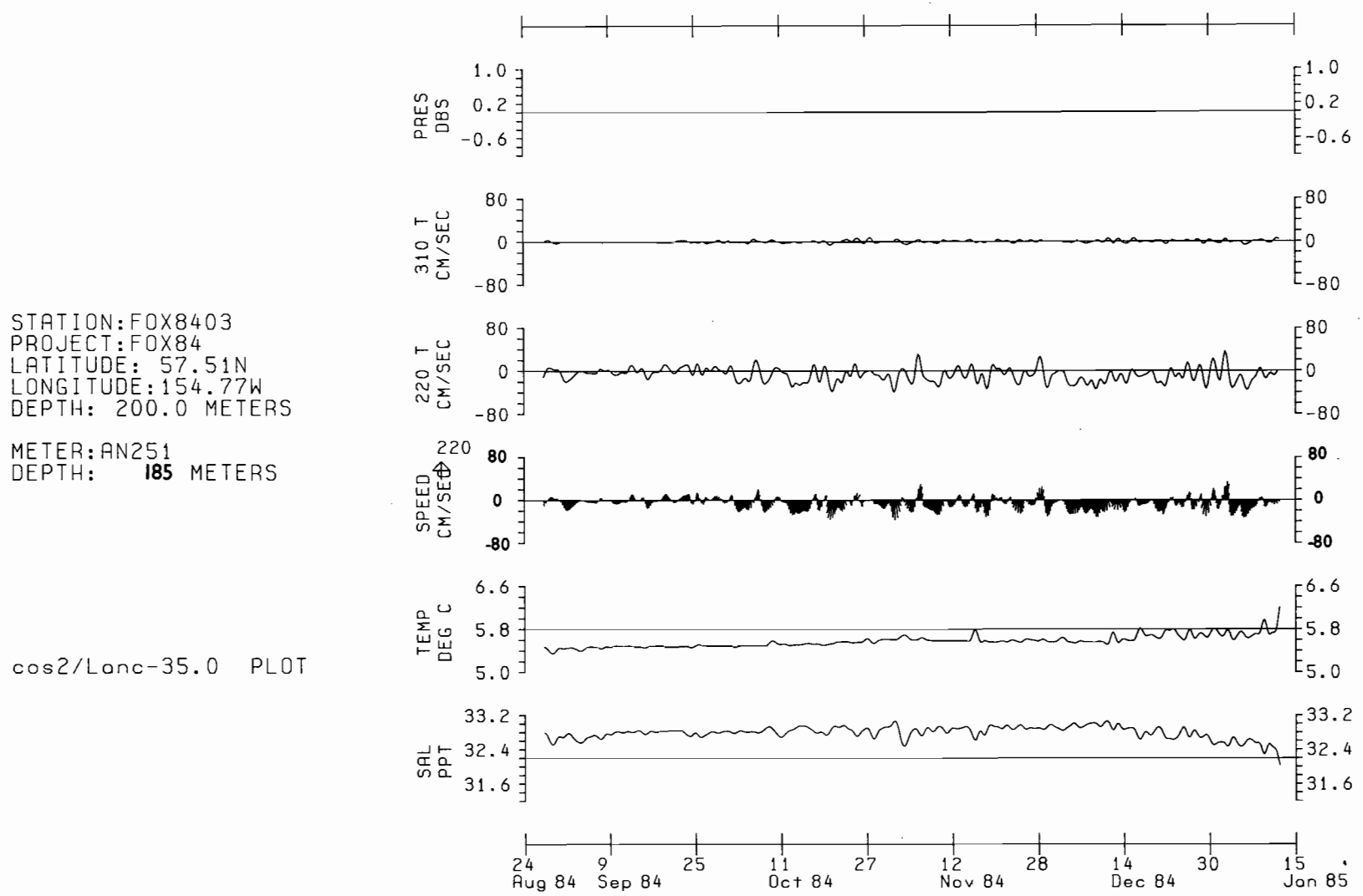

Figure 20.--Same as Figure 6, except for 3_5 at 185 meters.

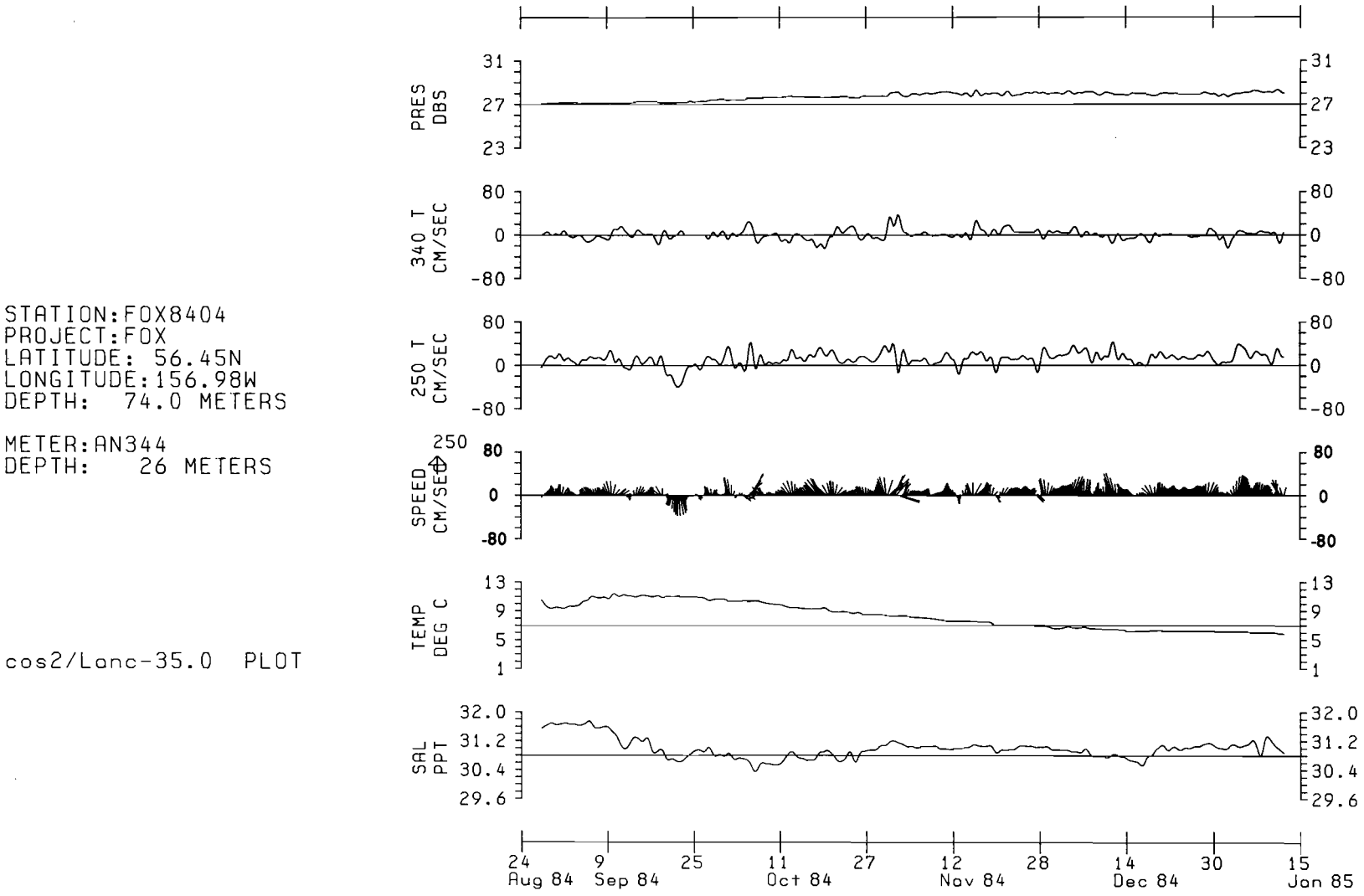

Figure 21.--Same as Figure 6, except for 4_1 at 26 meters.

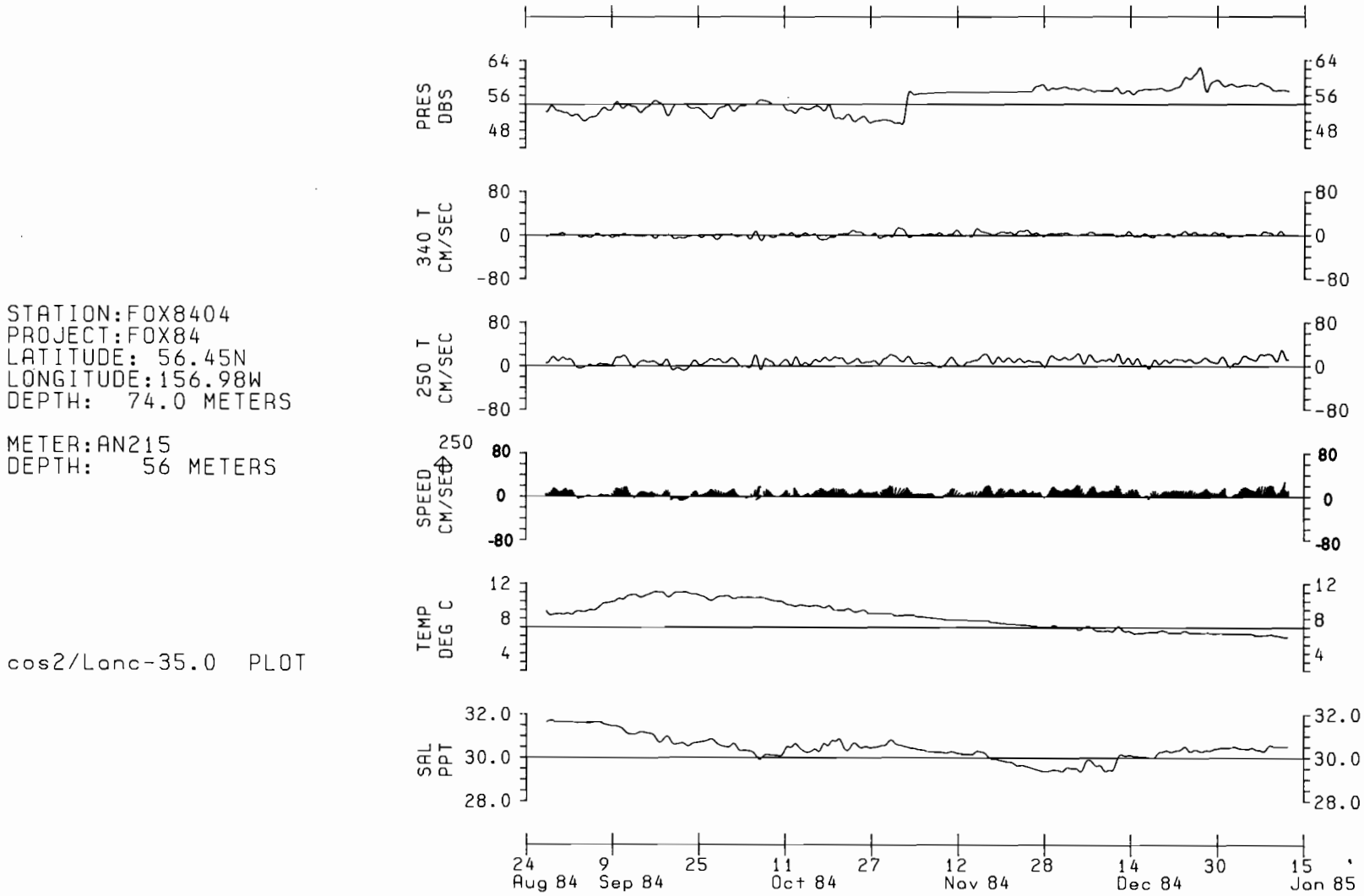

Figure 22.--Same as Figure 6, except for 4_2 at 56 meters.

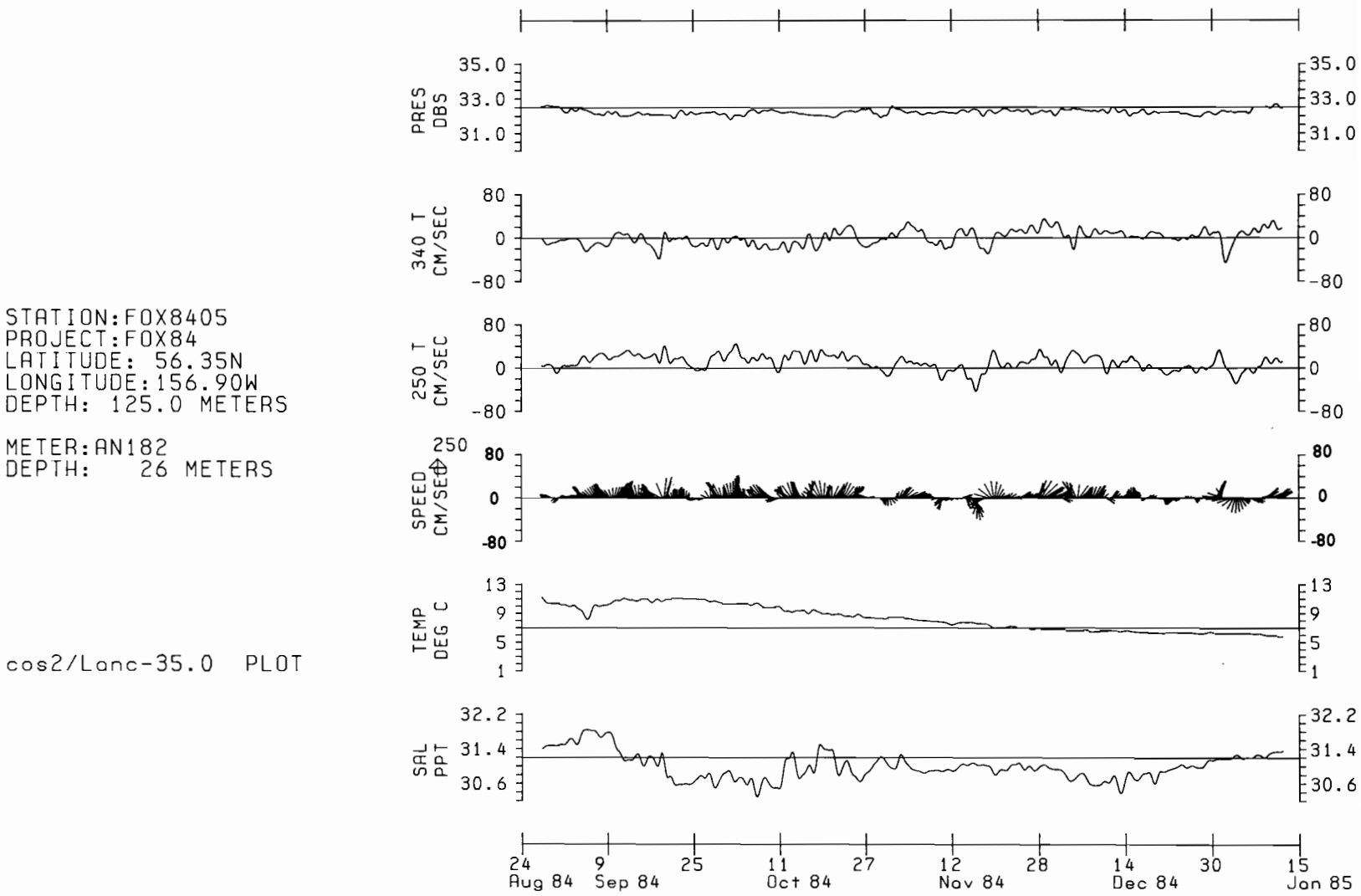

Figure 23.--Same as Figure 6, except for 5_1 at 26 meters.

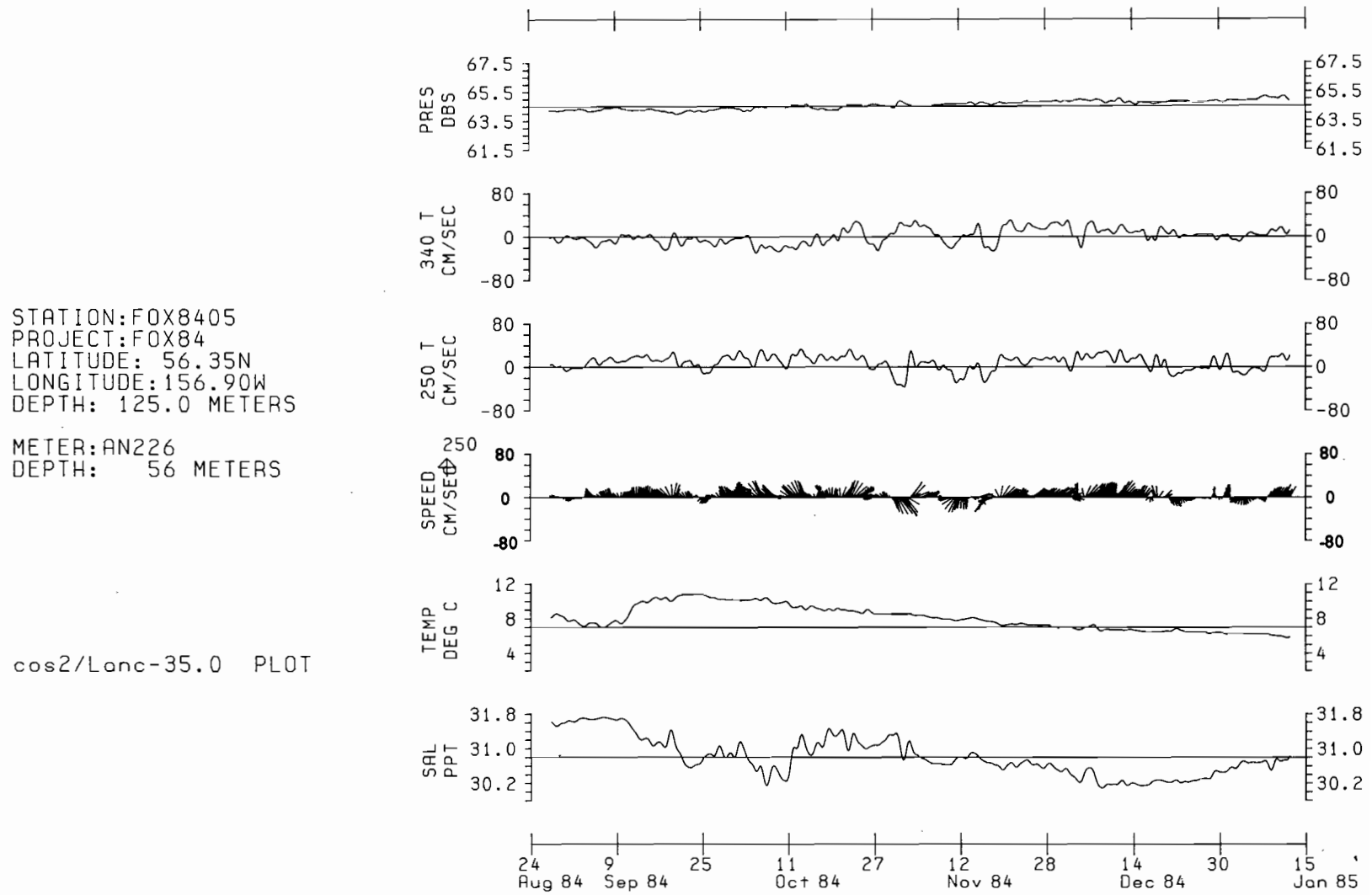

Figure 24.--Same as Figure 6, except for 5_2 at 56 meters.

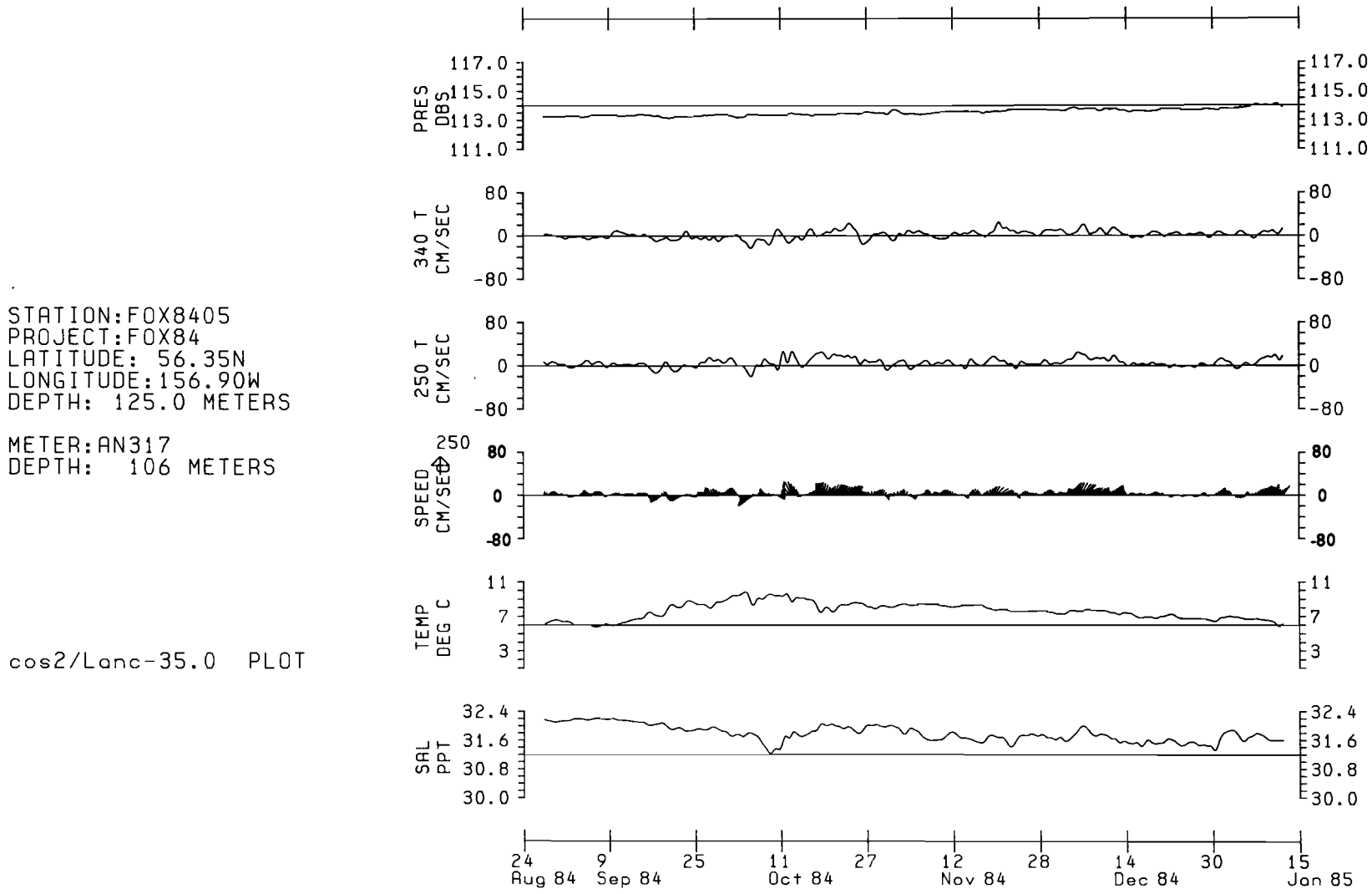

Figure 25.--Same as Figure 6, except for 5_3 at 106 meters.

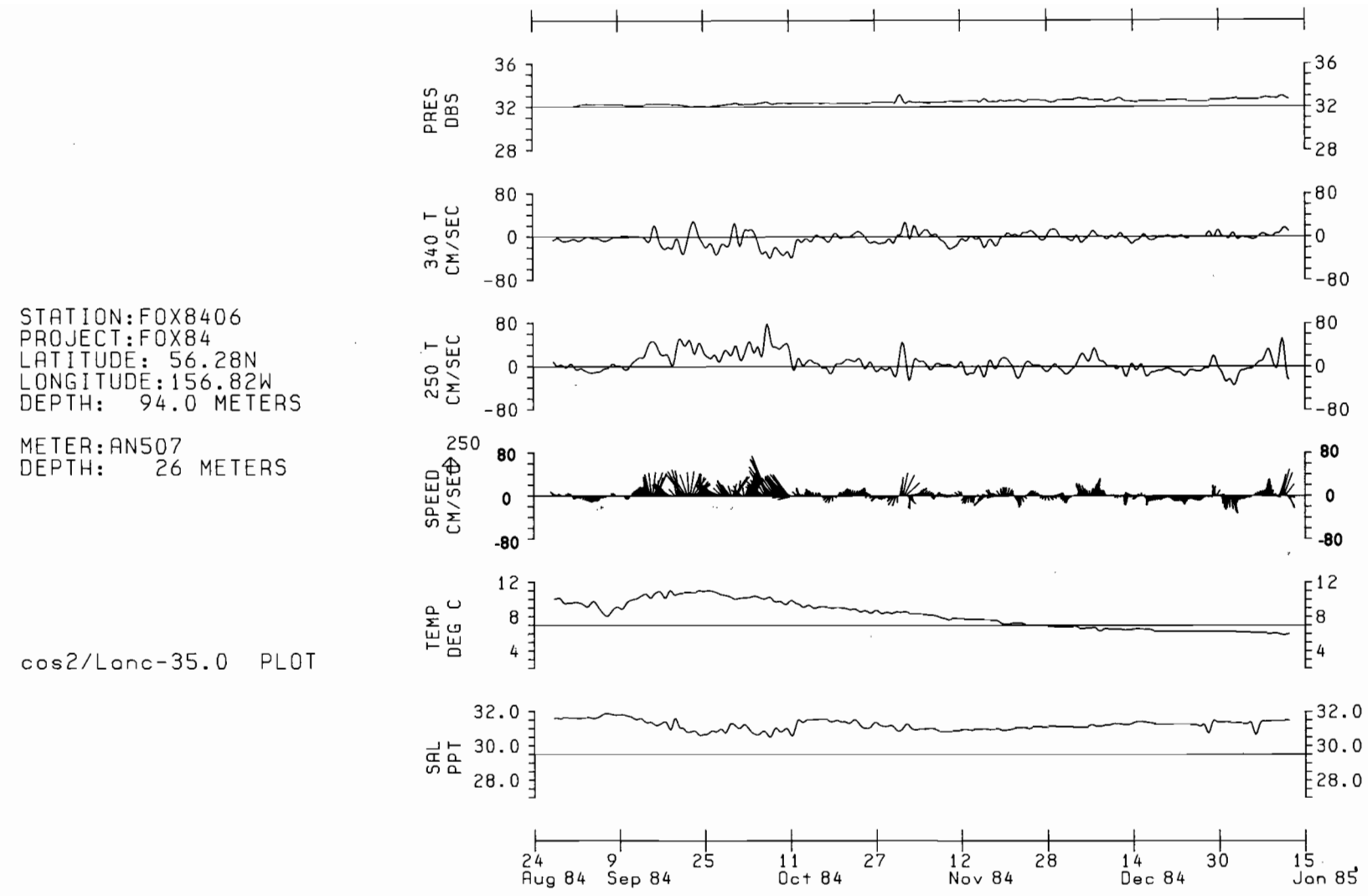

Figure 26.--Same as Figure 6, except for 6_1 at 26 meters.

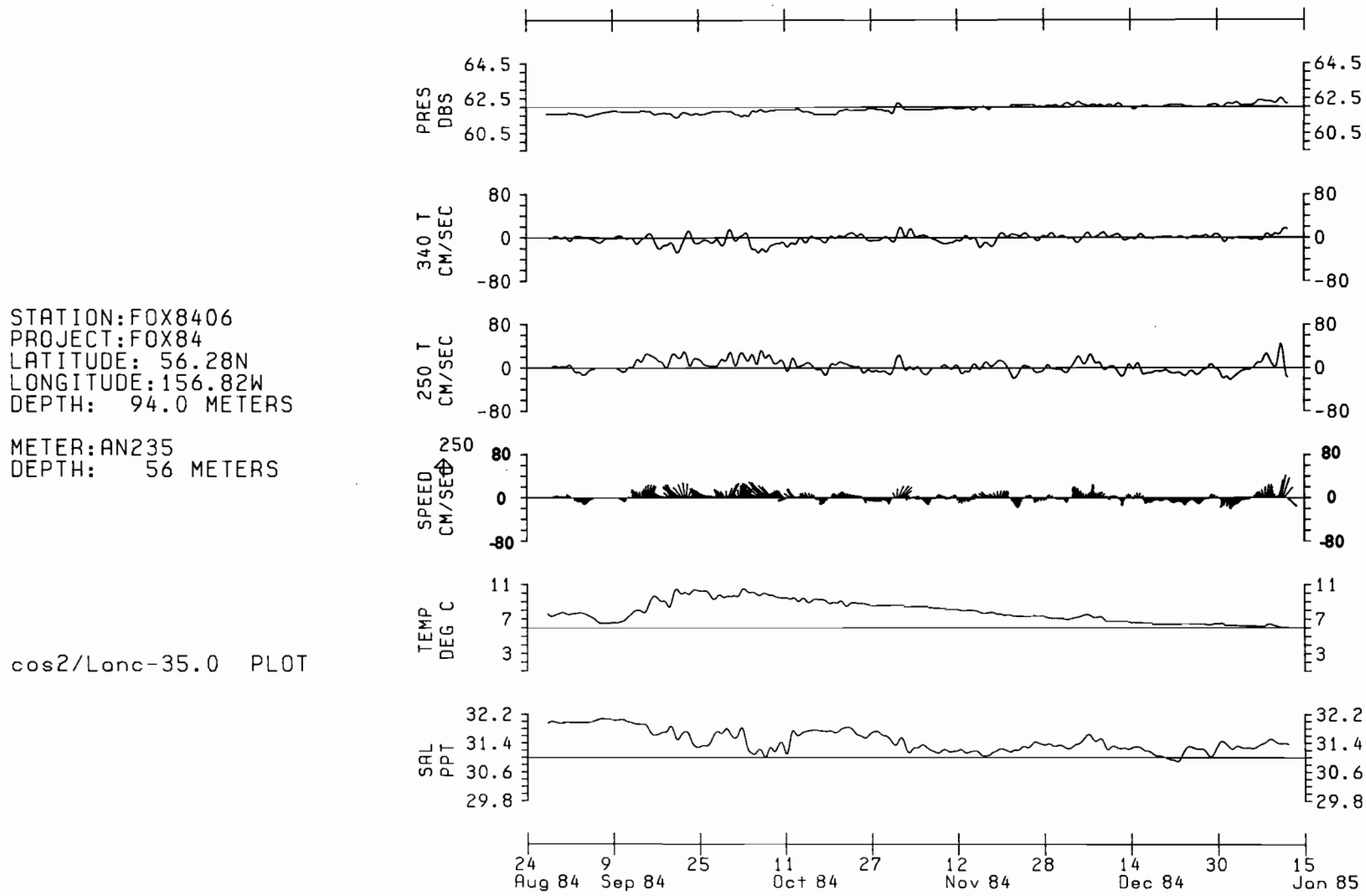

Figure 27.--Same as Figure 6, except for 6_2 at 56 meters.

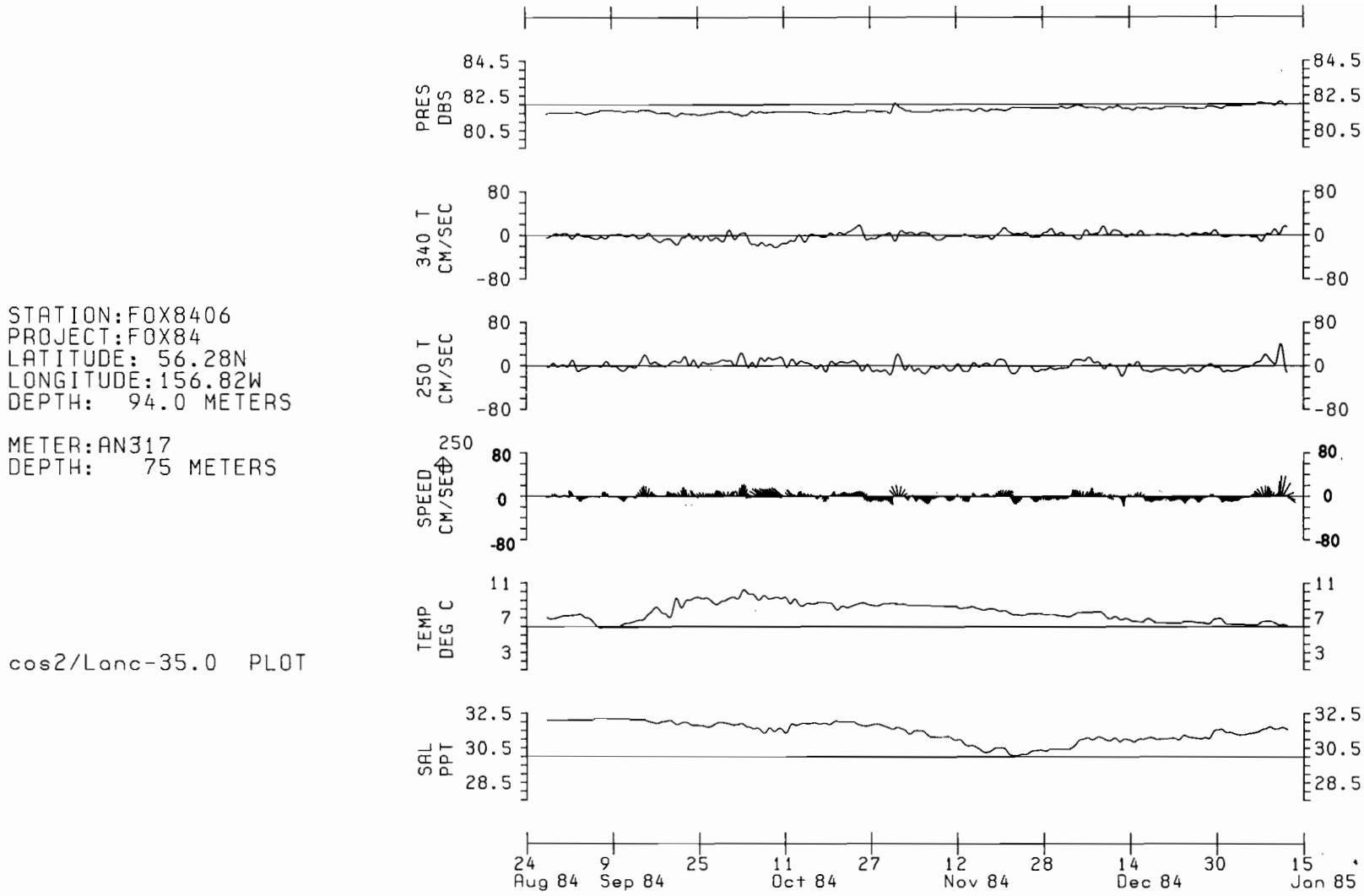

Figure 28.--Same as Figure 6, except for 6_3 at 75 meters.

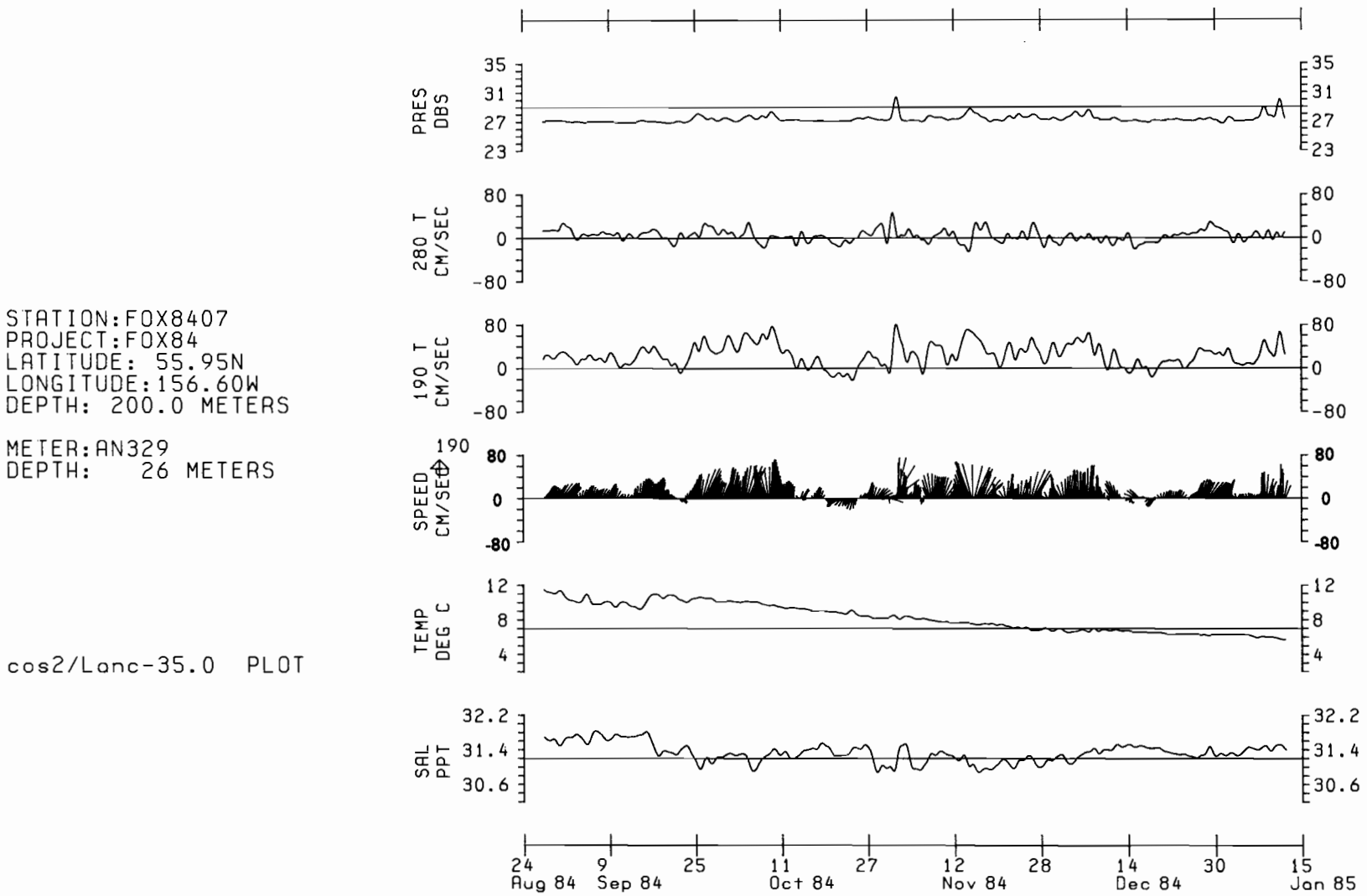

Figure 29.--Same as Figure 6, except for 7_1 at 26 meters.

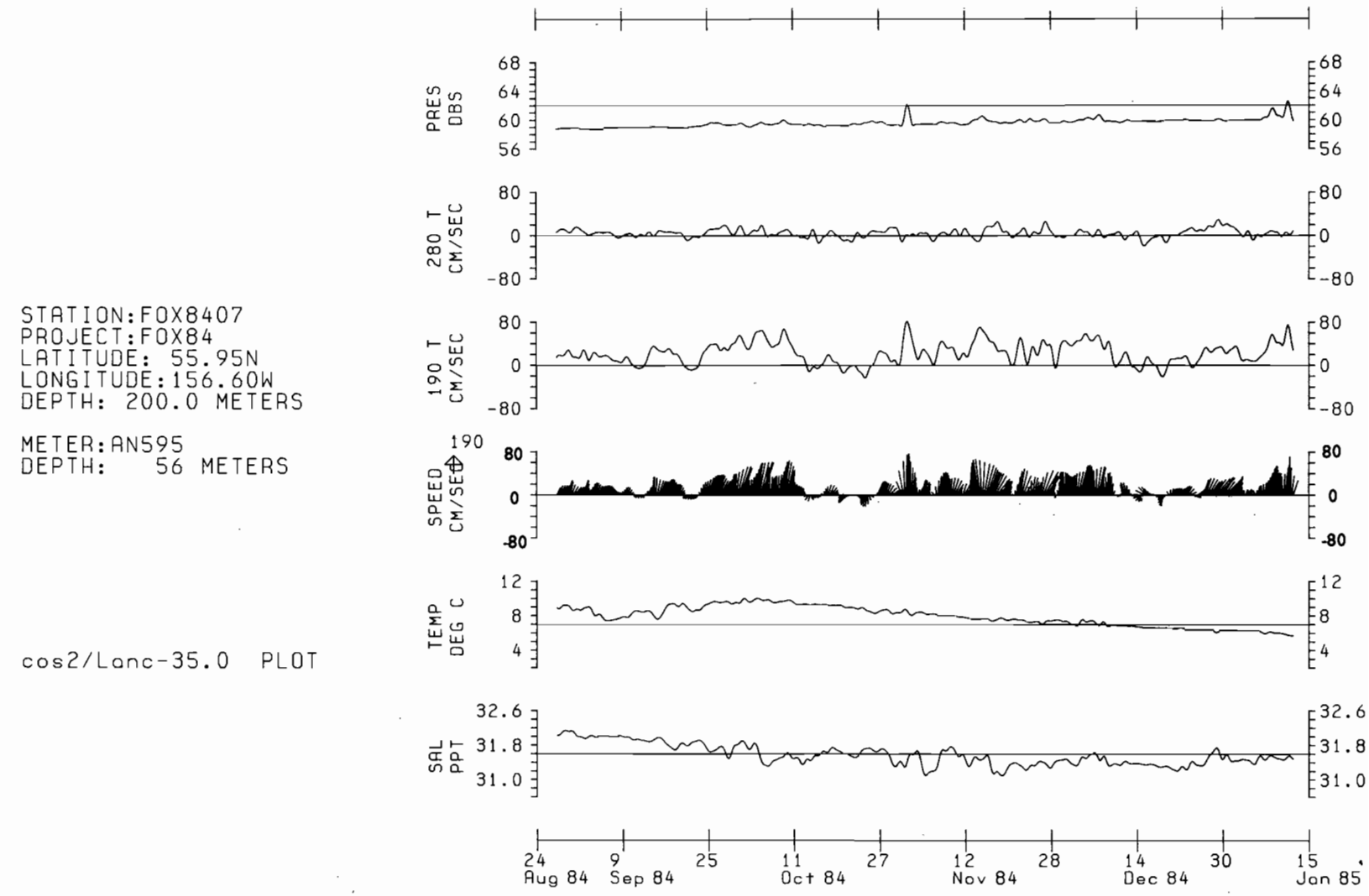

Figure 30.--Same as Figure 6, except for 7_2 at 56 meters.

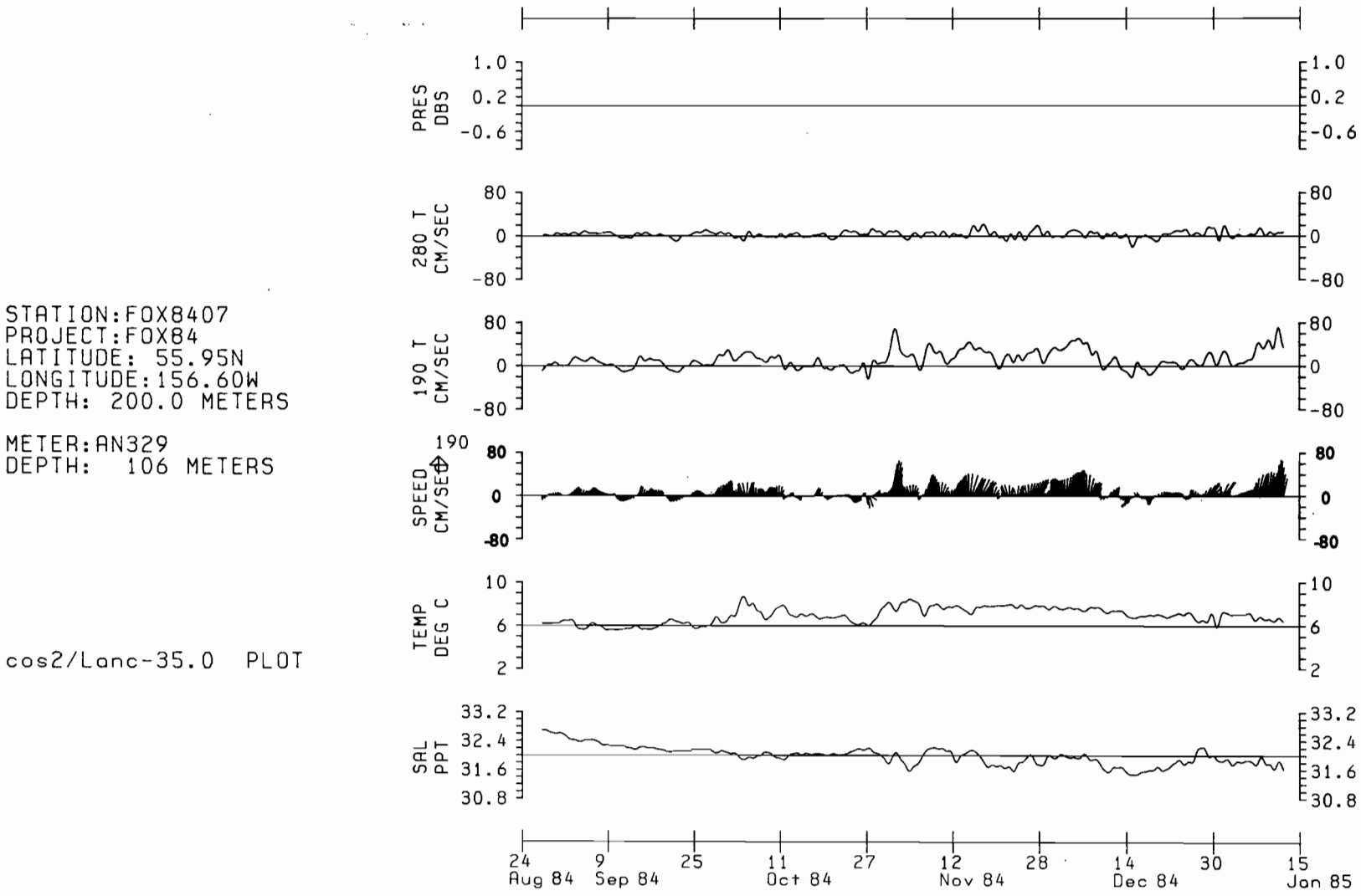

Figure 31.--Same as Figure 6, except for 7_3 at 106 meters.

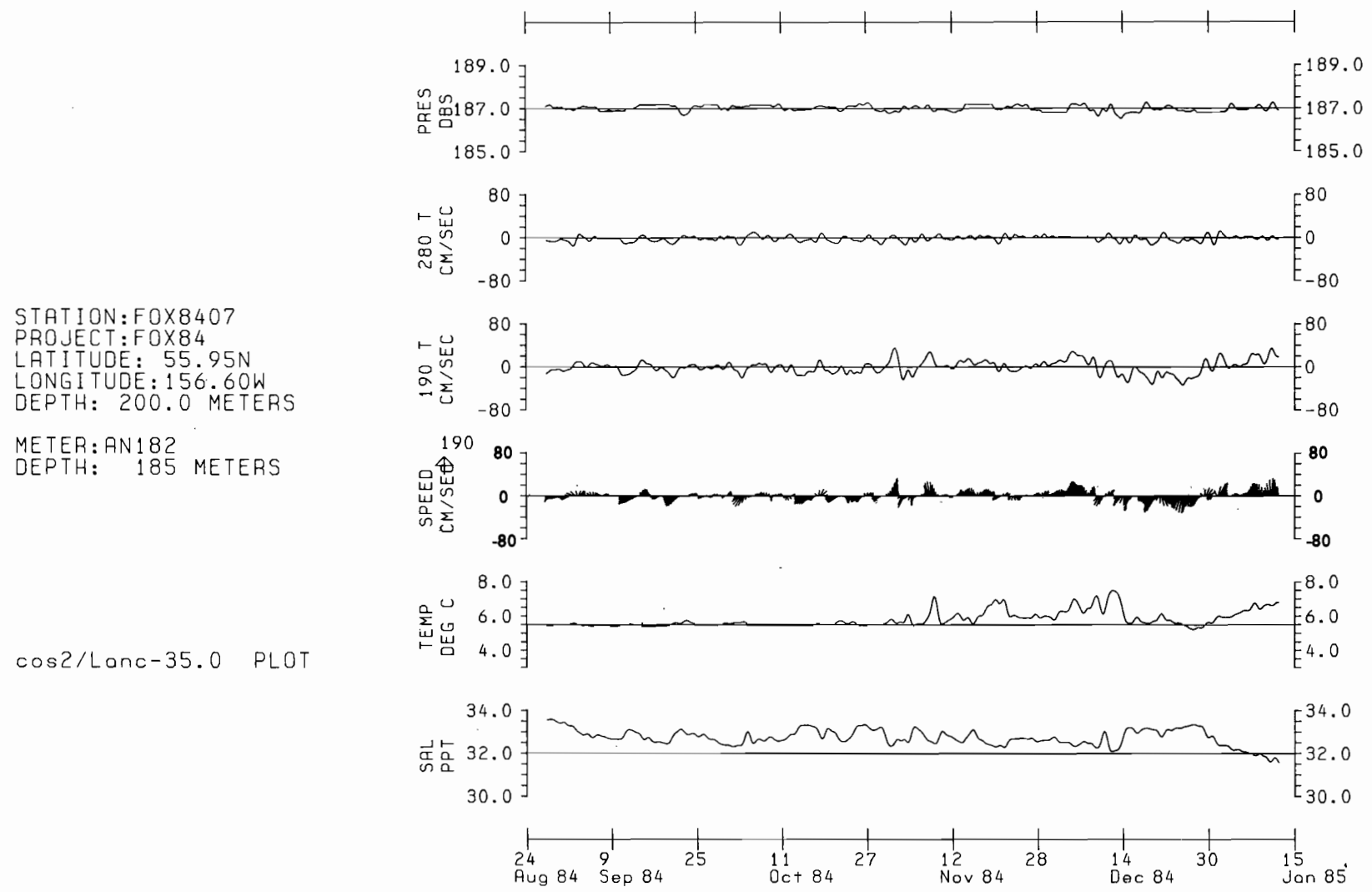

Figure 32.--Same as Figure 6, except for 7_4 at 185 meters.

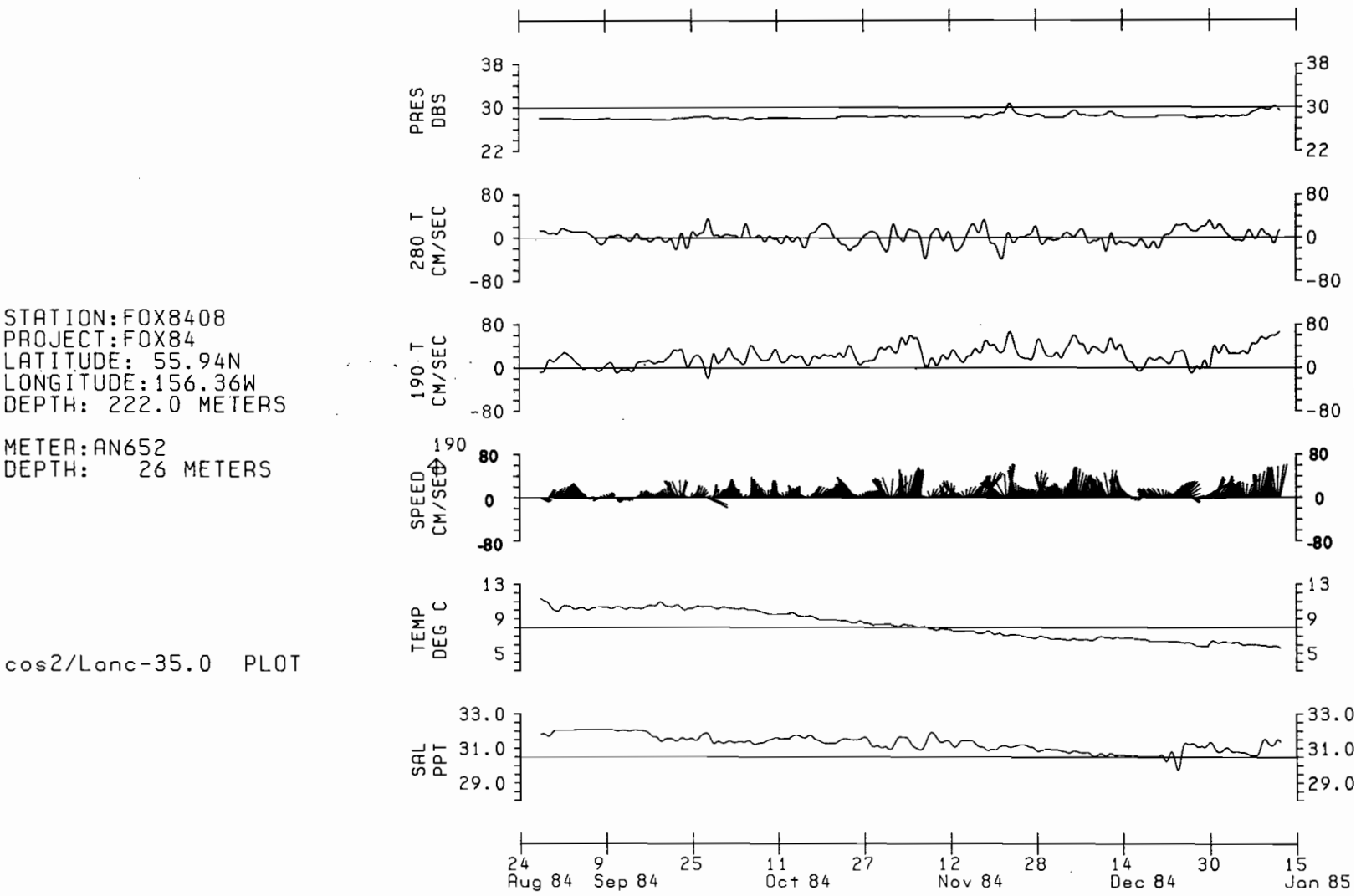

Figure 33.--Same as Figure 6, except for 8_1 at 26 meters.

STATION:FOX8408
PROJECT:FOX84
LATITUDE: 55.94N
LONGITUDE:156.36W
DEPTH: 222.0 METERS

METER:AN182
DEPTH: 56 METERS

cos2/Lanc-35.0 PLOT

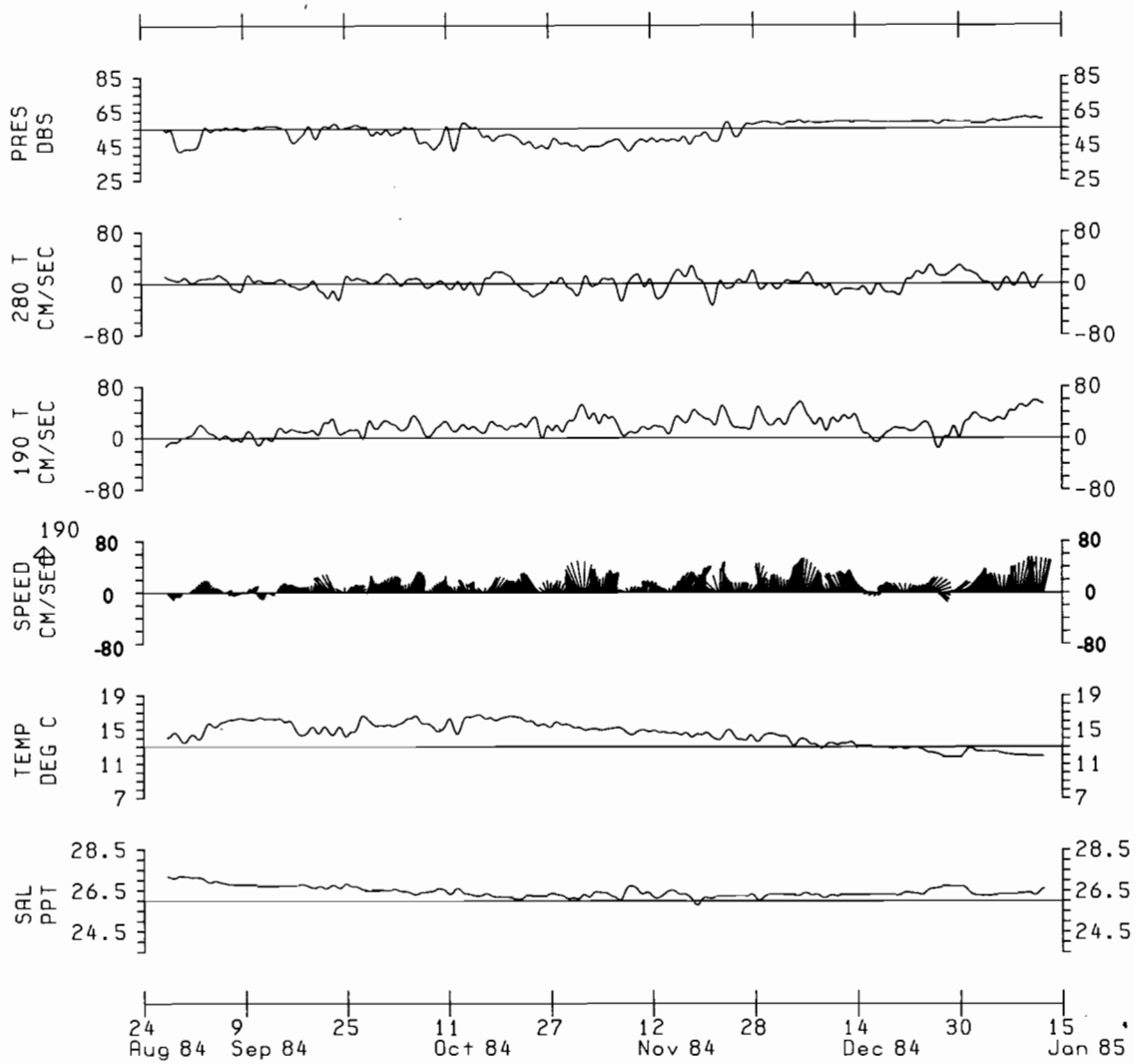

Figure 34.--Same as Figure 6, except for 8_2 at 56 meters.

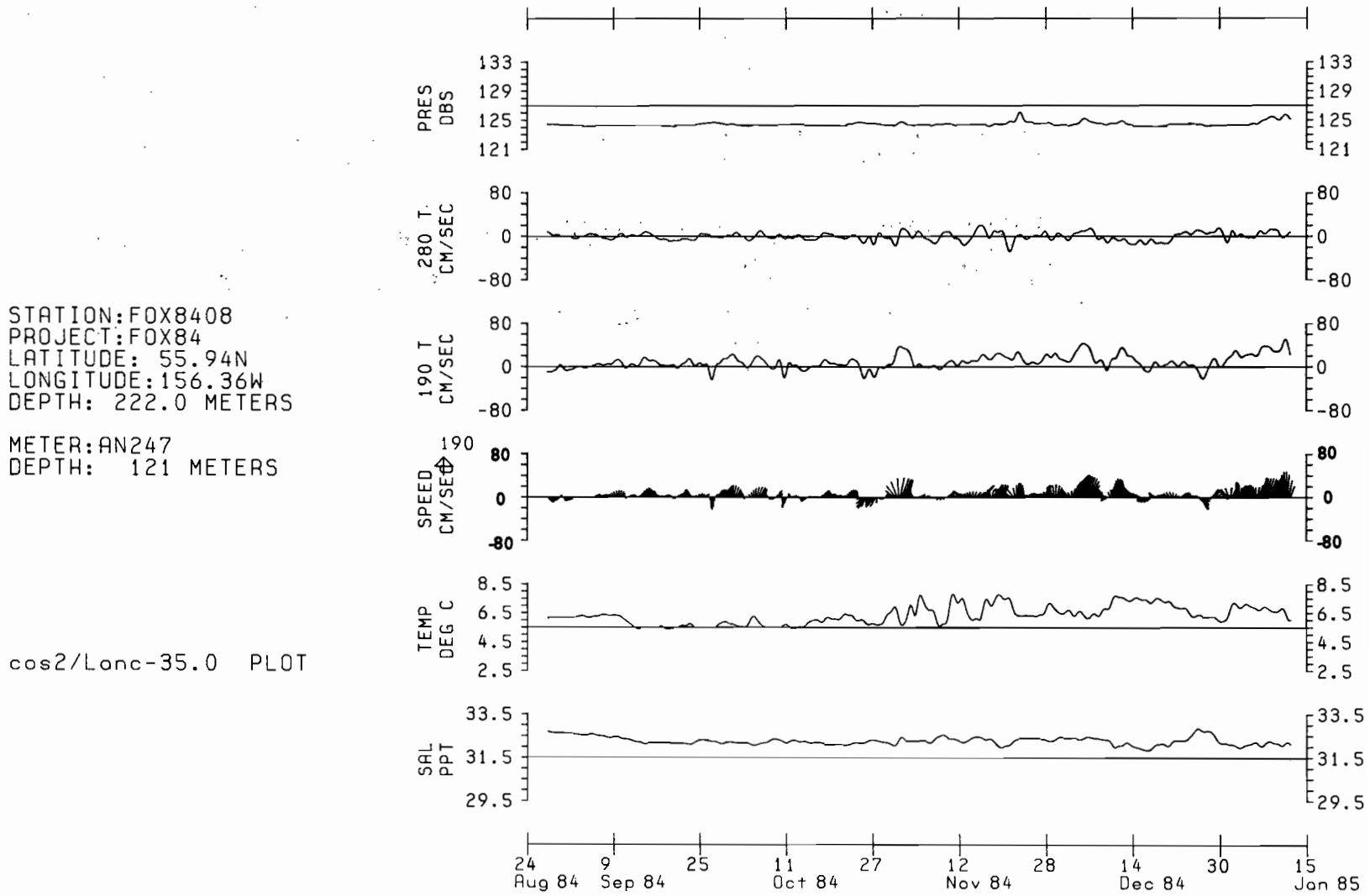

Figure 35.--Same as Figure 6, except for 8_3 at 121 meters.

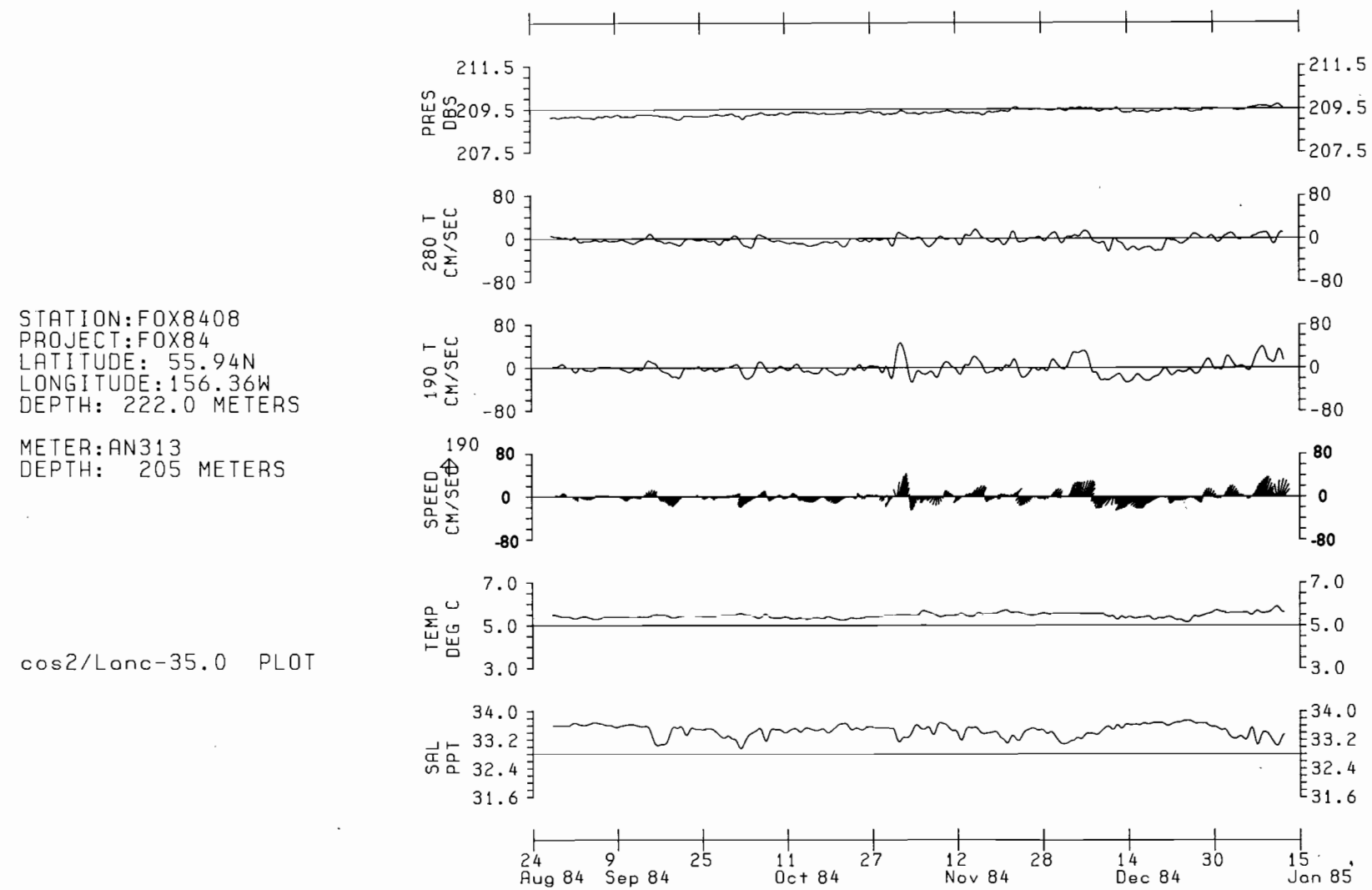

Figure 36.--Same as Figure 6, except for 8_4 at 205 meters.

STATION:FOX8409
PROJECT:FOX84
LATITUDE: 55.91N
LONGITUDE:155.15W
DEPTH: 185.0 METERS

METER:AN064
DEPTH: 26 METERS

cos2/Lanc-35.0 PLOT

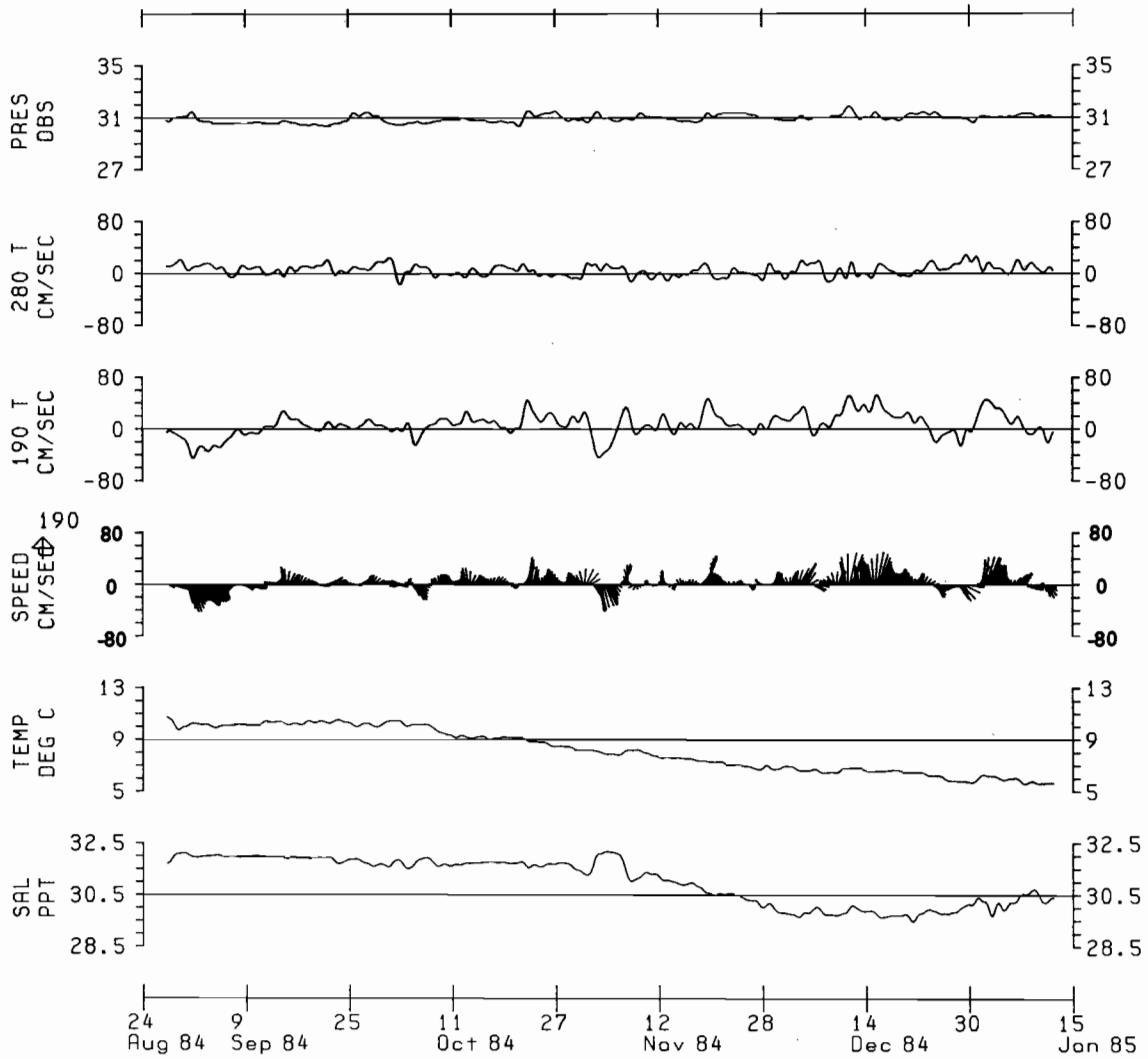

Figure 37.--Same as Figure 6, except for 9_1 at 26 meters.

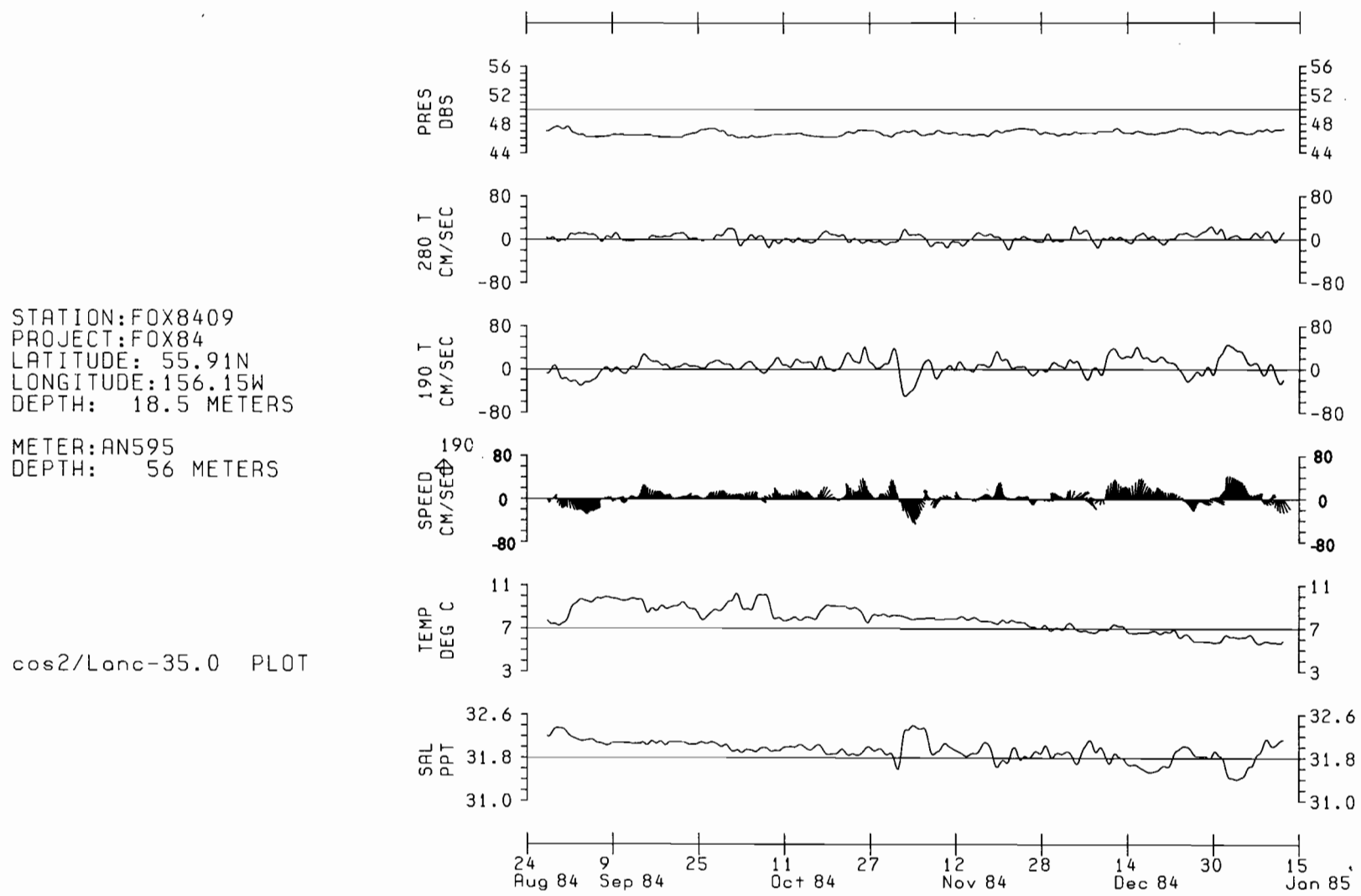

Figure 38.--Same as Figure 6, except for 9_2 at 56 meters.

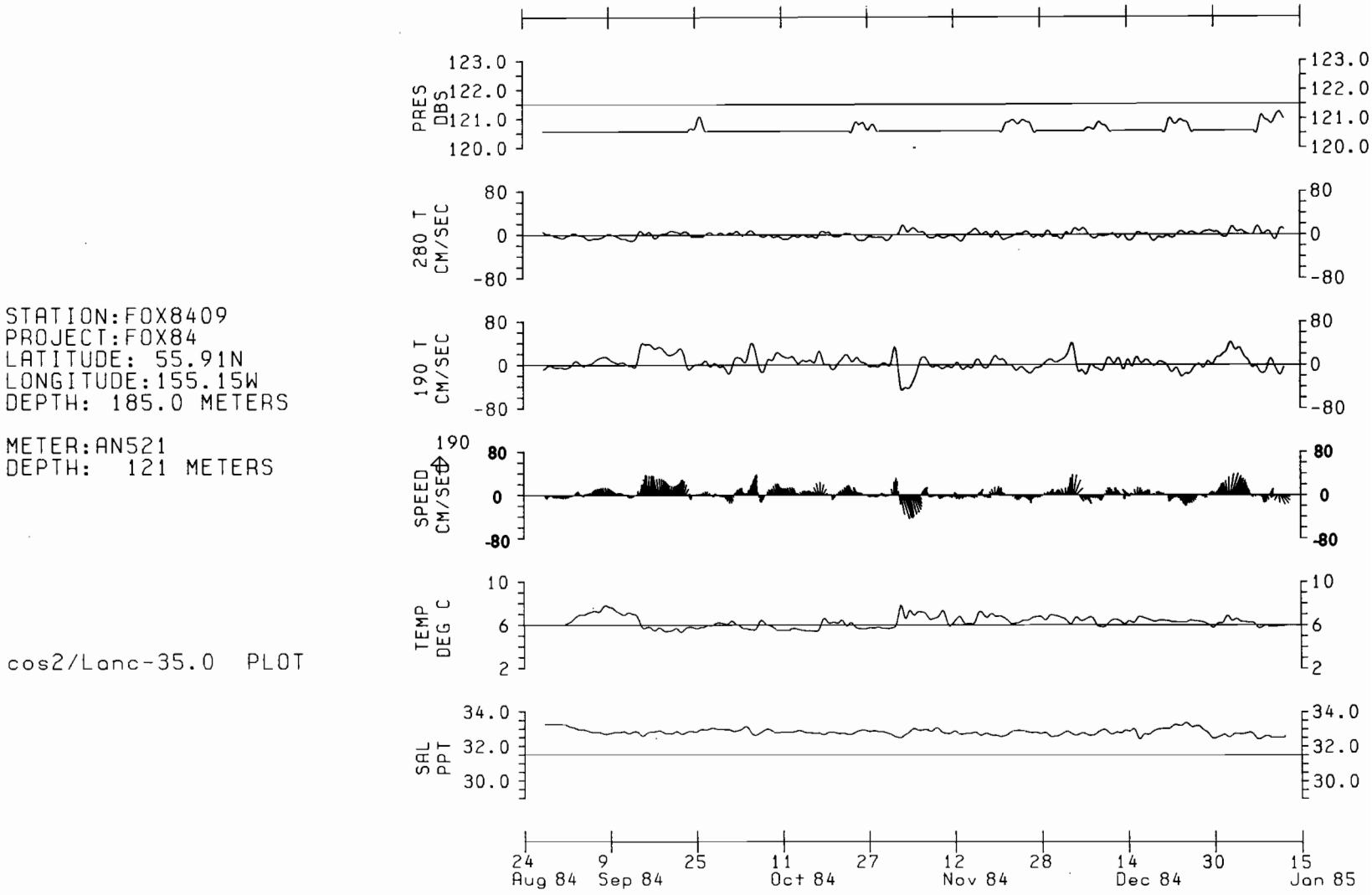

Figure 39.--Same as Figure 6, except for 9_3 at 121 meters.

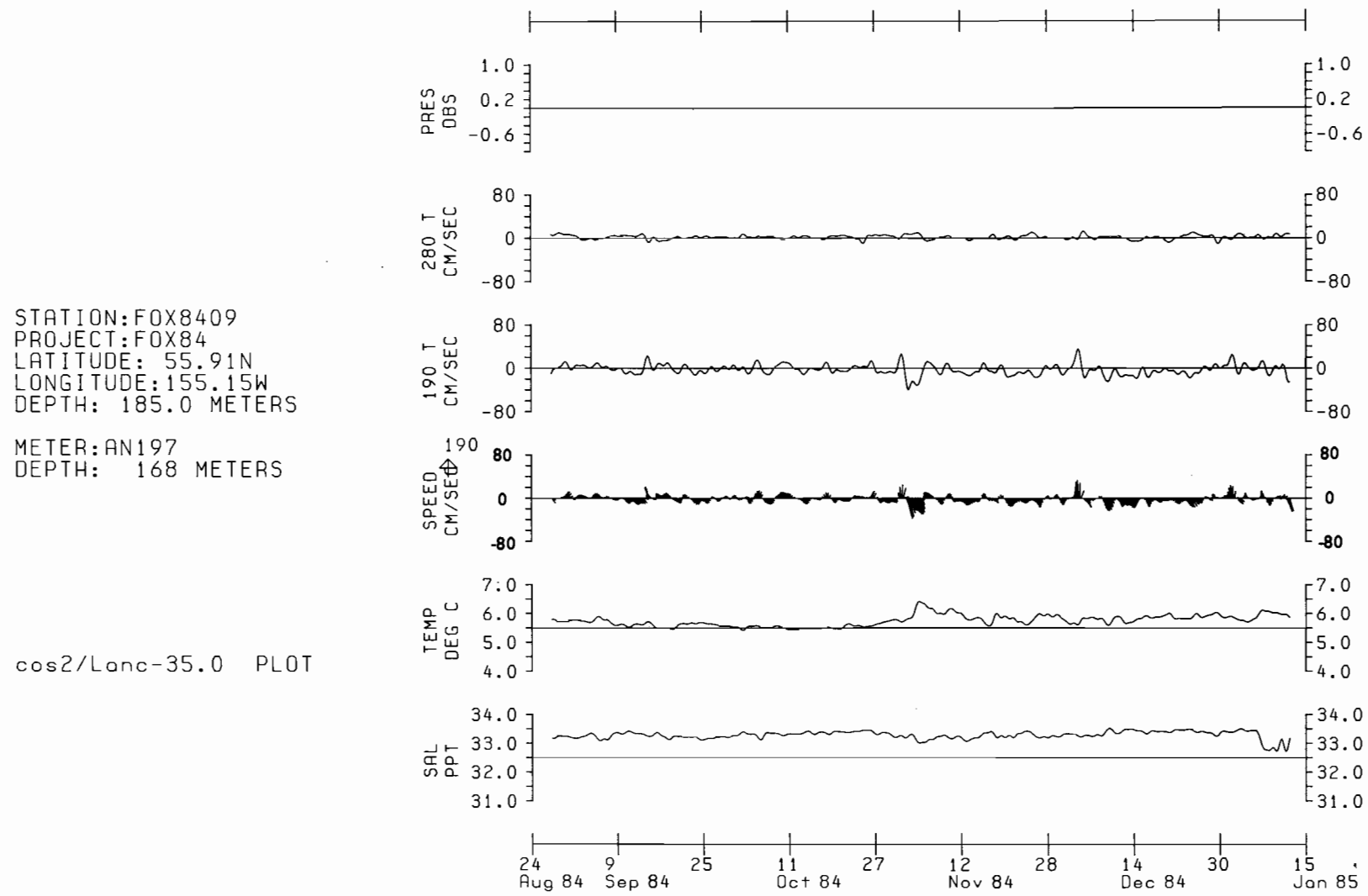

Figure 40.--Same as Figure 6, except for 9_4 at 168 meters.

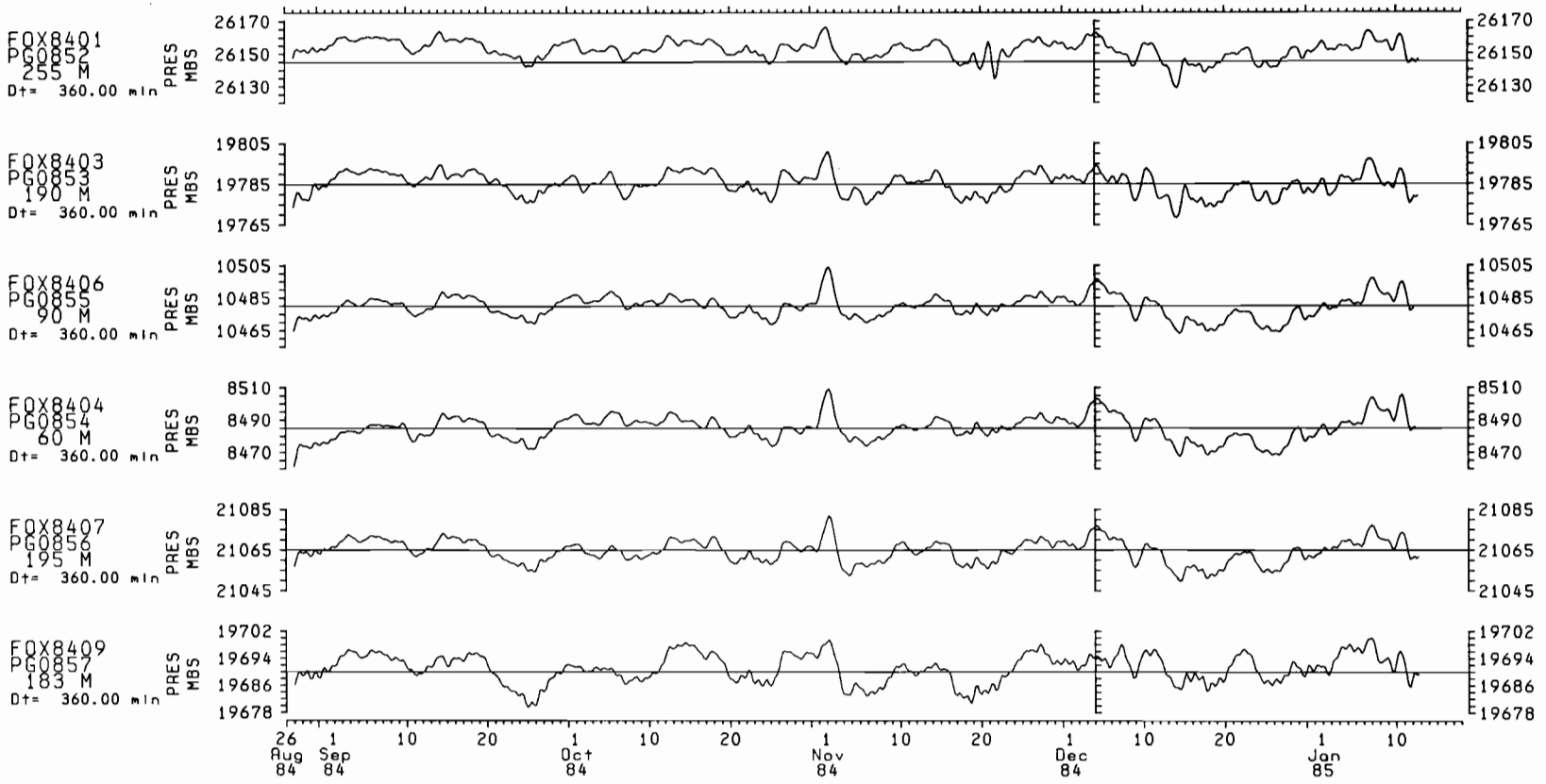

Figure 41.--Time series plot of bottom pressure gauge records. The horizontal axis is drawn at the mean value and the units are millibars.

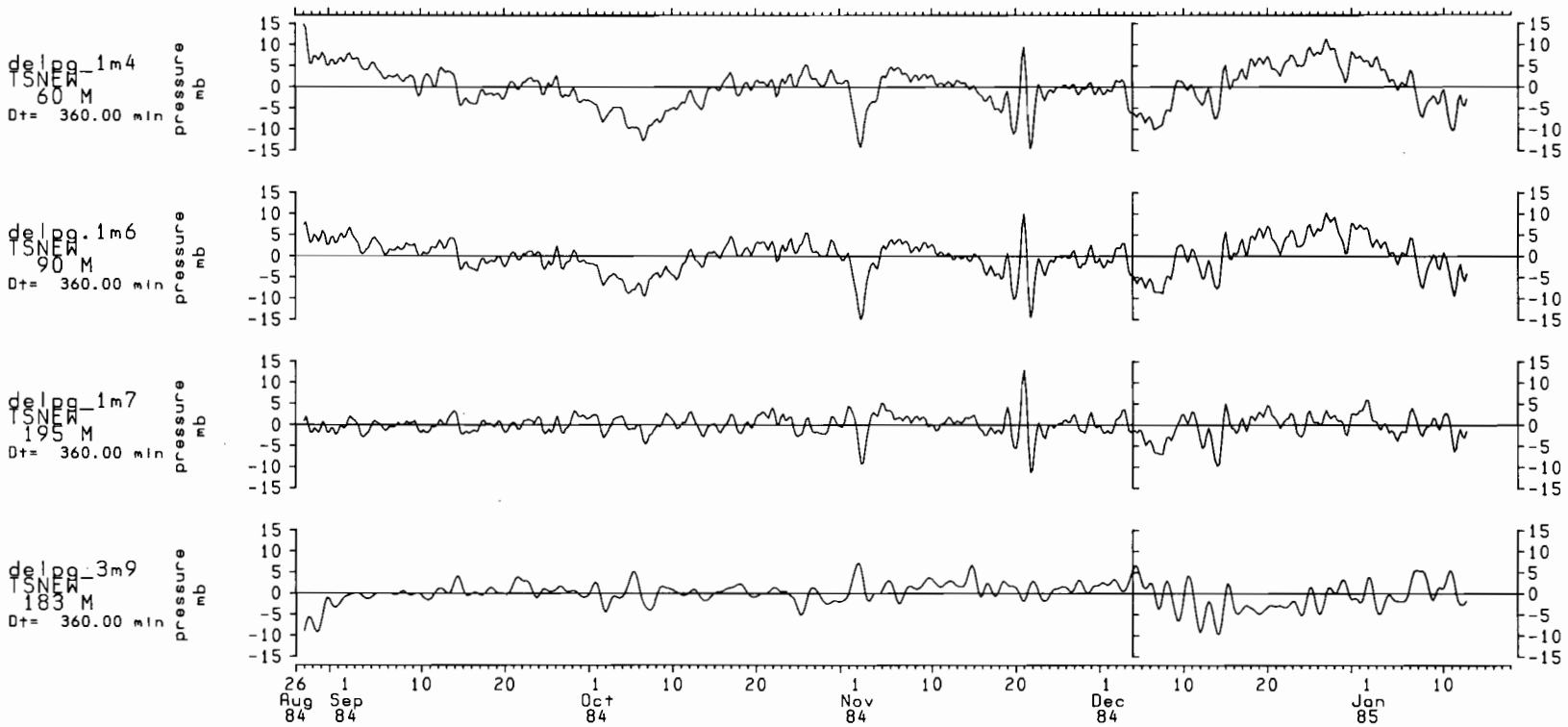

Figure 42.--Time series plots of pressure differences series generated from demeaned and detrended bottom pressure series. These four are the "downstream" differences.

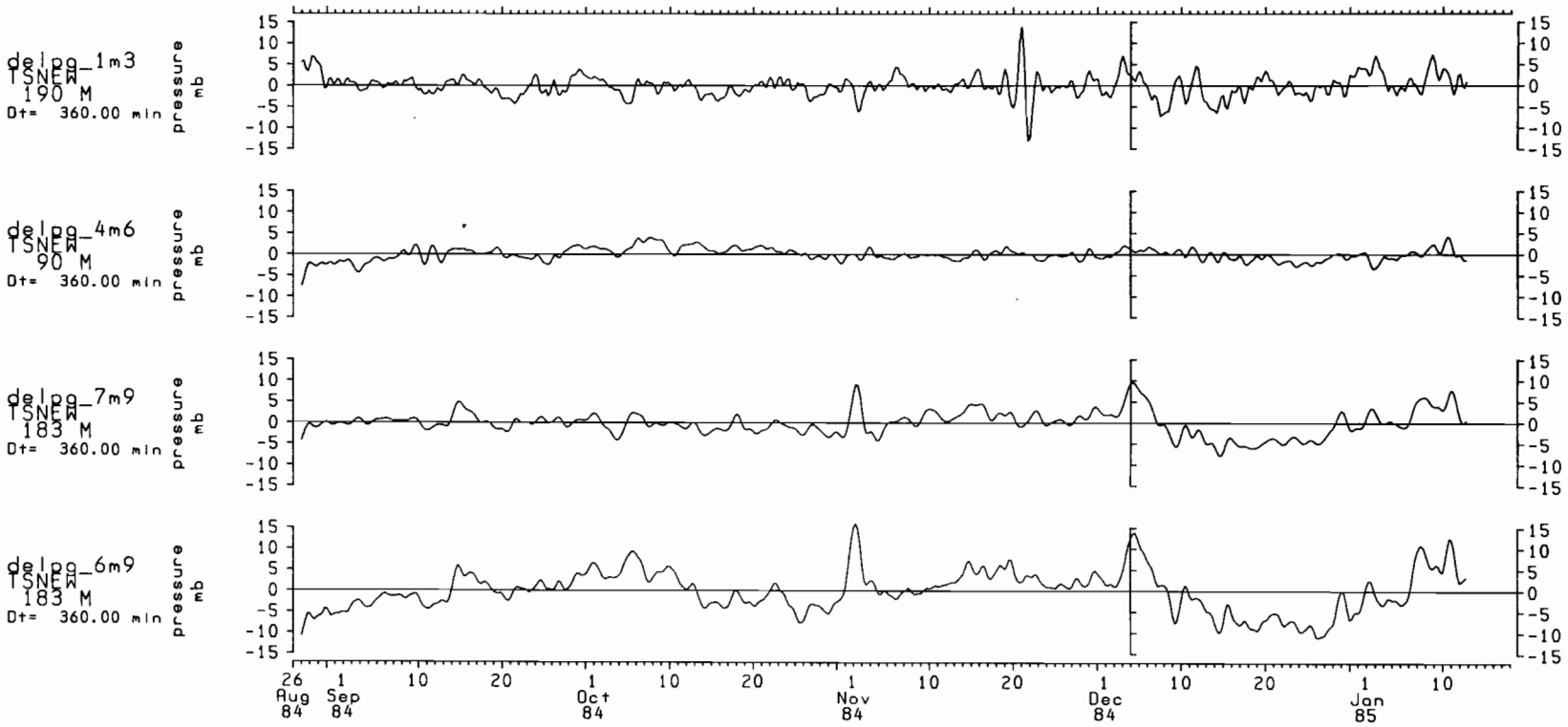

Figure 43.--Same as Figure 42 except for "cross-stream" differences.

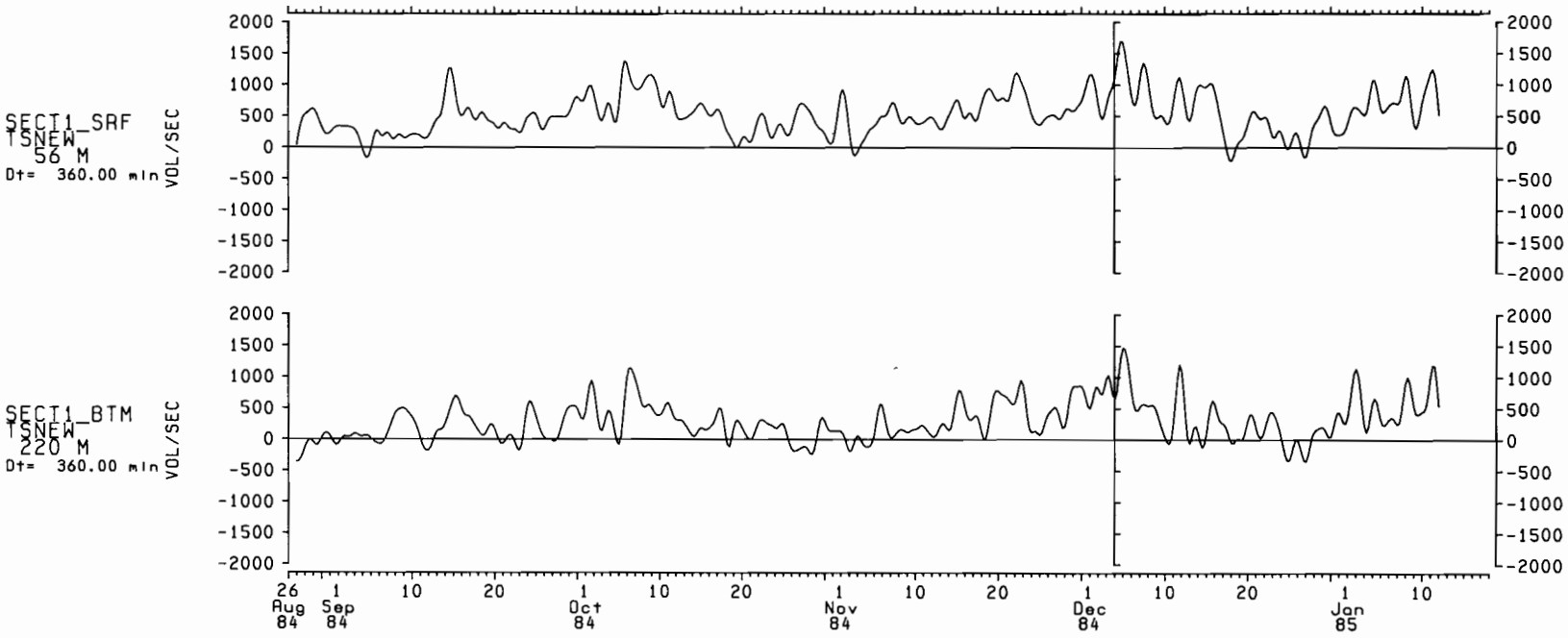

Figure 44.--Time series of integrated transport for Section #1. The surface series was constructed from low-pass filtered records at depths of 56 m and above and the bottom series is from the remaining records in a section (see Figure 2). The value units are 10^3 m^3/s.

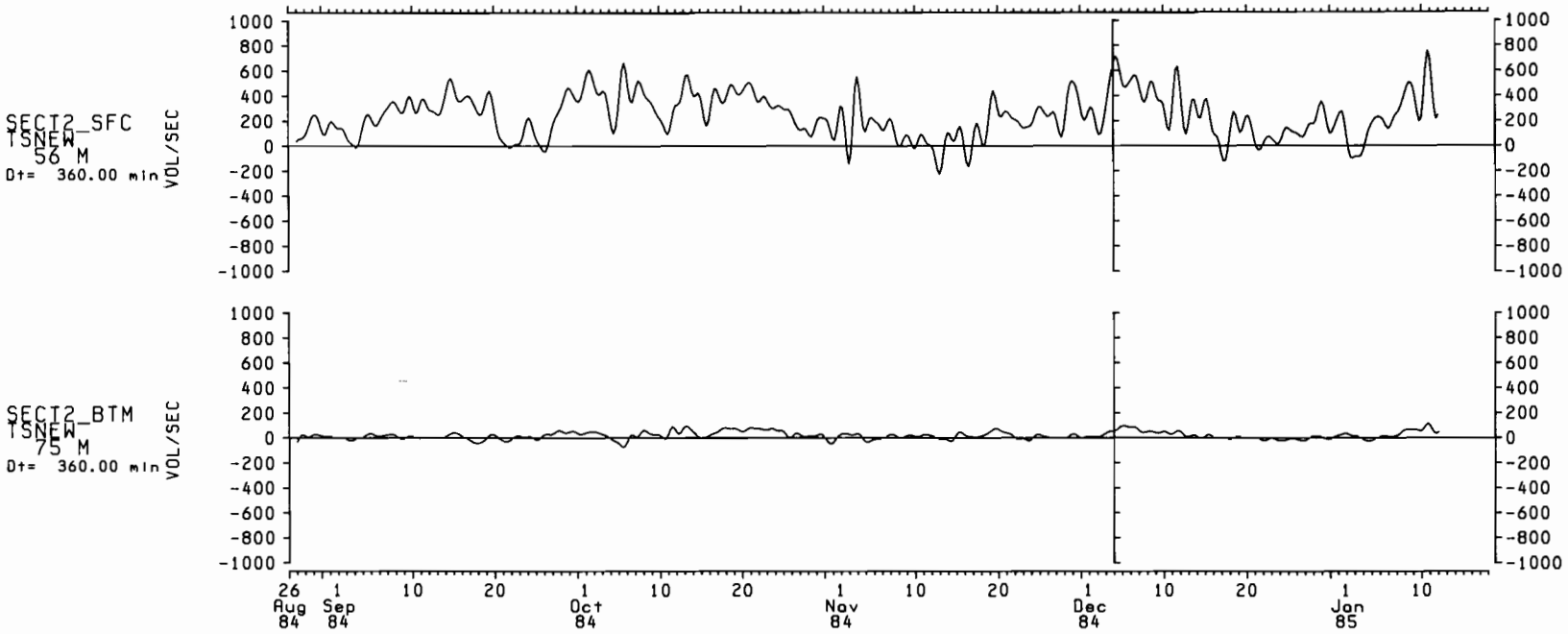

Figure 45.--Same as Figure 44A, except for Section #2.

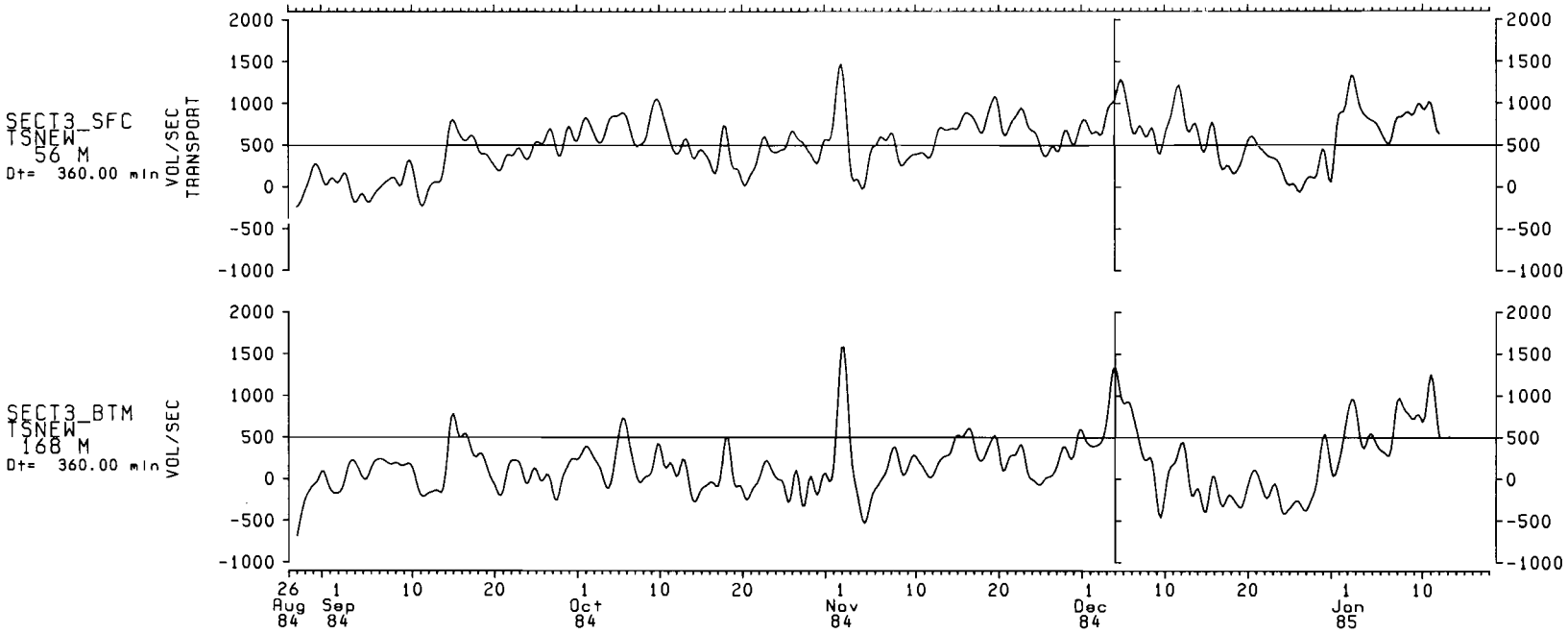

Figure 46.--Same as Figure 44A, except for Section #3.

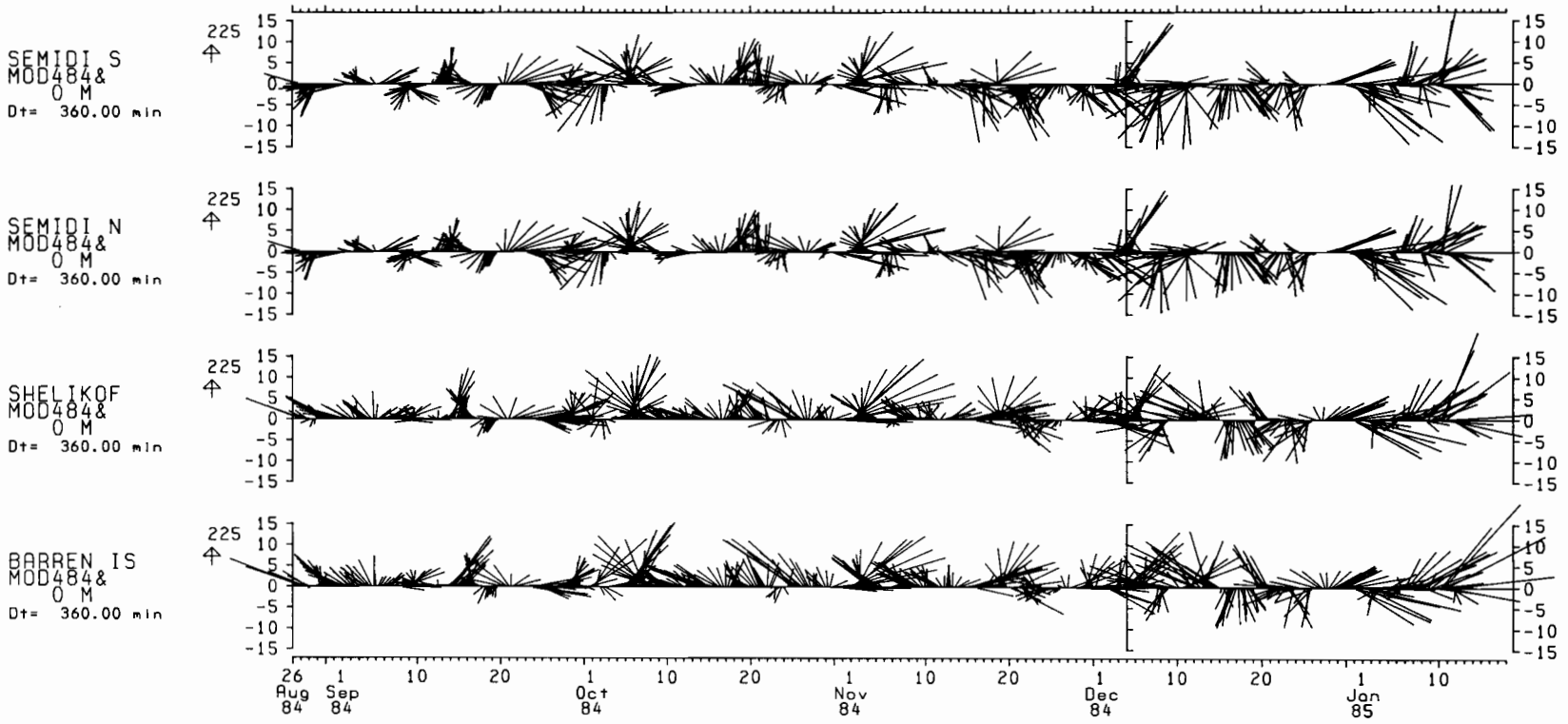

Figure 47.--Stick vector plots of the geostrophic wind series generated from surface atmospheric pressure analyses. The vertical axis is directed along the Alaska Peninsula at 225 T (oceanographic directional convention) and the vertical scale is in meters/second.

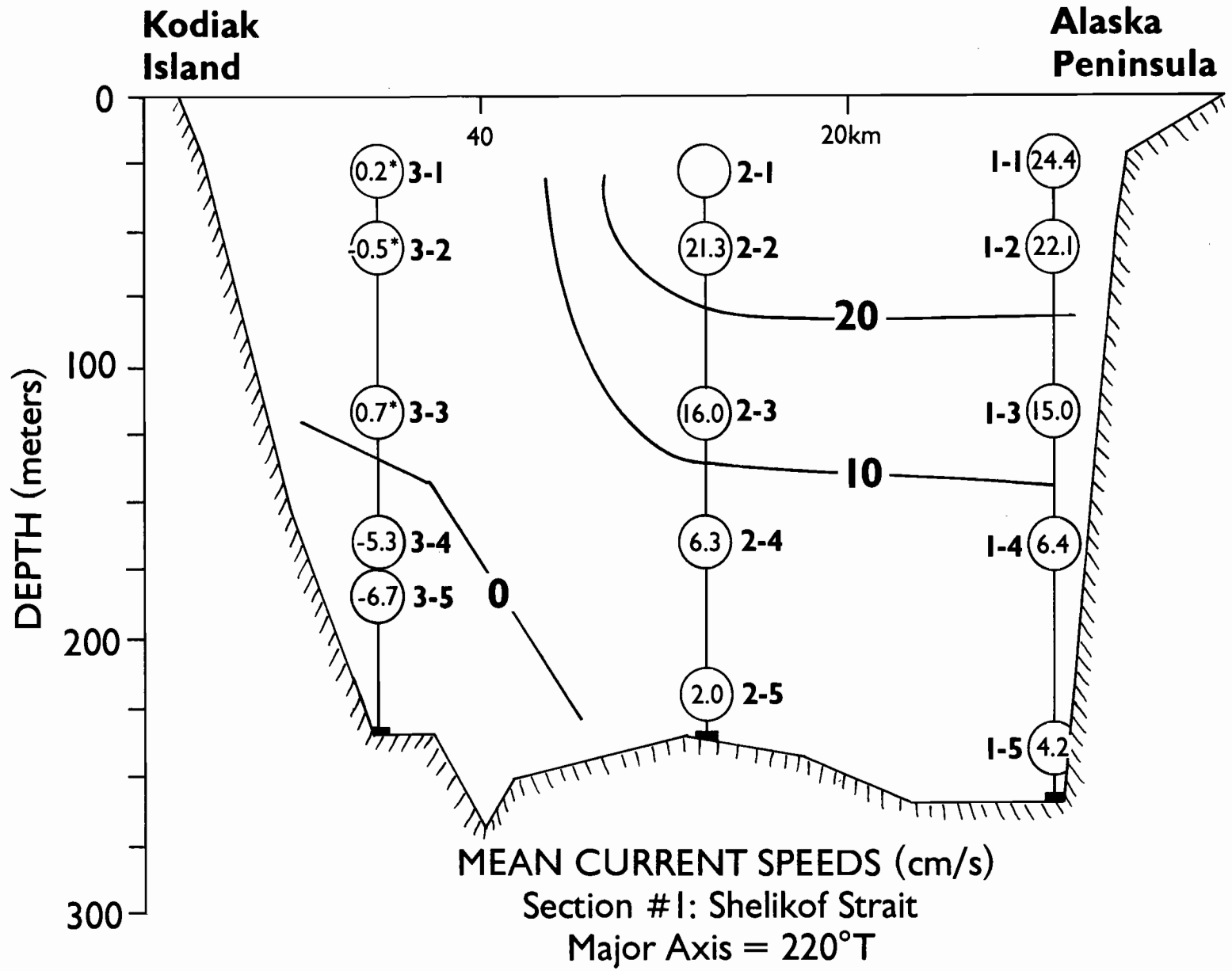

Figure 48.--Mean current speeds plotted on a cross-sectional plot of the instruments for Section #1. The speeds are in cm/s and directed along the major axis as noted on the figure. An asterisk indicates the reported value does not exceed the RMS error for that location.

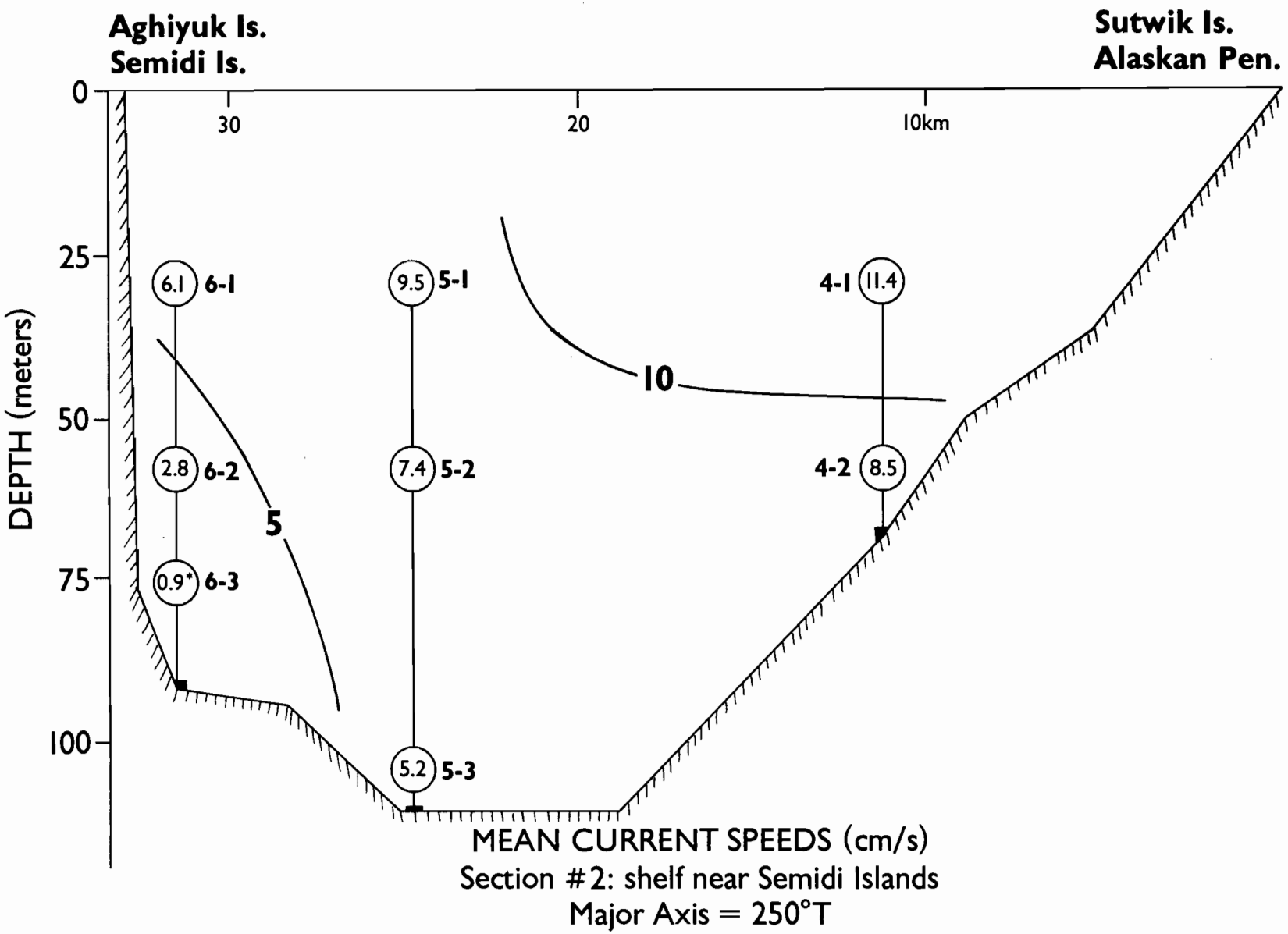

Figure 49.--Same as Figure 48, except for Section #2.

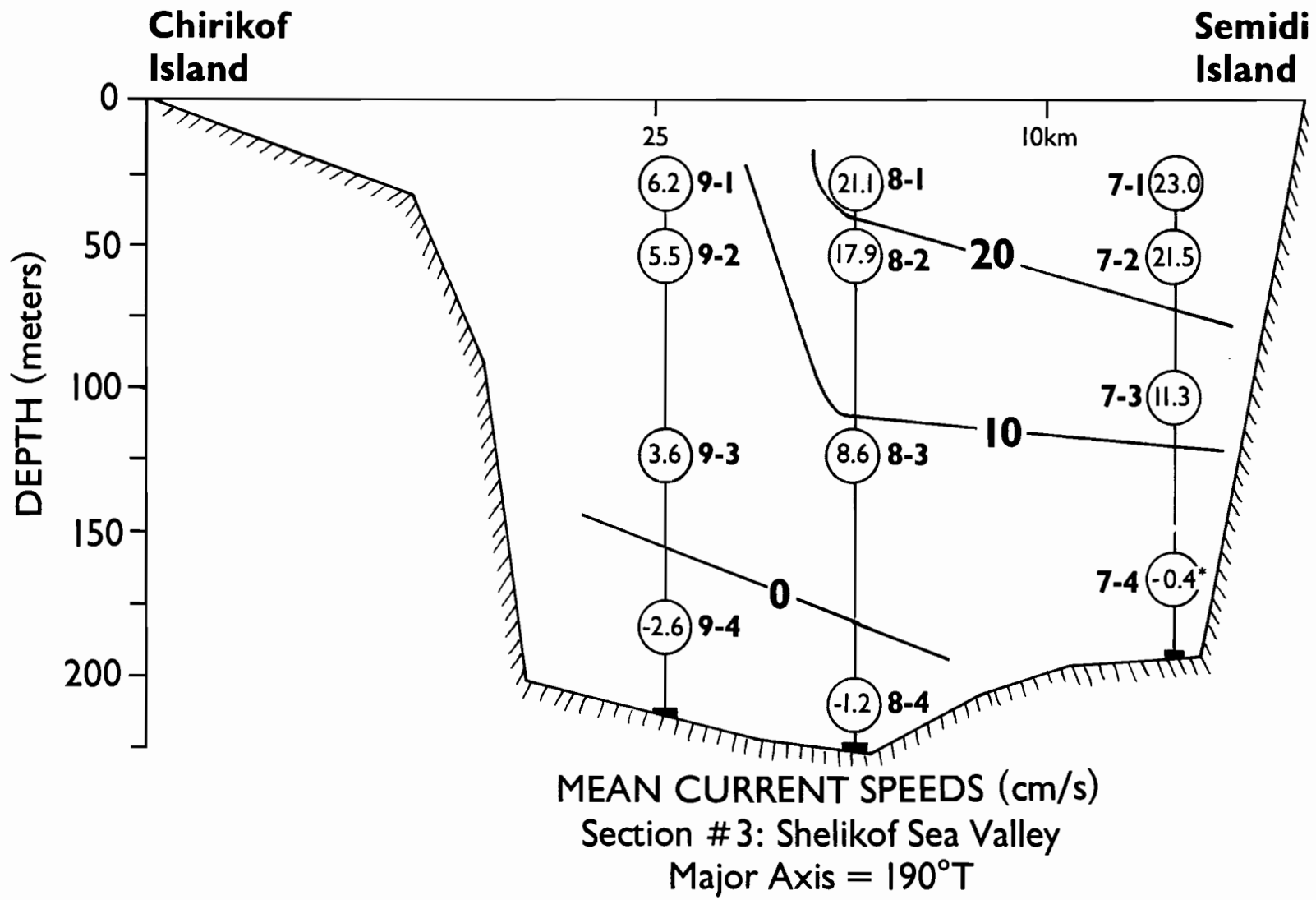

Figure 50.--Same as Figure 48, except for Section #3.

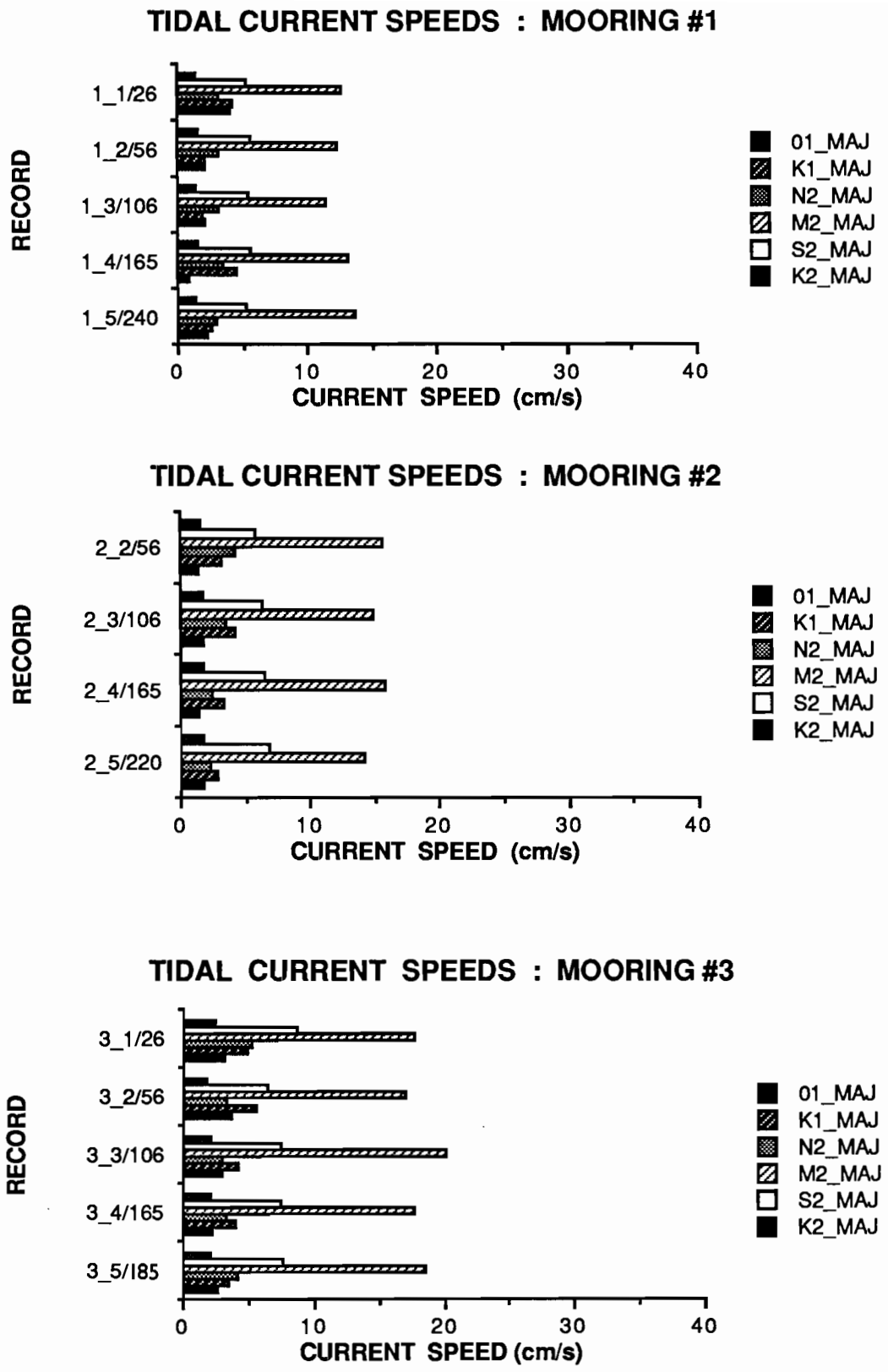

Figure 51.--Tidal current speeds generated from succesive 29-day harmonic analysis for transport section #1.

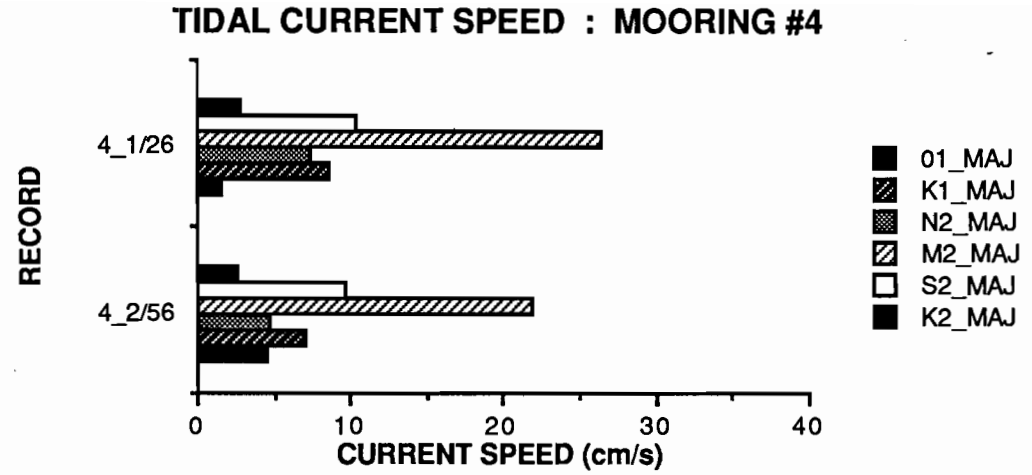

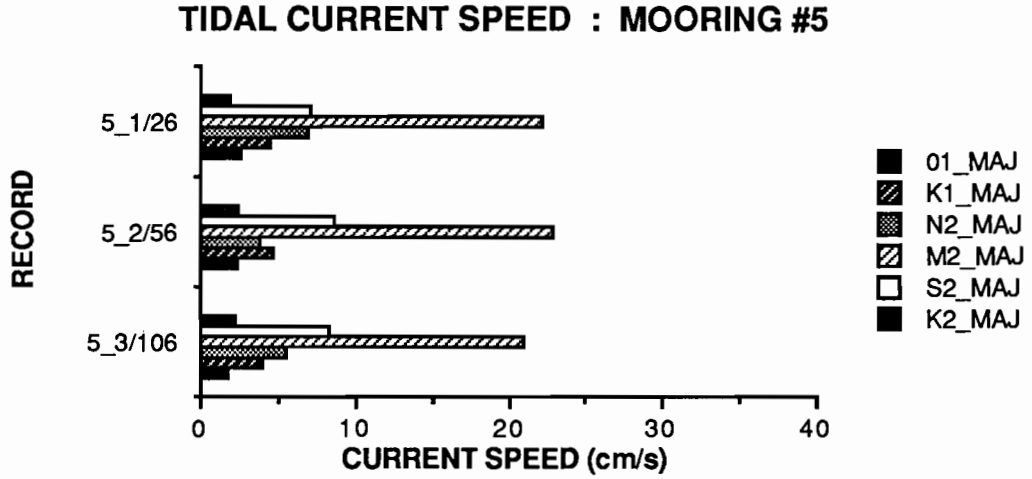

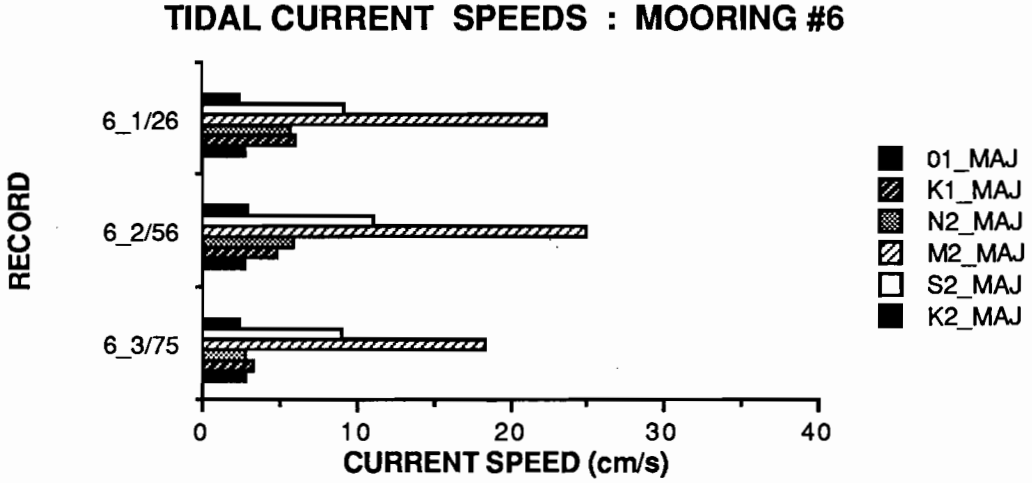

Figure 52.--Same as Figure 51, except for transport section #2.

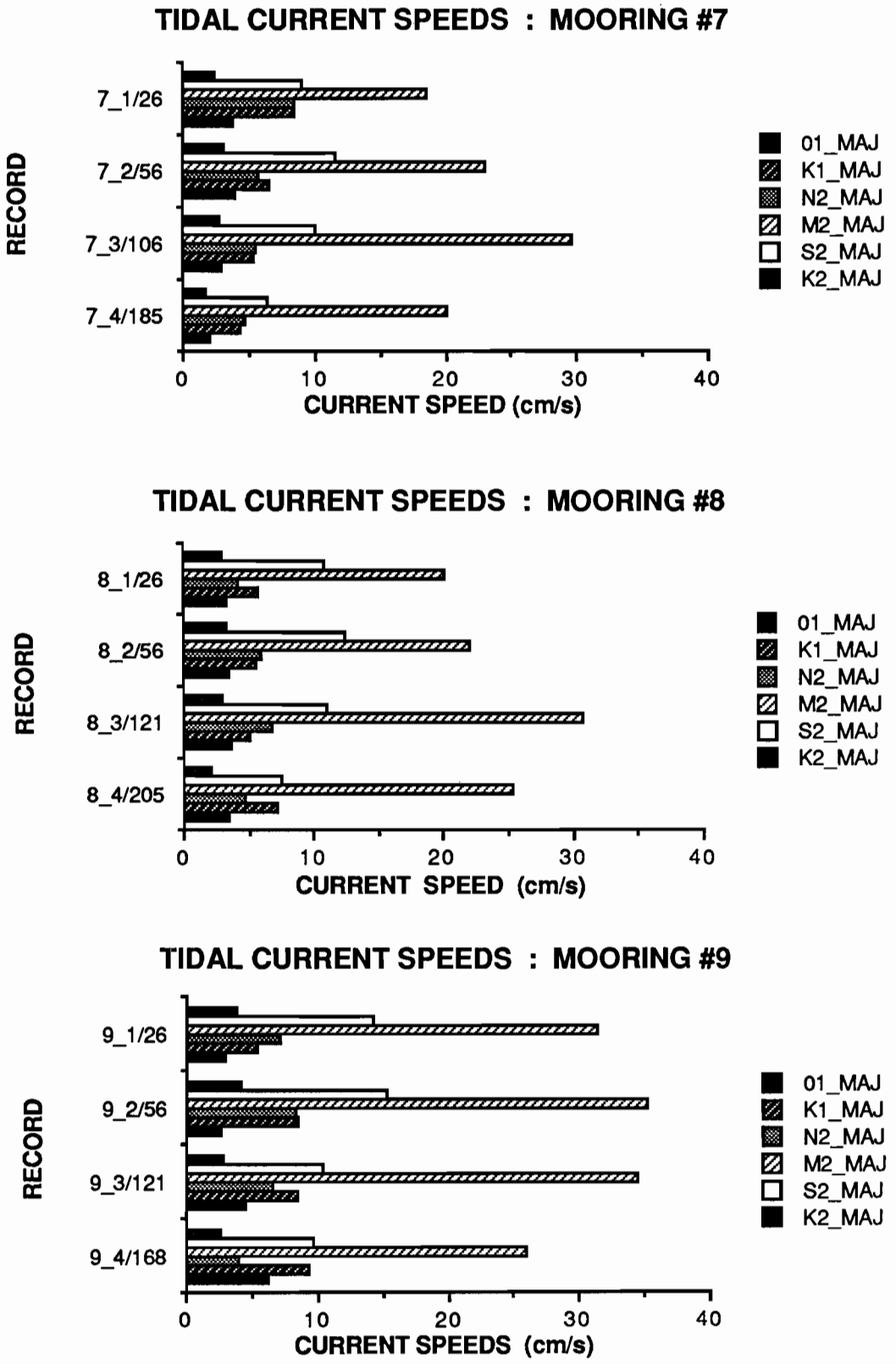

Figure 53.--Same as Figure 51, except for transport section #3.

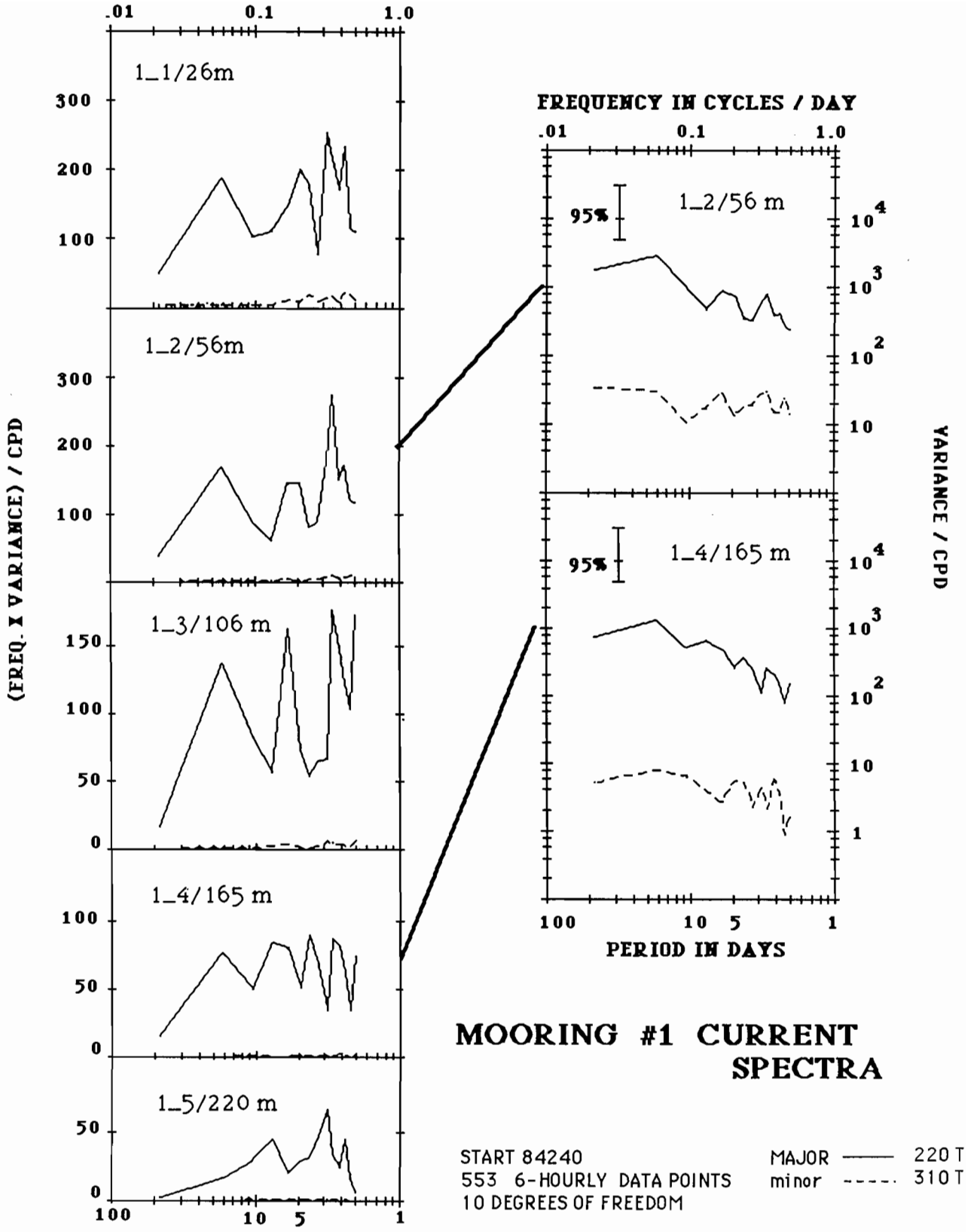

Figure 54.--Spectra of the current meter records for Mooring #1 in both the variance preserving format (to the left) and the spectral density function. All series start on JD 240 in 1984 (25 August) and have 10 degrees of freedom. The solid line represents the major axis component and the dashed line represents the orthogonal minor axis.

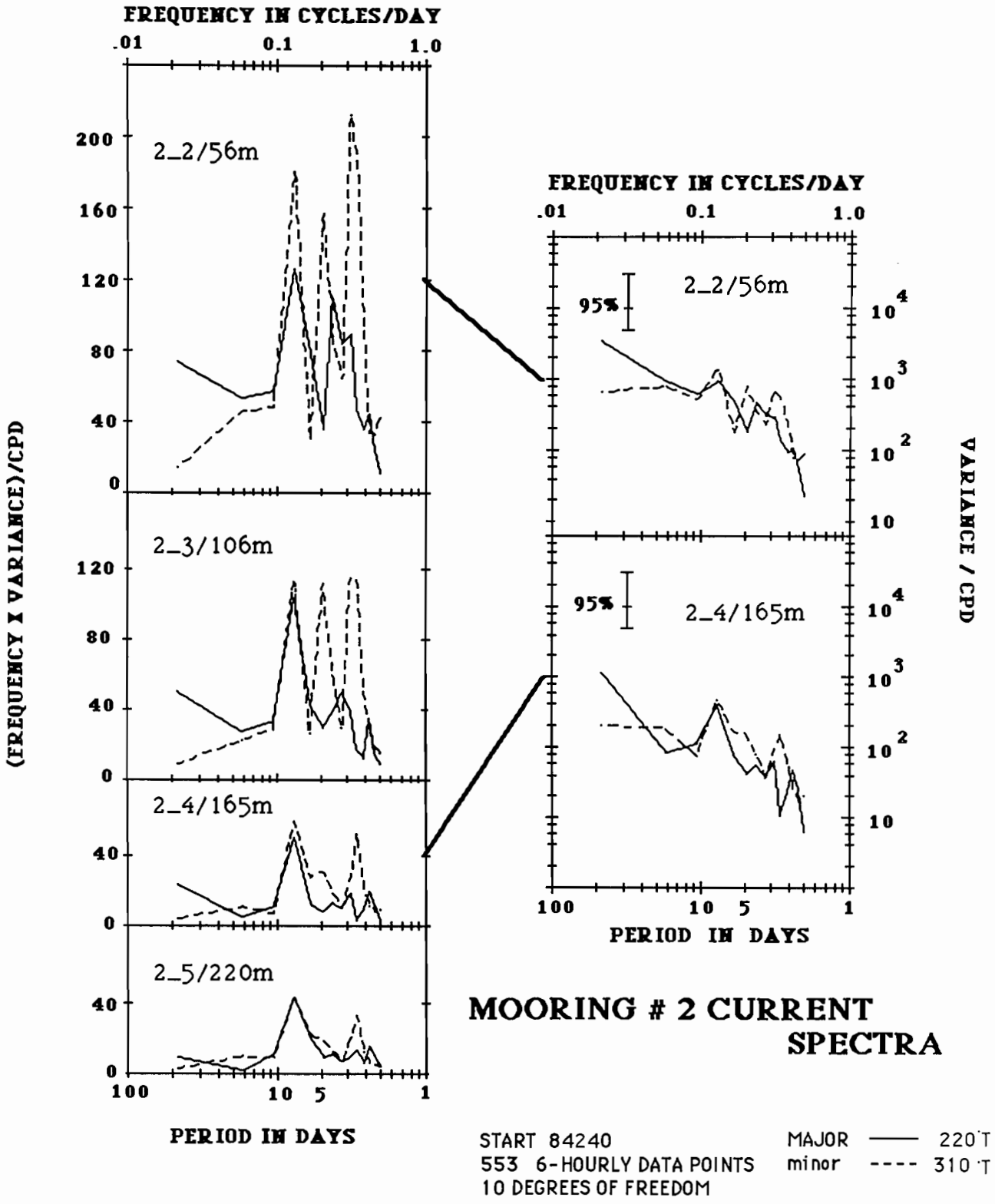

Figure 55.--Same as Figure 54, except for Mooring #2.

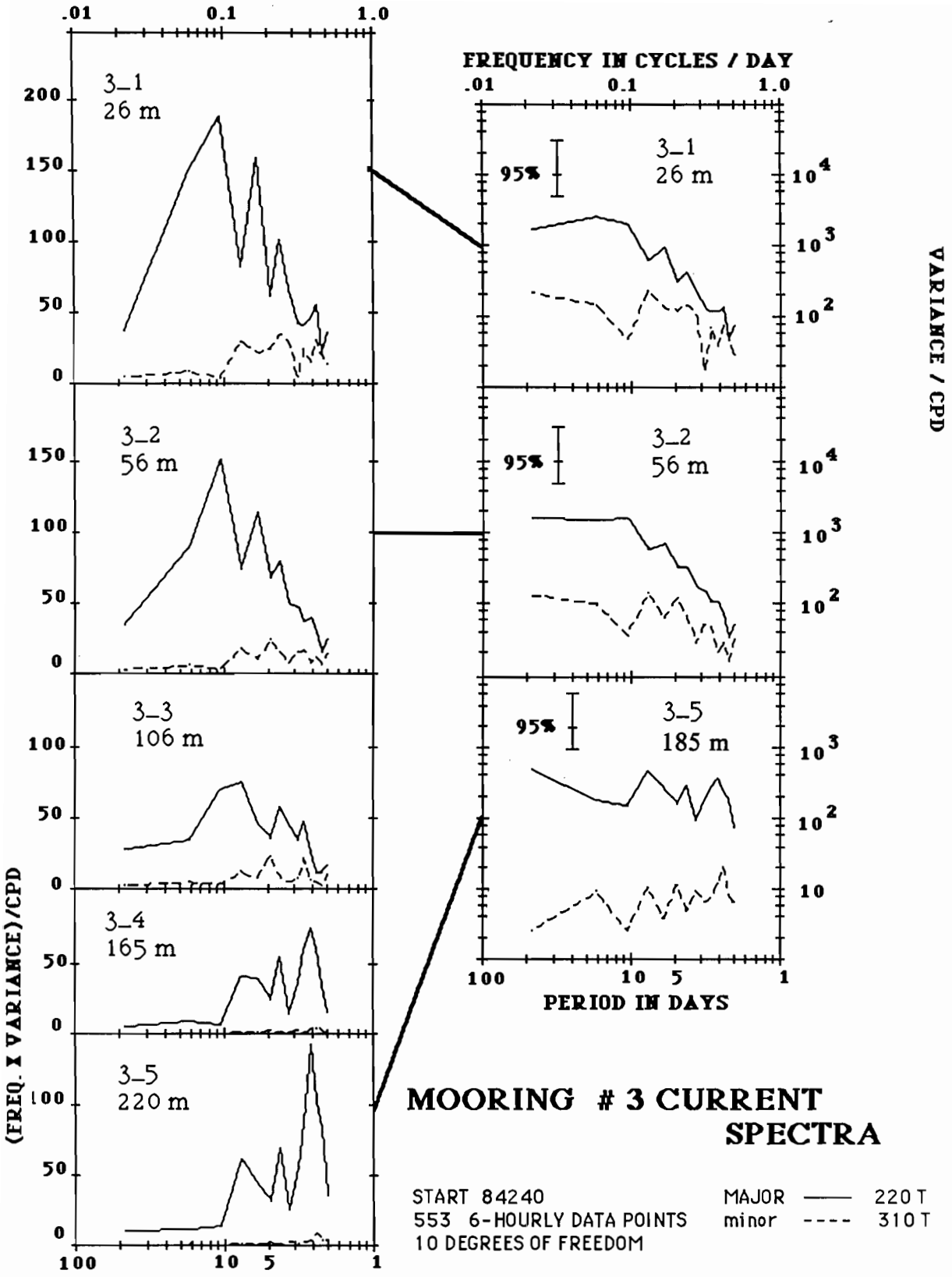

Figure 56.--Same as Figure 54, except for Mooring #3.

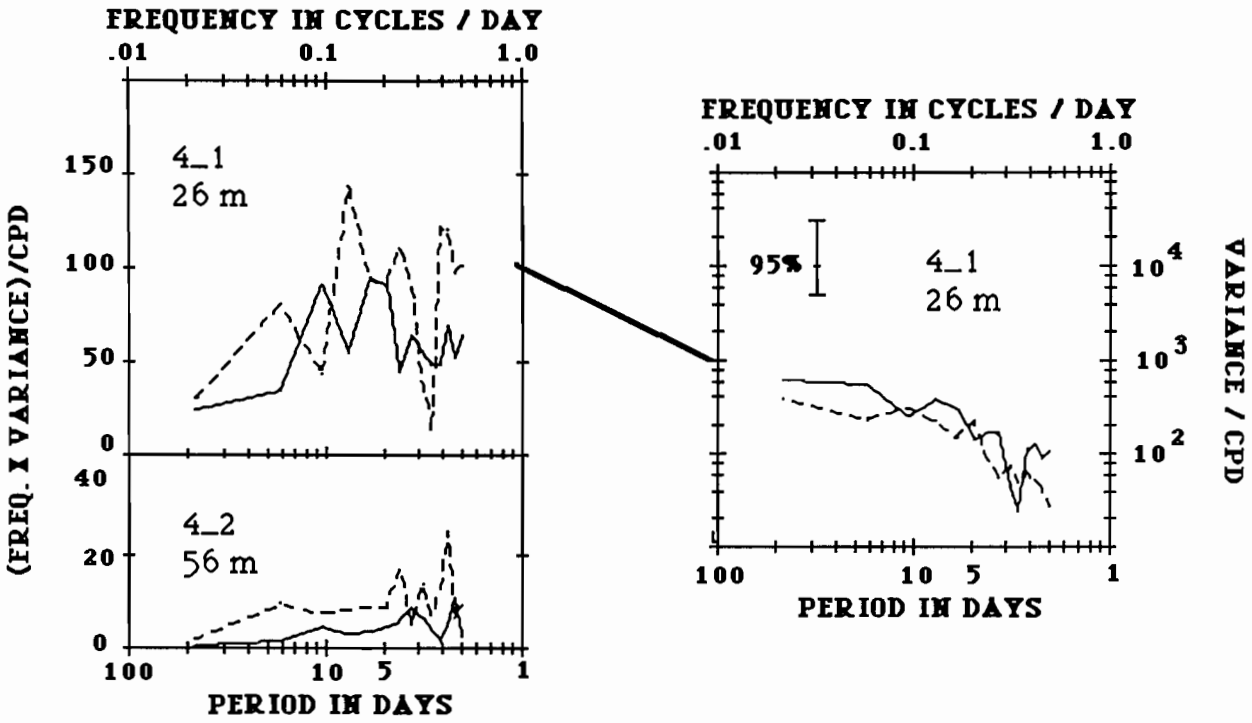

MOORING # 4 CURRENT SPECTRA

START 84240
553 6-HOURLY DATA POINTS
10 DEGREES OF FREEDOM

MAJOR —— 250 T
minor ---- 340 T

Figure 57.--Same as Figure 54, except for Mooring #4.

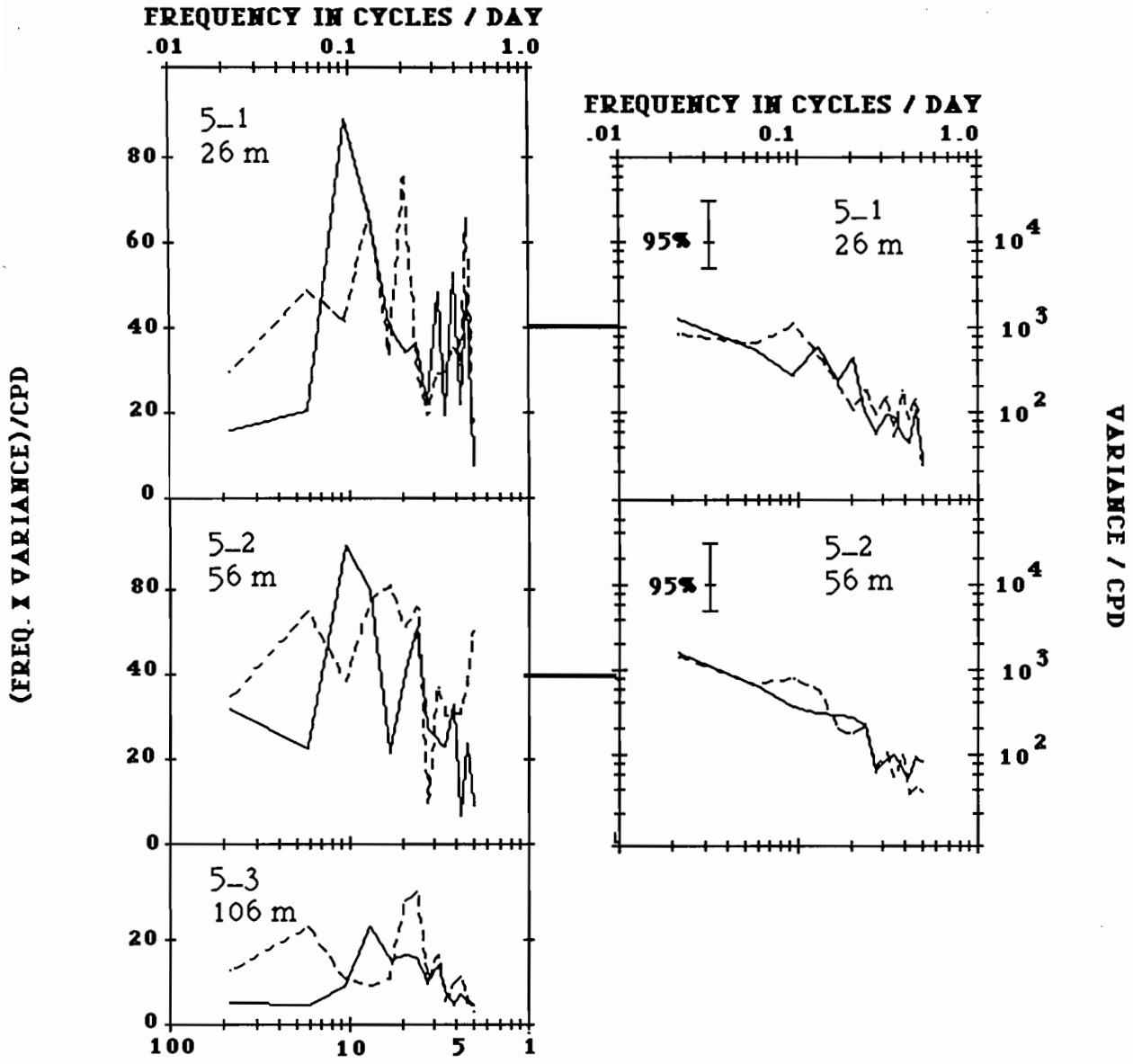

MOORING # 5 CURRENT SPECTRA

START 84240
553 6-HOURLY DATA POINTS
10 DEGREES OF FREEDOM

MAJOR —— 250 T
minor ---- 340 T

Figure 58.--Same as Figure 54, except for Mooring #5.

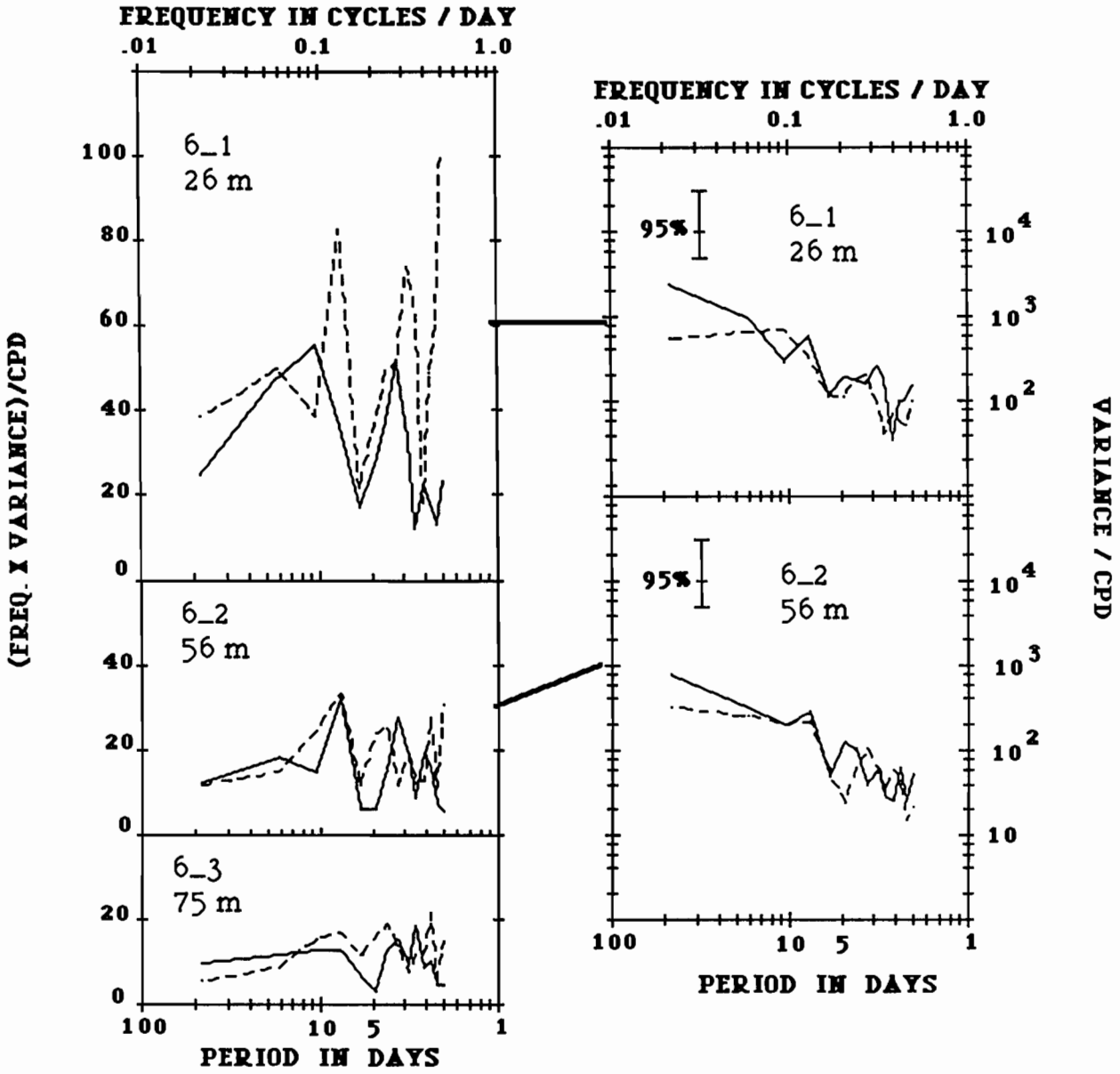

MOORING # 6 CURRENT SPECTRA

START 84240
553 6-HOURLY DATA POINTS
10 DEGREES OF FREEDOM

MAJOR —— 250 T
minor ---- 340 T

Figure 59.--Same as Figure 54, except for Mooring #6.

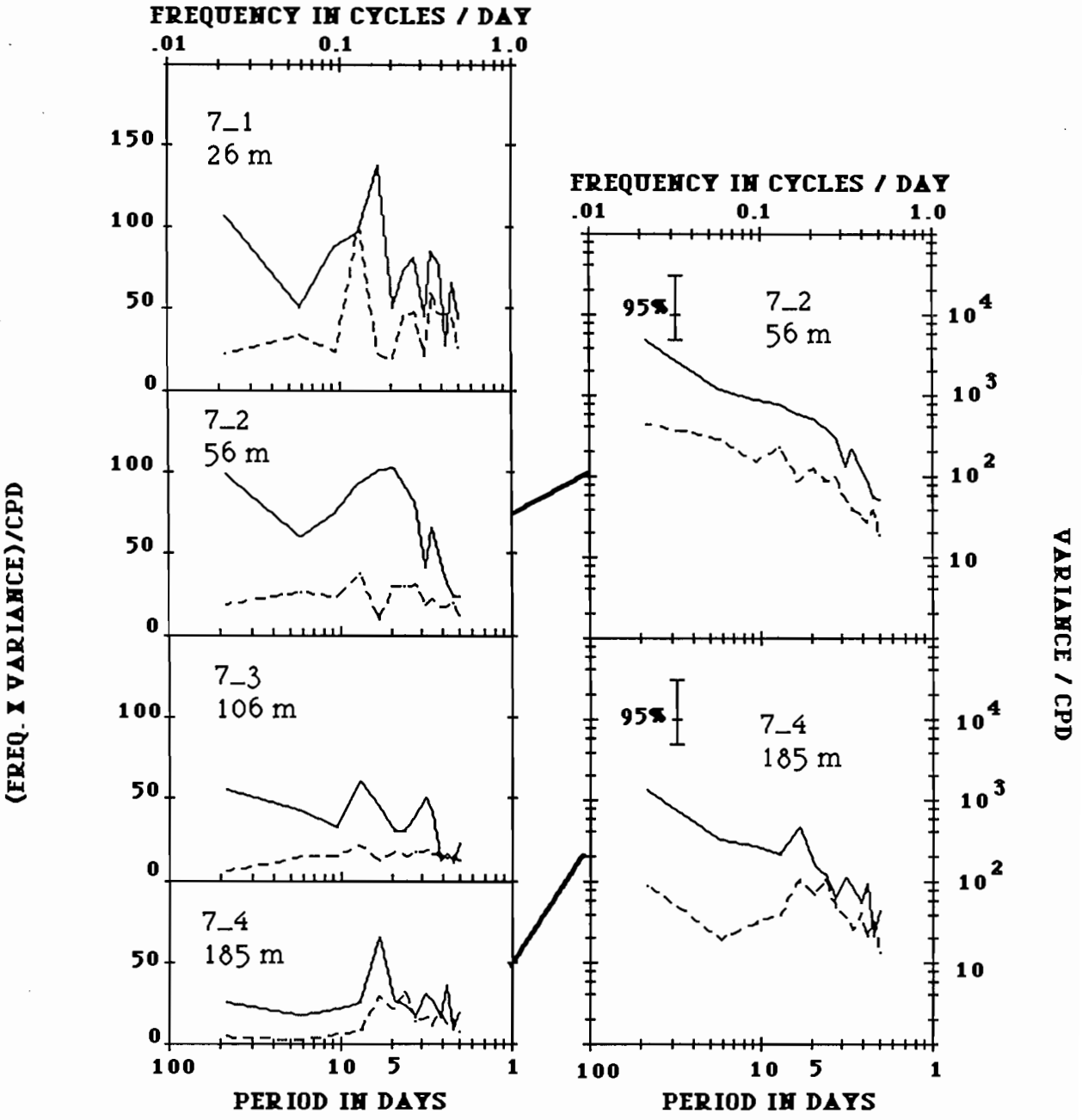

MOORING # 7 CURRENT SPECTRA

START 84240
553 6-HOURLY DATA POINTS
10 DEGREES OF FREEDOM

MAJOR —— 190 T
minor --- 280 T

Figure 60.--Same as Figure 54, except for Mooring #7.

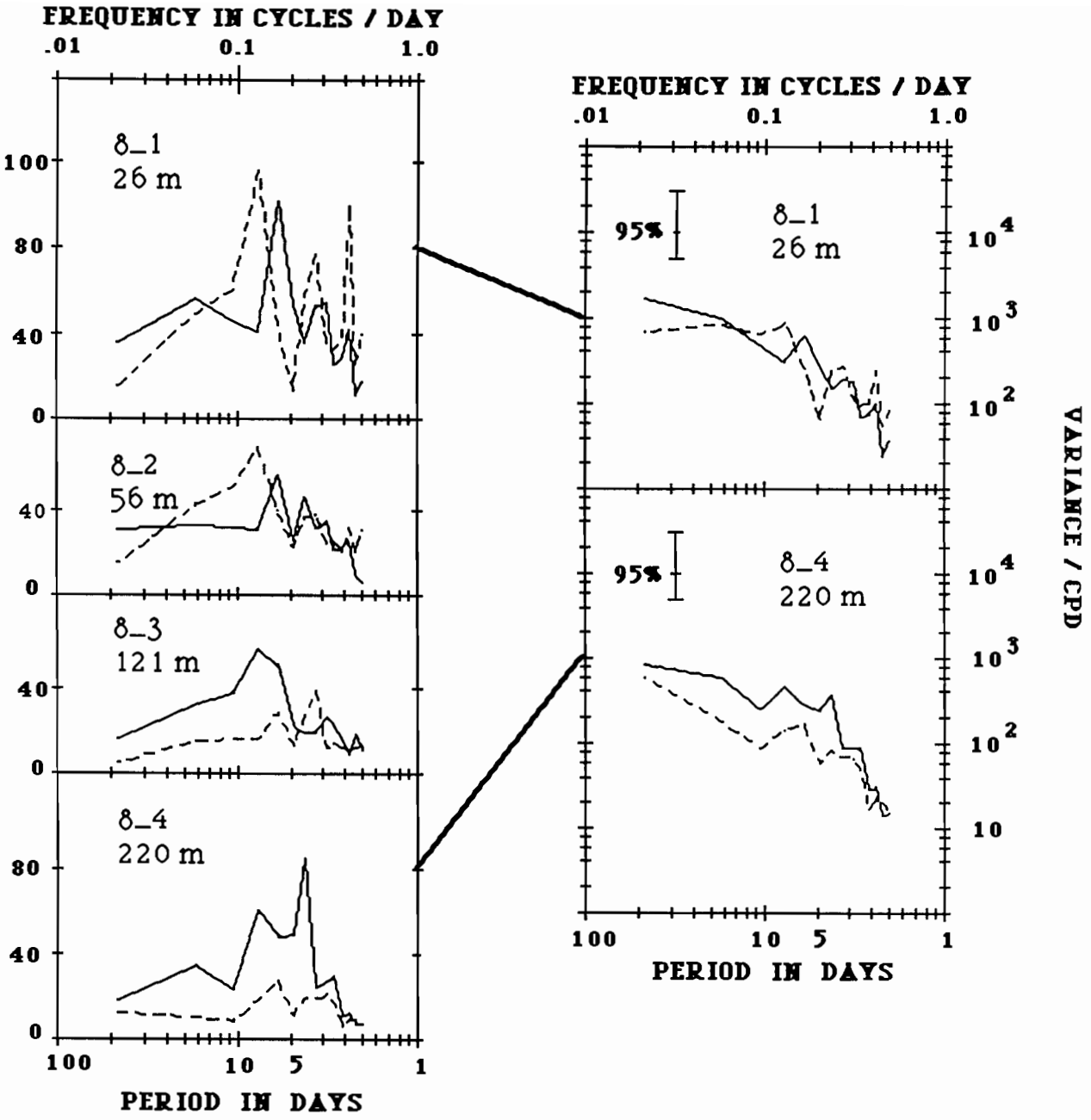

MOORING # 8 CURRENT SPECTRA

START 84240
553 6-HOURLY DATA POINTS
10 DEGREES OF FREEDOM

MAJOR —— 190 T
minor ---- 280 T

Figure 61.--Same as Figure 54, except for Mooring #8.

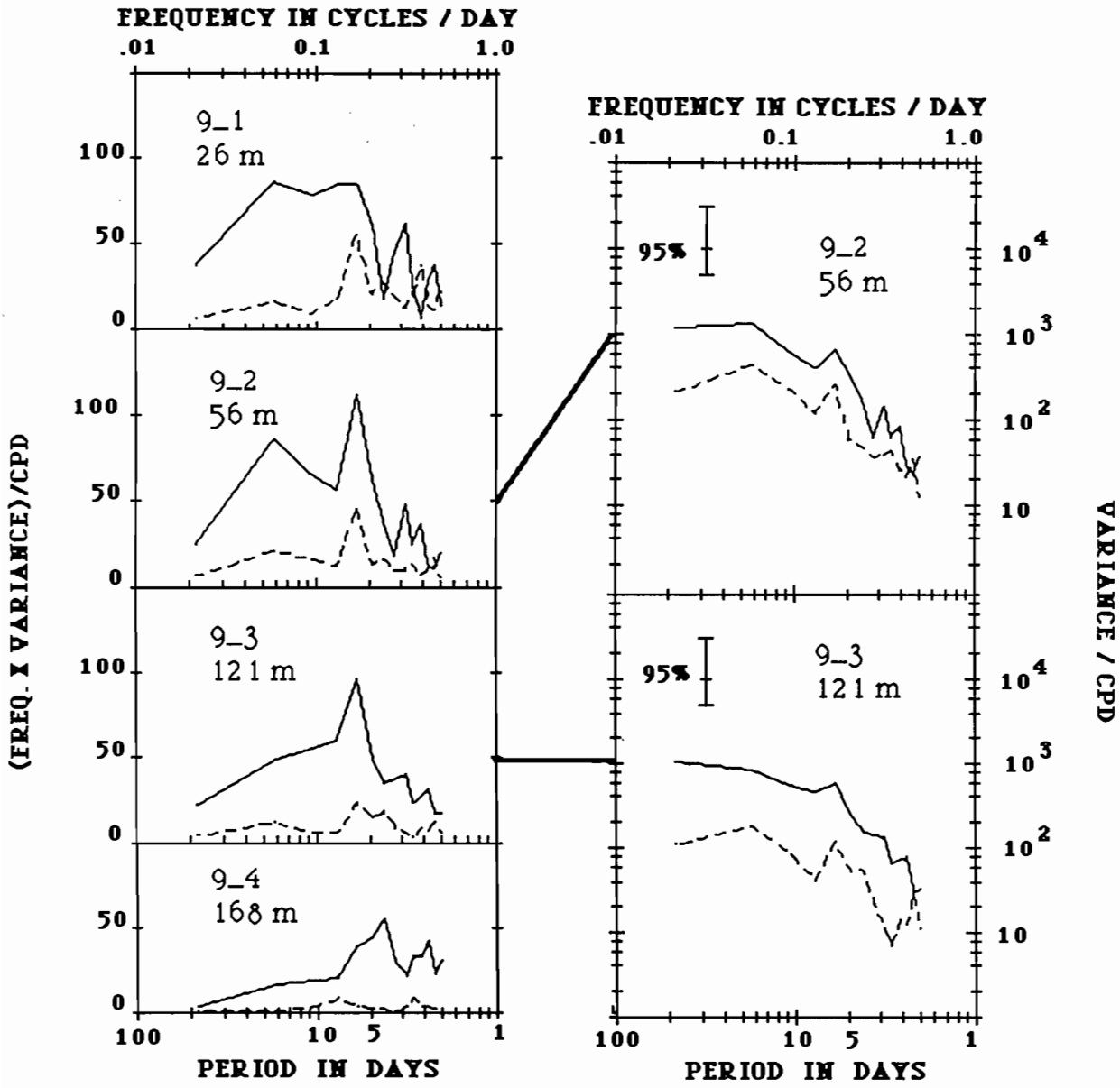

MOORING # 9 CURRENT SPECTRA

START 84240
553 6-HOURLY DATA POINTS
10 DEGREES OF FREEDOM

MAJOR —— 190 T
minor ---- 280 T

Figure 62.--Same as Figure 54, except for Mooring #9.

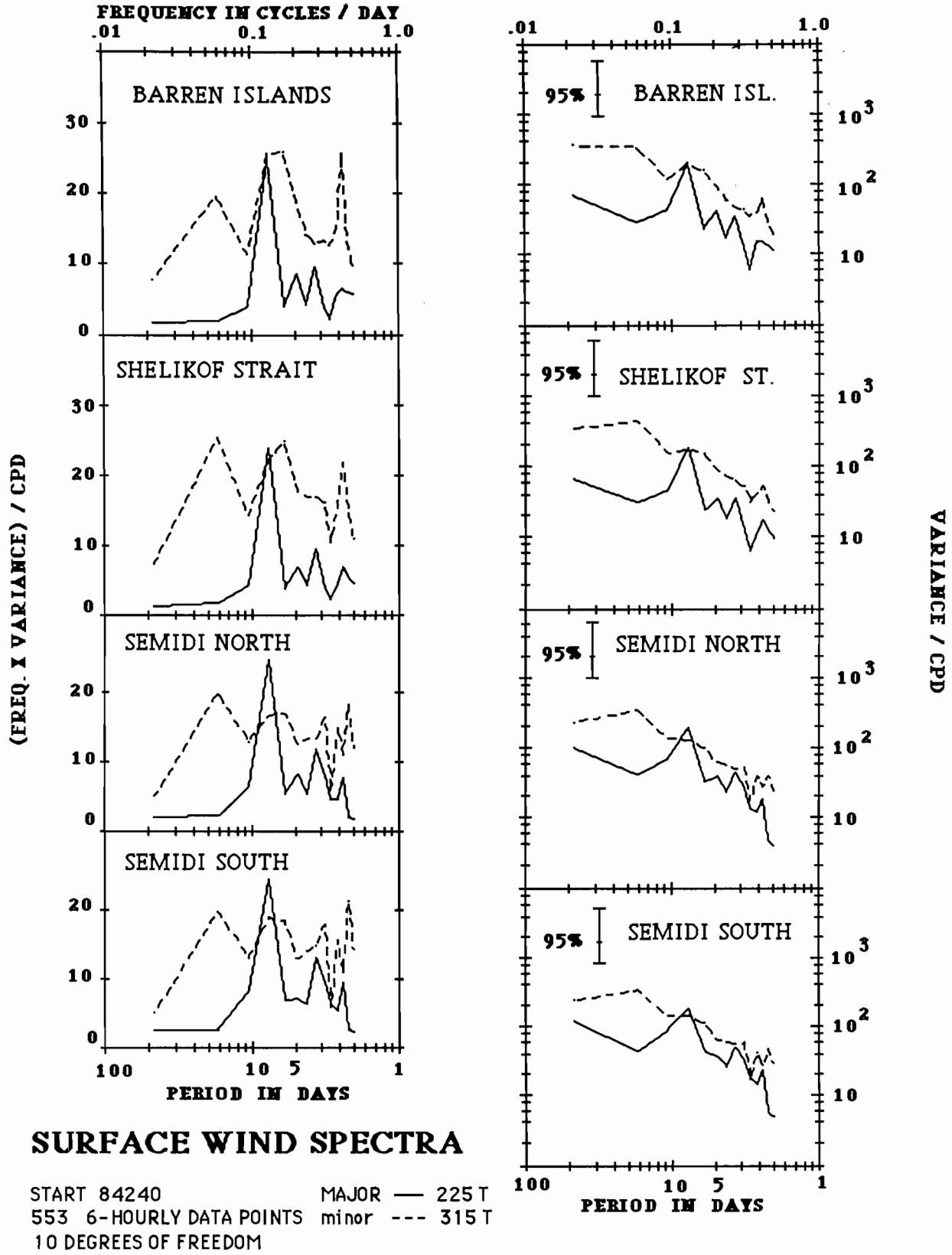

Figure 63.--Same as Figure 54, except for the surface wind series.

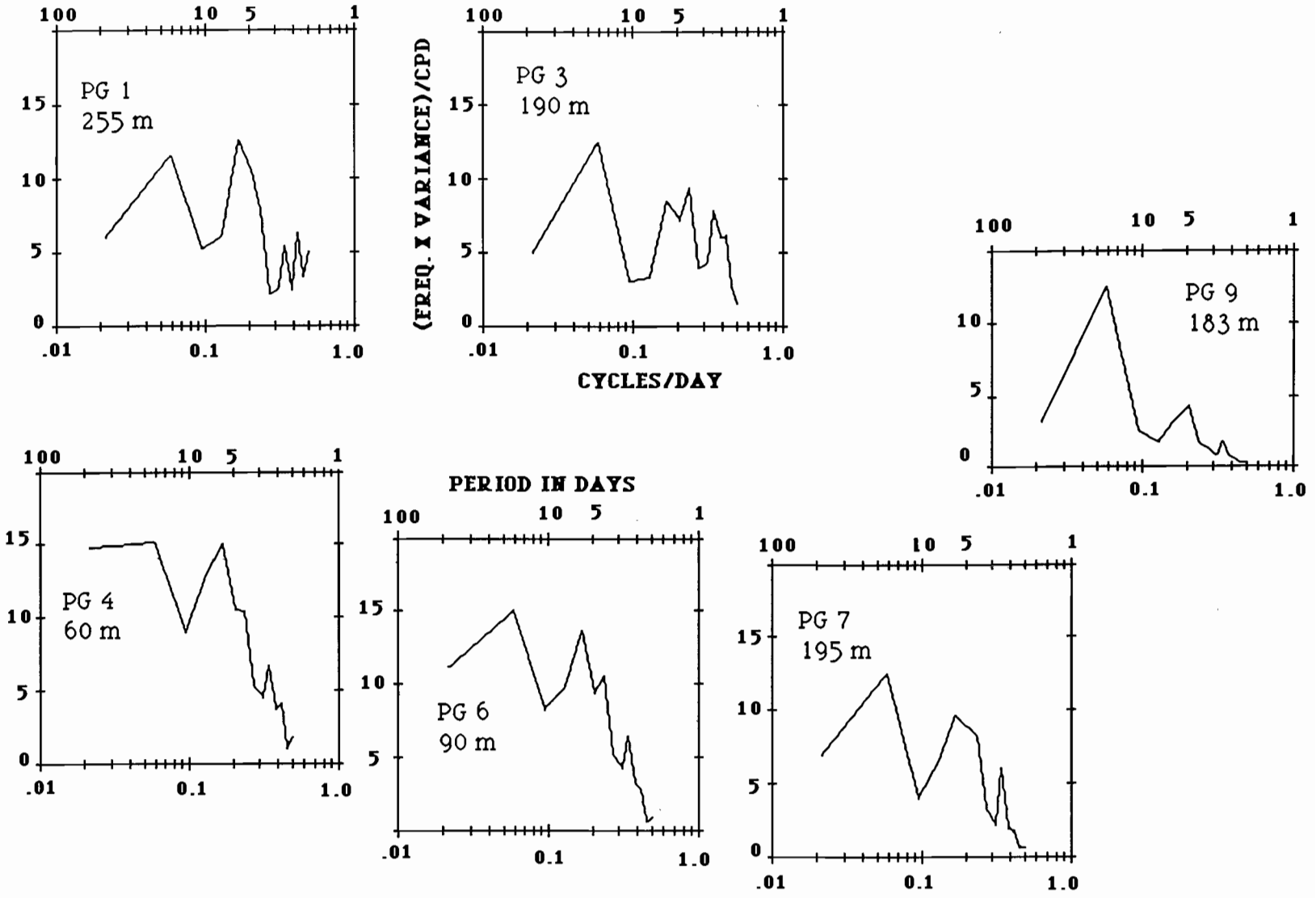

Figure 64.--Variance preserving spectra of the bottom pressure gauge records.

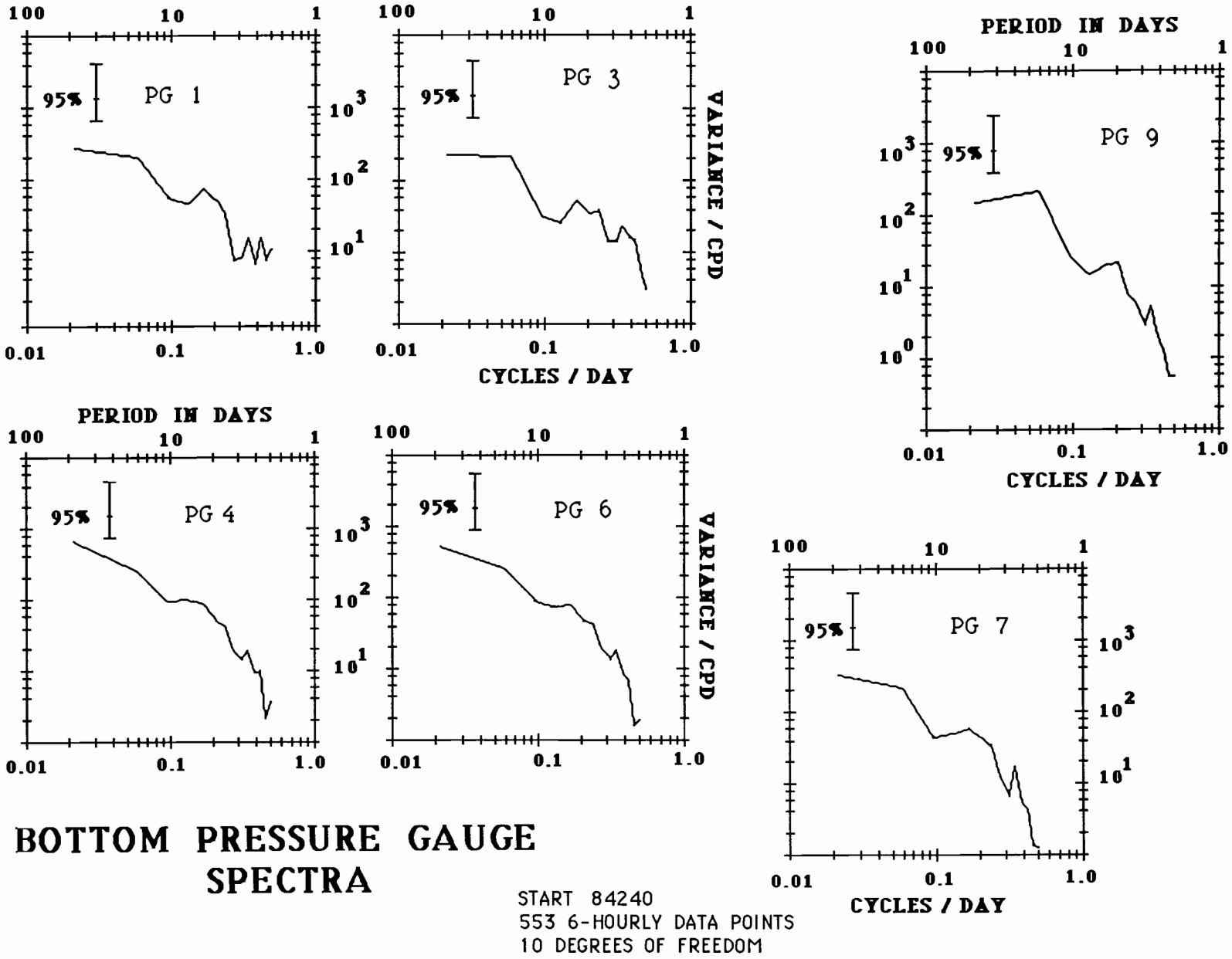

Figure 65.--Spectral density plot of the bottom pressure gauge records.

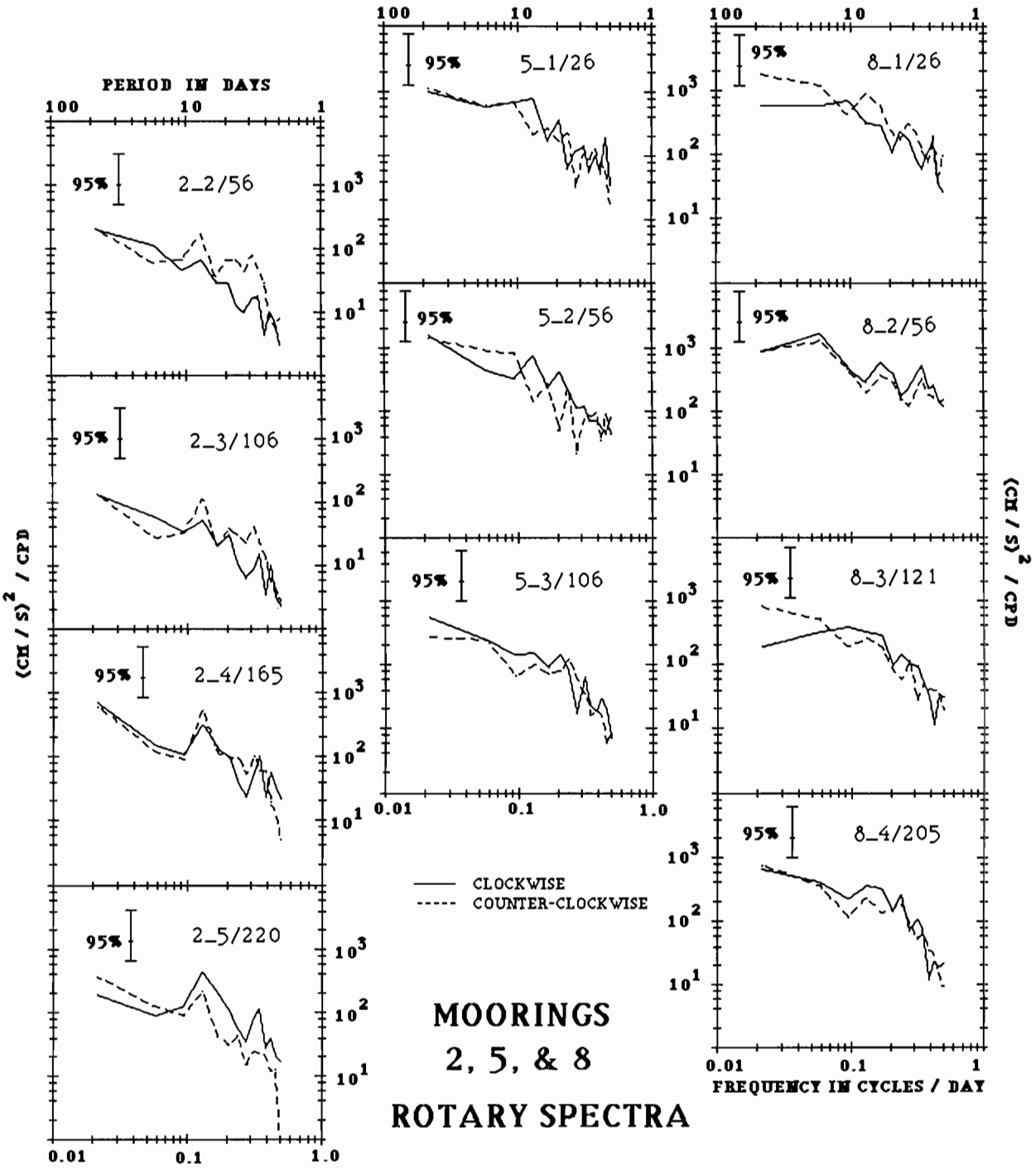

Figure 66.--Spectral density plot for the rotary spectra of Moorings 2, 5, and 8. All series start on JD 240 in 1984 and have 10 degrees of freedom. The solid line represents the clockwise components of the rotational spectrum and the dashed line represents the counterclockwise component.

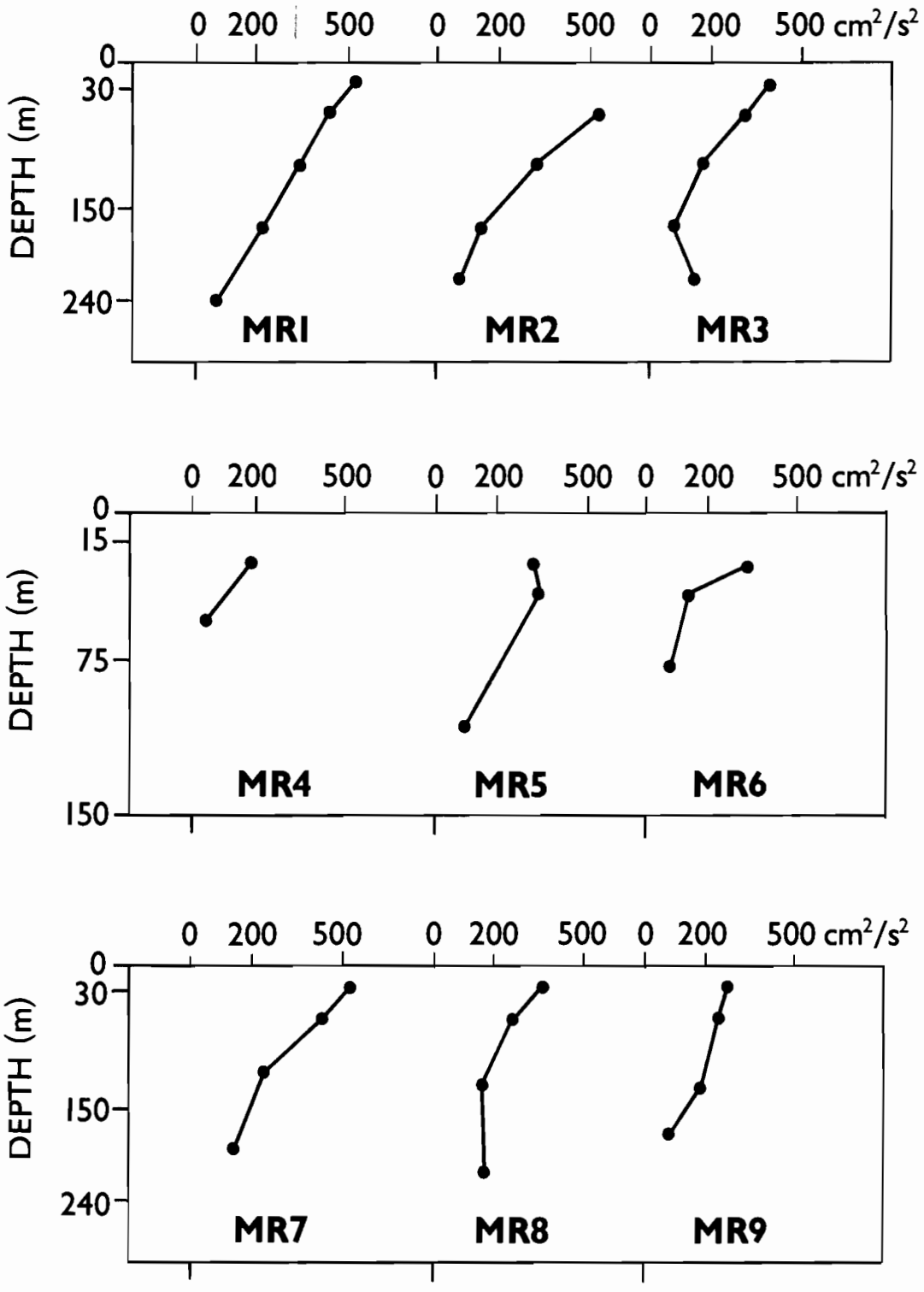

Figure 67.--Plot of total variance versus depth for all nine moorings. Units are cm^2/s^2.

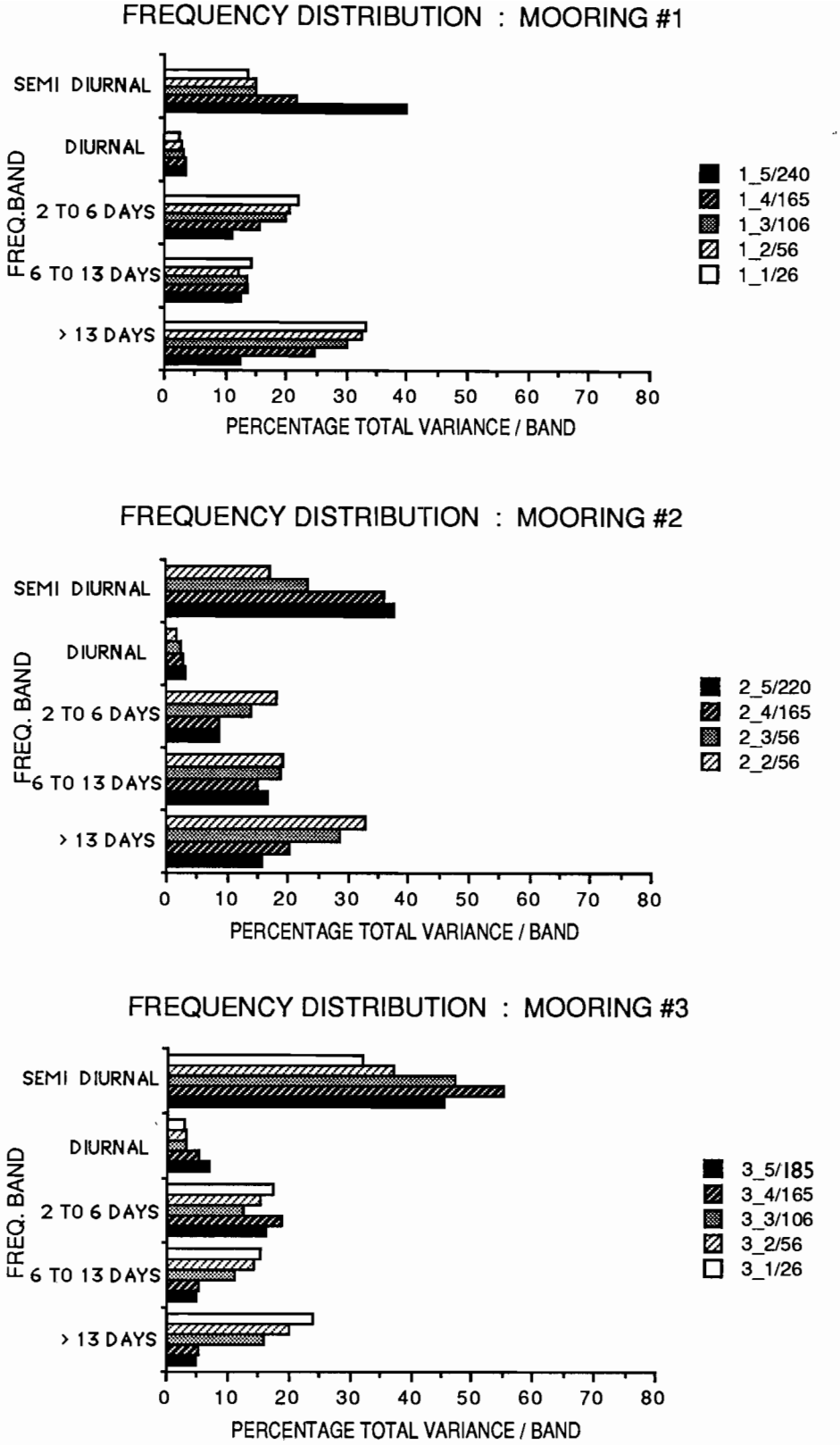

Figure 68.--Frequency distribution bar graph for the three moorings along transport section #1. The length of the bar represents the percentage of the total variance in the series that lies within a specified band. These plots were generated from spectra with 553 six-hourly data points and 30 degrees of freedom. Precise bandwidth information is contained in Table 17.

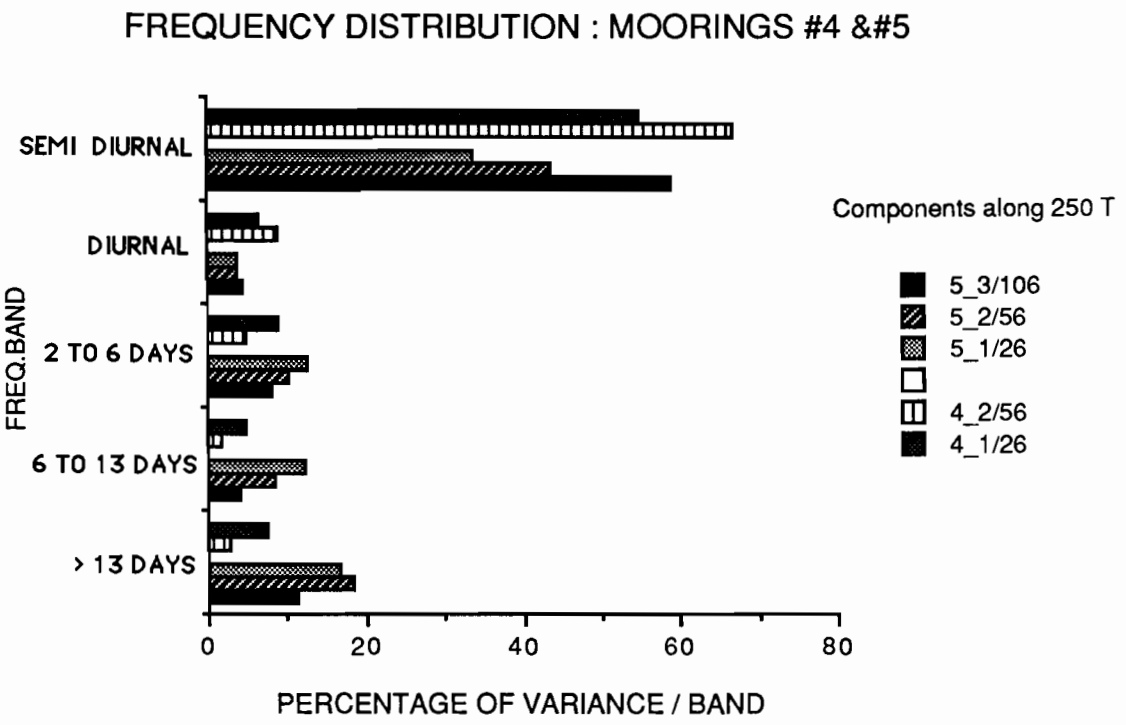

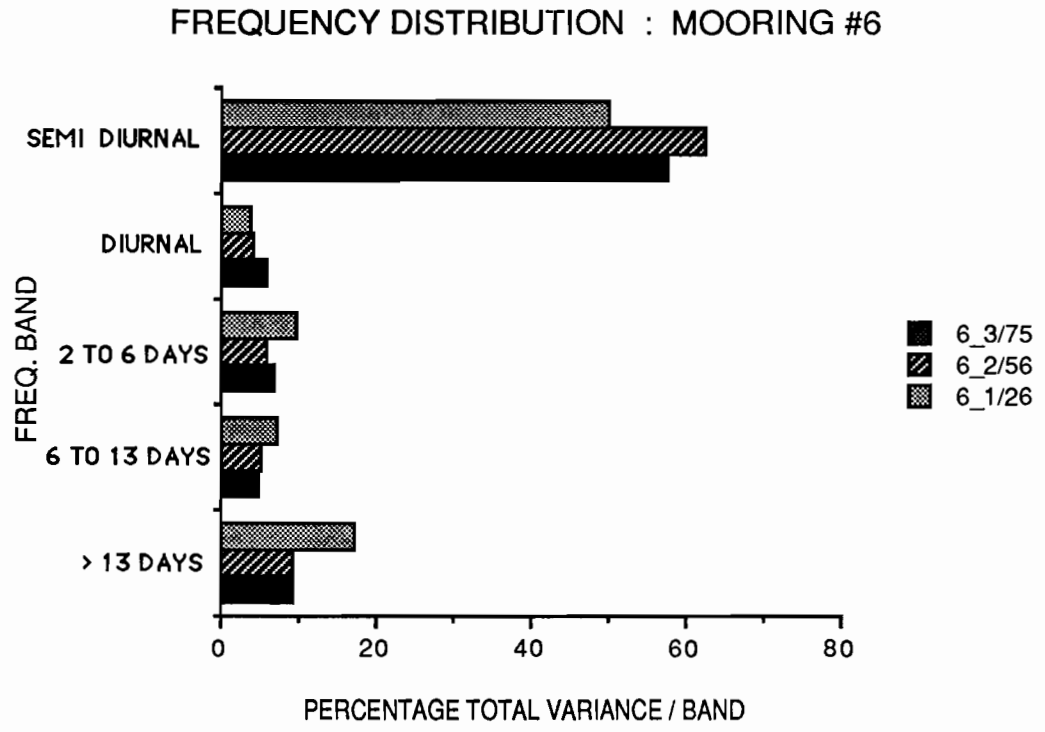

Figure 69.--Same as Figure 68, except for transport section #2.

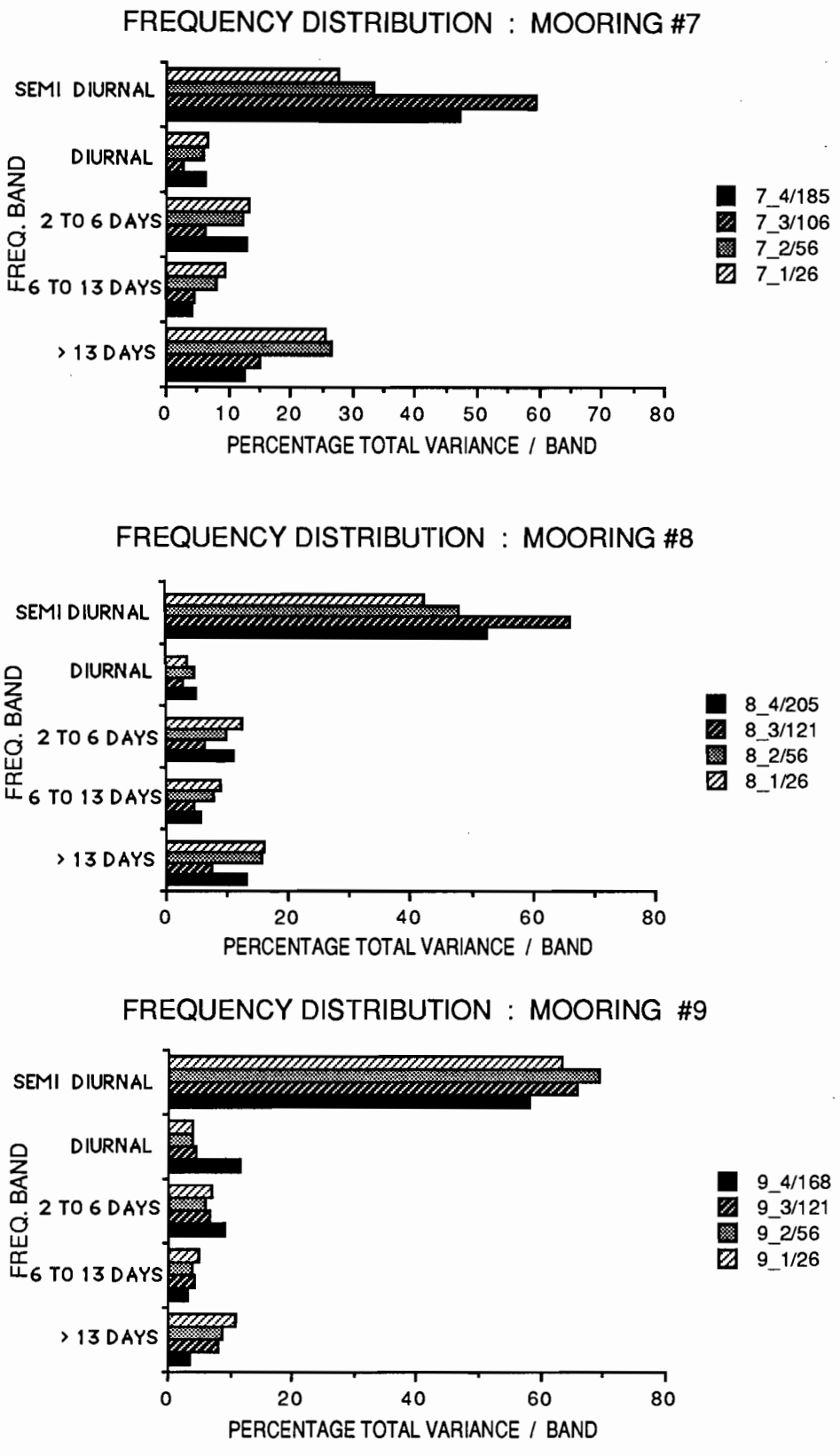

Figure 70.--Same as Figure 68, except for transport section #3.

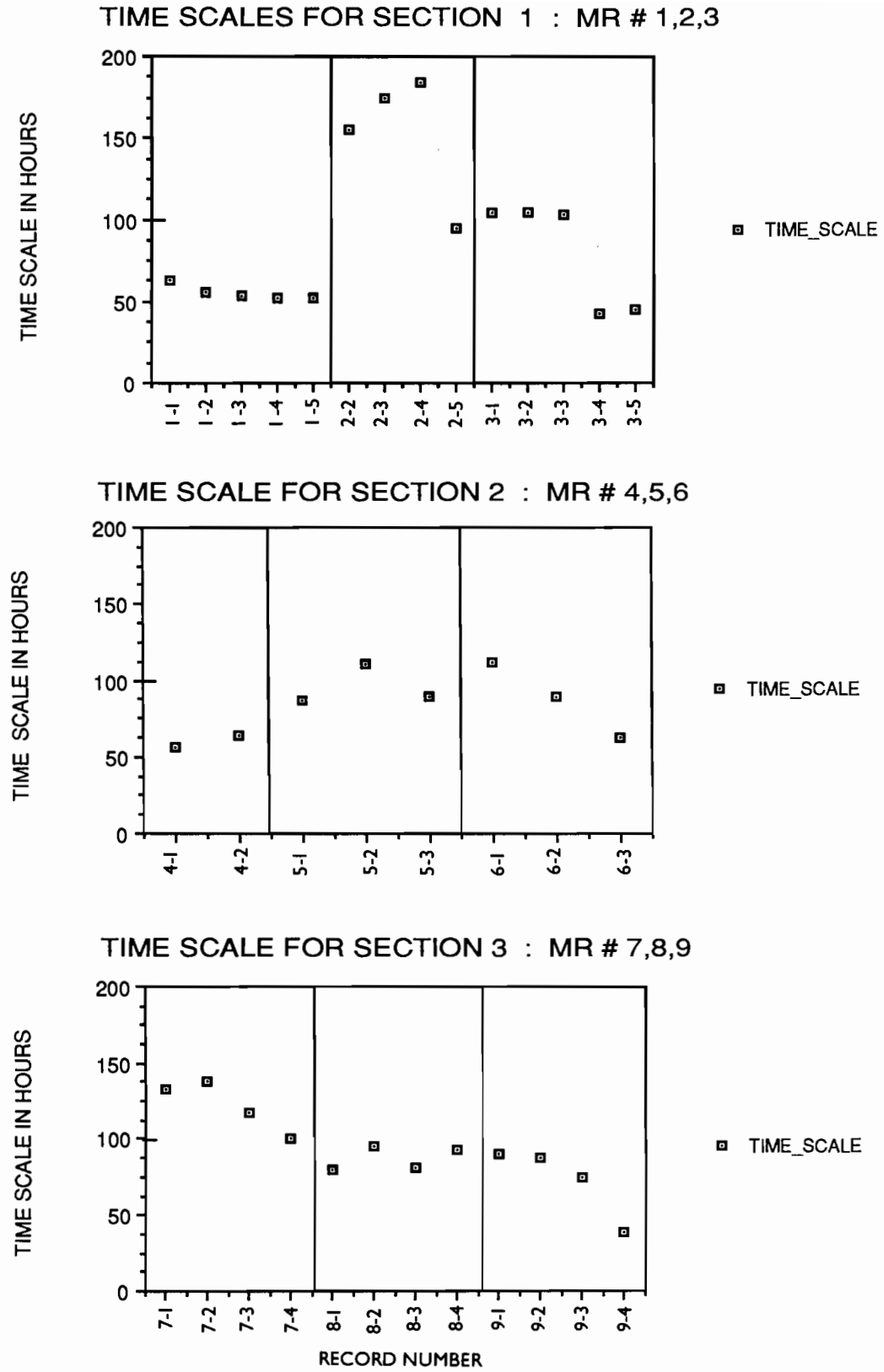

Figure 71.--Plot of the time scale for each record in hours. The integral time scale (Allen and Kundu, 1982) is a measure of the time between "independent" observations of a non-random time series. The time scale, $T = \sum_{n=-n_o}^{n=n_o} r_1(n\Delta t) \cdot r_2(n\Delta t) \cdot \Delta t$ where r_1, r_2 are lagged autocorrelation coefficients for variables 1 and 2, respectively. Δt is the time interval between data point (Δt 6 hrs).

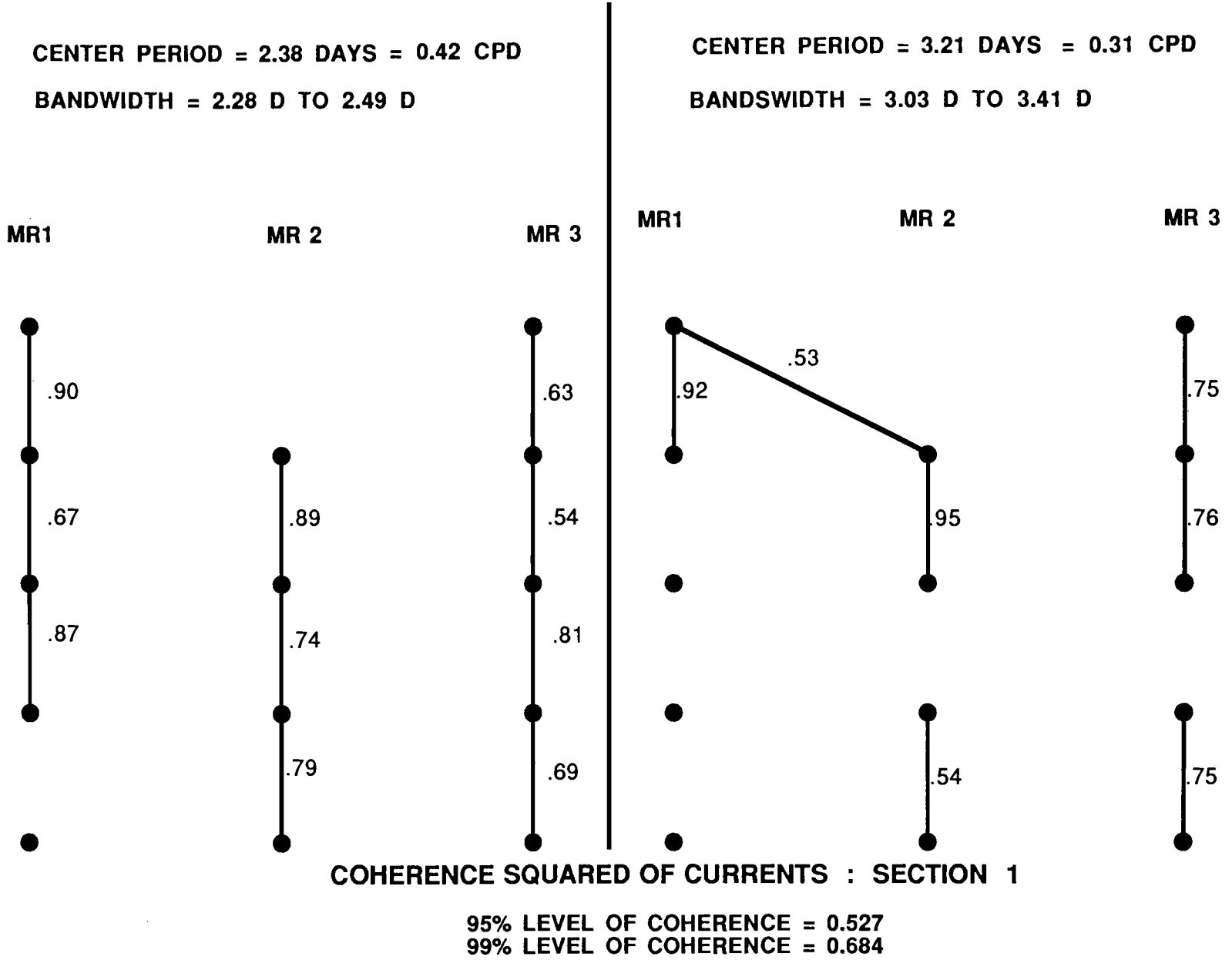

Figure 72.--Schematic of coherence squared between current meters for section #1 for the 2.38 and 3.21 day bands. Solid lines connect records where there is significant coherence. An estimate of the spectral bandwidth is included.

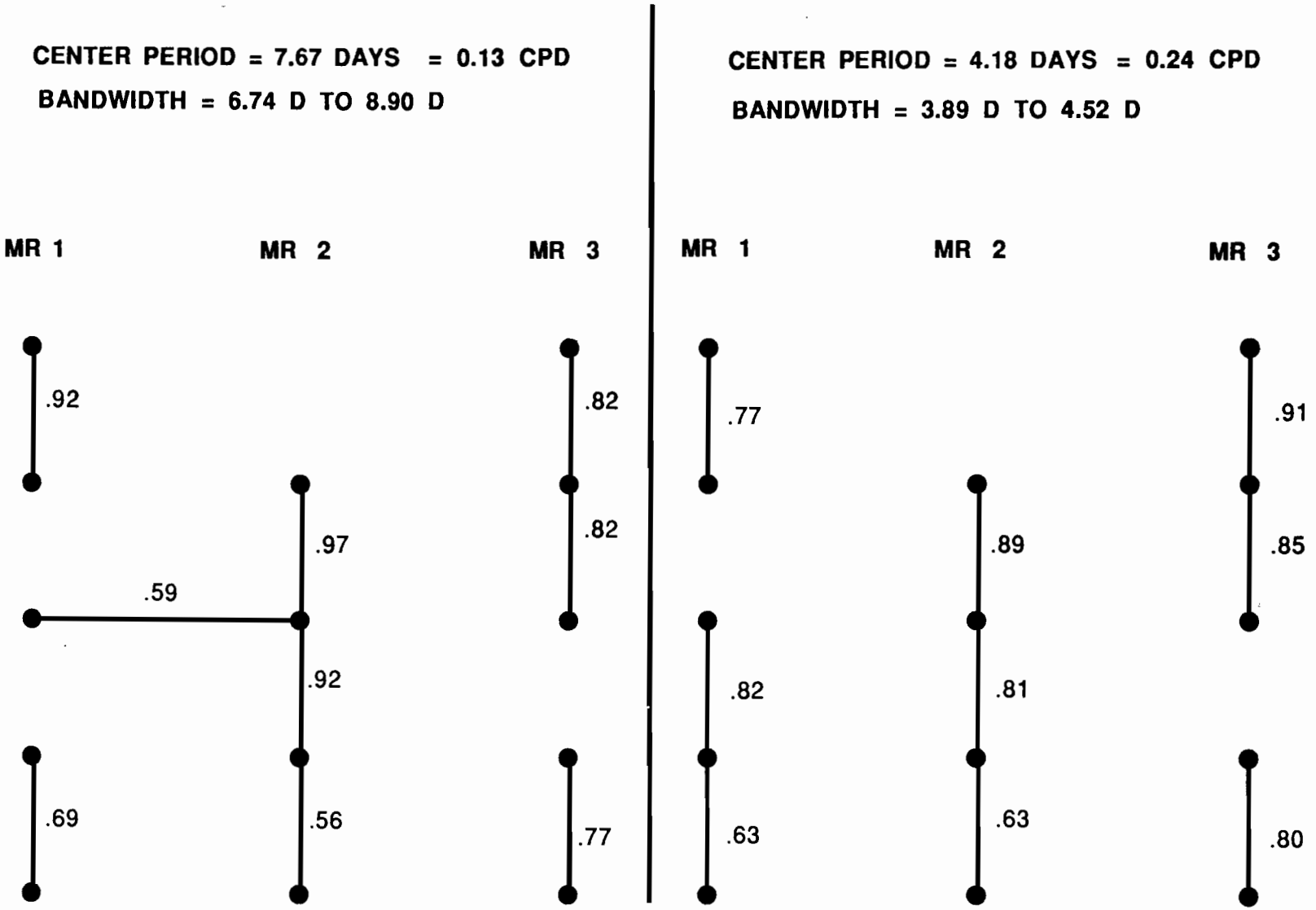

COHERENCE SQUARED OF CURRENTS : SECTION 1

95% LEVEL OF COHERENCE = 0.527
99% LEVEL OF COHERENCE = 0.684

Figure 73.--Same as Figure 70, except for the 4.18 and 7.67 day bands.

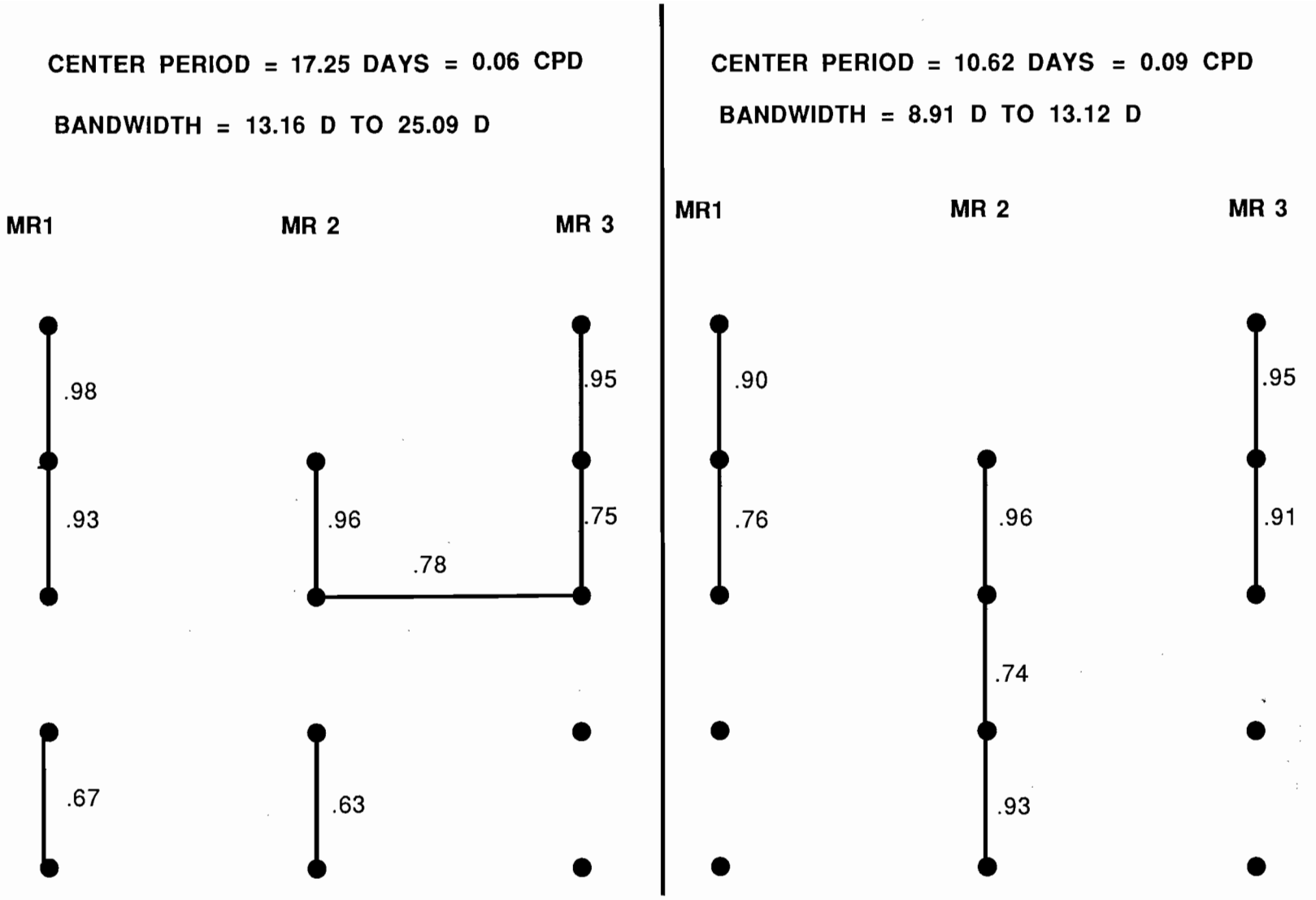

COHERENCE SQUARED OF CURRENTS : SECTION 1

95% LEVEL OF COHERENCE = 0.527
99% LEVEL OF COHERENCE = 0.684

Figure 74.--Same as Figure 70, except for the 10.62 and 17.25 day bands.

COHERENCE SQUARED OF CURRENTS : SECTIONS 2 AND 3

95% LEVEL OF COHERENCE = 0.527
99% LEVEL OF COHERENCE = 0.684

CENTER PERIOD = 2.38 DAYS = 0.42 CPD

BANDWIDTH = 2.28 D TO 2.49 D

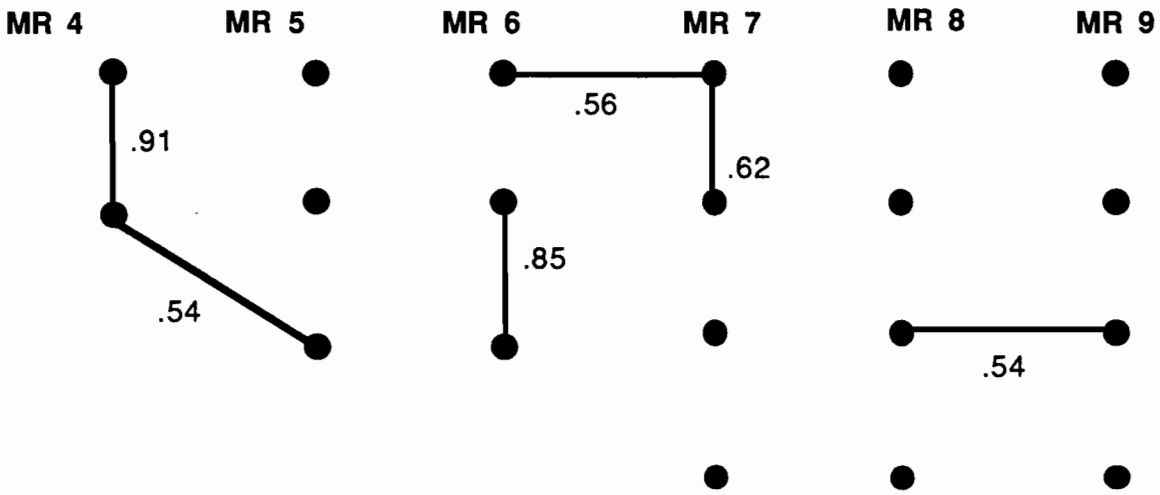

CENTER PERIOD = 3.21 DAYS = 0.31 CPD

BANDWIDTH = 3.03 D TO 3.41 D

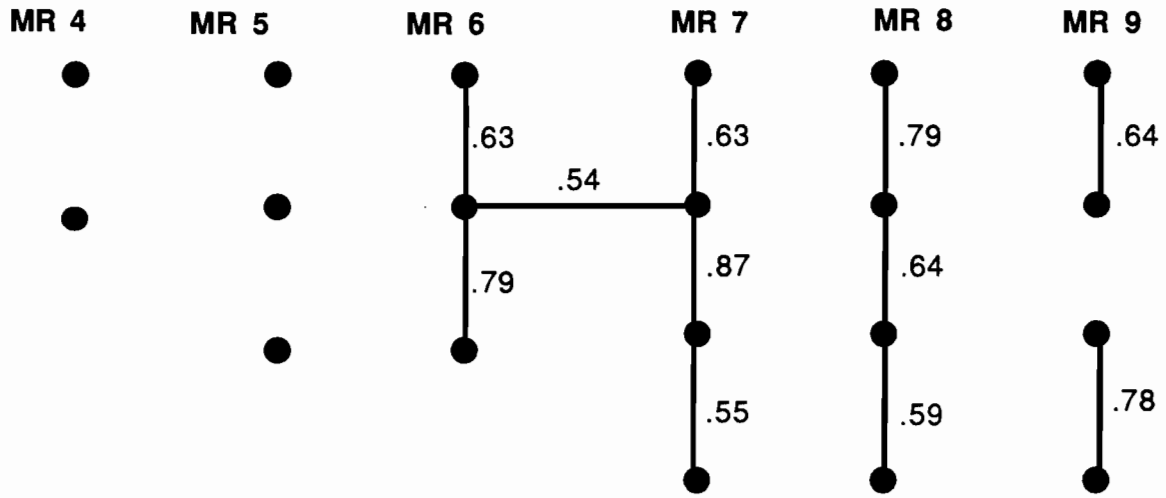

Figure 75.--Schematic of coherence between current meters for Sections #2 and #3 for the 2.38 and 3.21 day bands. Solid lines connect records where there is significant coherence.

COHERENCE SQUARED FOR CURRENTS : SECTIONS 2 AND 3

95% LEVEL OF COHERENCE = 0.527
99% LEVEL OF COHERENCE = 0.684

CENTER PERIOD = 4.18 DAYS = 0.24 CPD
BANDWIDTH = 3.89 D TO 4.52 D

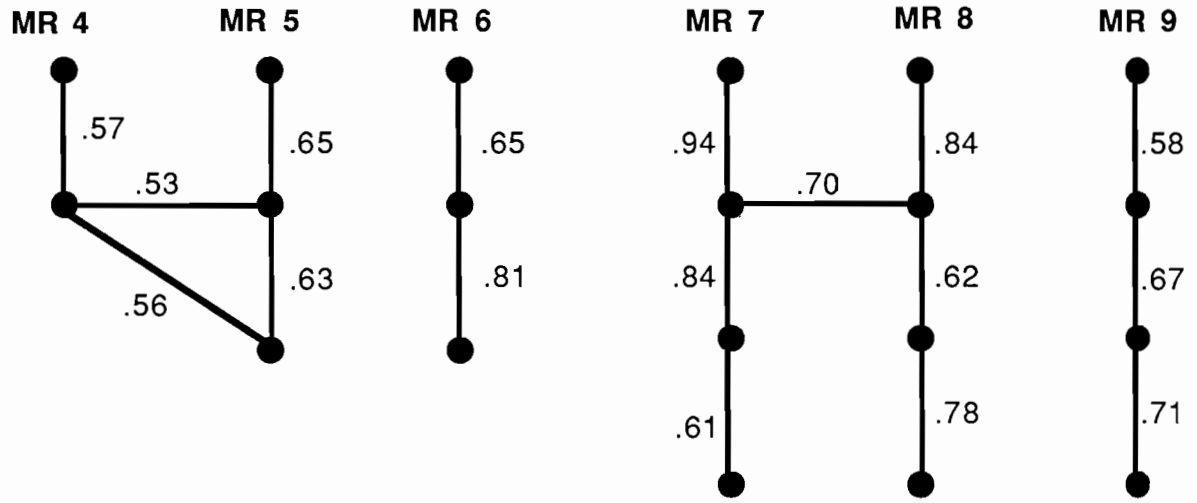

CENTER PERIOD = 7.67 DAYS = 0.13 CPD
BANDWIDTH = 6.74 D TO 8.90 D

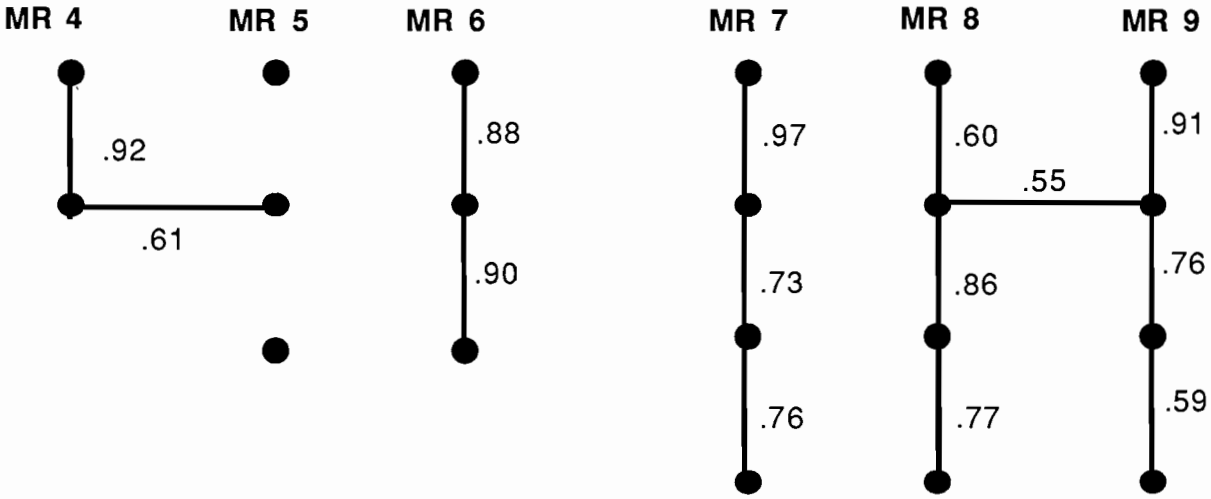

Figure 76.--Same as Figure 73, except for 4.18 and 7.67 day bands.

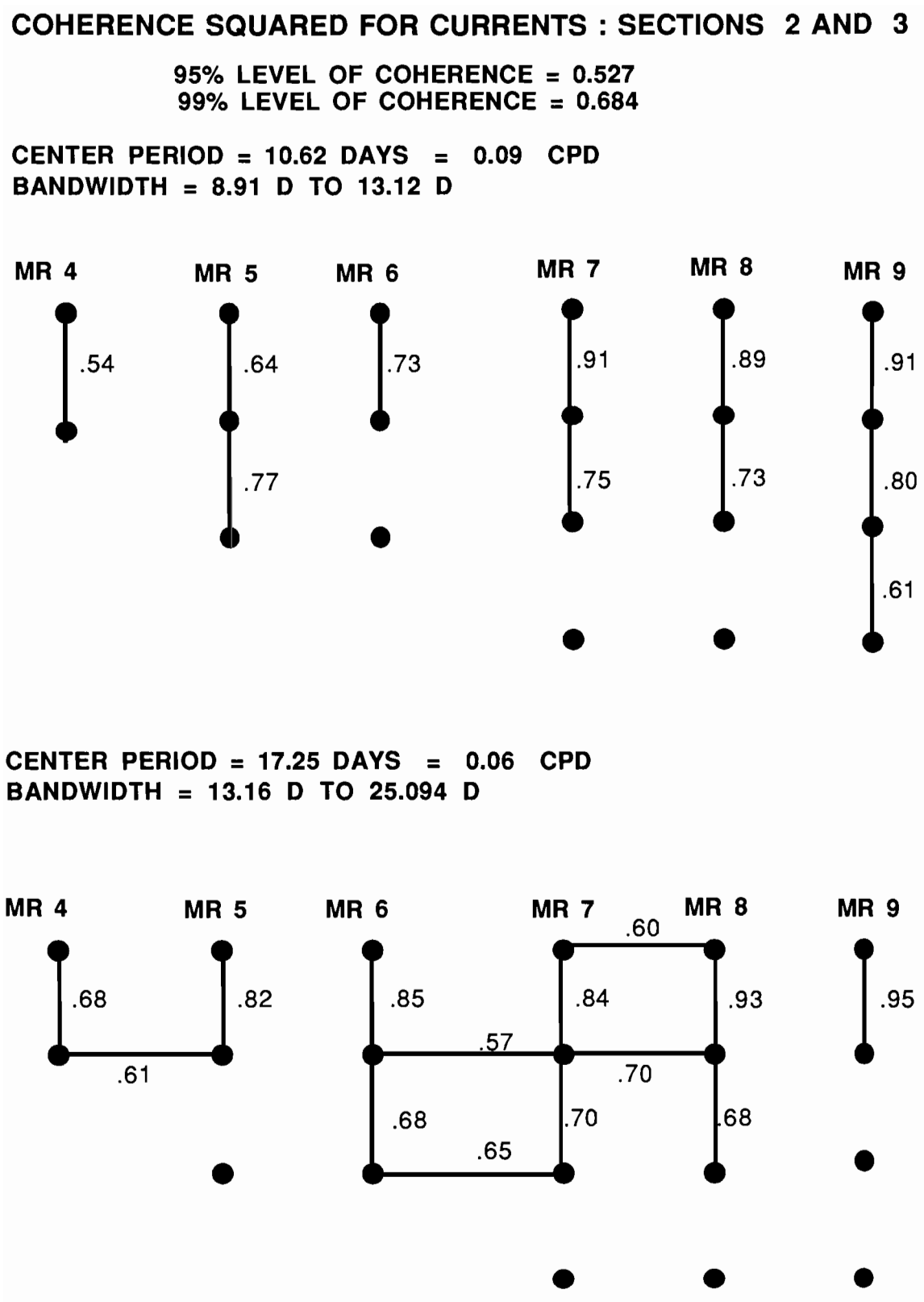

Figure 77.--Same as Figure 73, except for 10.62 and 17.25 day bands.

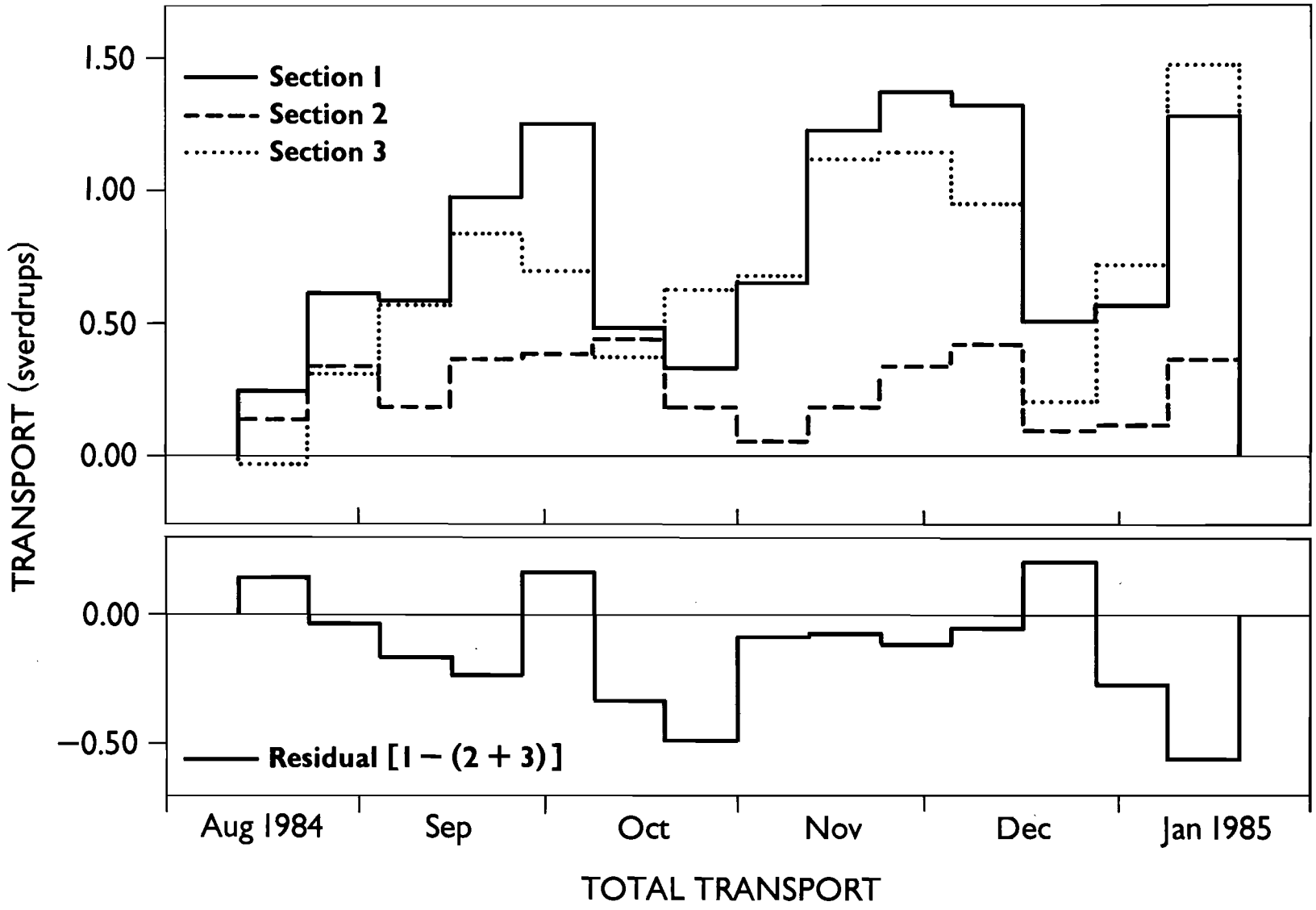

Figure 78.--Ten day averages of transport through each Section. The residual current remaining after the transport through Section 1 is subtracted from the sum of that through Sections 2 and 3 is plotted in the bottom panel.

TABLES

Table 1.--Duration and location of the current meter records showing the instruments on each mooring.

Mooring	Latitude (°W)	Longitude (°N)	Start/End JD	Days	Instruments CM	Instruments BP
1	57.72	155.26	84235/85016	147	5	X
2	57.60	155.01	84235/85016	147	5	
3	57.51	154.77	84235/85015	146	5	X
4	56.45	156.98	84236/85207	337	2	X
5	56.35	156.90	84236/85207	337	3	
6	56.28	156.82	84236/85207	337	3	X
7	55.95	156.60	84237/85206	335	4	X
8	55.94	156.36	84237/85206	335	4	
9	55.91	155.15	84237/85206	335	4	X

Table 2.--Current meter statistics for Moorings #1, #2, and #3. The RMS error is calculated as $\{S/(L/t)^{1/2}\}$ where S is the standard deviation of the series, L is the length of the series in hours and t is the integral time scale after Allen and Kundu, 1982. The variance is calculated along the principal axes shown as U and V and is written as MAJOR/minor axis variance. DIR is the axis of greatest variance and the ellipse is the quotient $(MAJOR^{1/2}/minor^{1/2})$.

Meter	V(220T) (cm/s)	U(310T) (cm/s)	Dir (°T)	Variance (cm^2/s^2)	Ellipse
1-1/26m	24.4 ± 3.1	-1.7 ± 0.5	214	506/23	4.7
1-2/56m	22.1 ± 2.6	0.4 ± 0.4	220	411/12	5.9
1-3/106m	15.0 ± 2.3	0.4 ± 0.3	224	320/08	6.4
1-4/165m	6.4 ± 1.8	-0.2 ± 0.2	223	215/02	9.7
1-5/240m	4.2 ± 1.1	0.6 ± 0.2	227	81/02	6.6
2-2/56m	21.3 ± 3.5	3.5 ± 1.8	231	297/228	1.1
2-3/106m	16.0 ± 2.9	3.6 ± 1.4	223	196/141	1.2
2-4/165m	6.3 ± 2.0	1.6 ± 1.0	58	78/61	1.1
2-5/220m	2.0 ± 1.1	0.0 ± 0.9	74	45/45	1.0
3-1/26m	0.2 ± 3.2	0.3 ± 0.8	219	337/52	2.6
3-2/56m	-0.5 ± 2.8	-0.2 ± 0.7	220	252/36	2.7
3-3/106m	0.7 ± 2.2	0.8 ± 0.6	218	153/25	2.5
3-4/165m	-5.3 ± 1.0	0.0 ± 0.2	227	86/05	4.3
3-5/220m	-6.7 ± 1.4	0.1 ± 0.2	225	139/05	5.3

Table 3.--Current meter statistics for Moorings #4, #5, and #6. Calculations are the same as in Table 2.

Meter	V(250T) (cm/s)	U(340T) (cm/s)	Dir (°T)	Variance (cm^2/s^2)	Ellipse
4-1/26m	11.4 ± 1.6	1.0 ± 1.0	247	130/72	1.3
4-2/56m	8.5 ± 0.9	1.3 ± 0.5	265	38/13	1.7
5-1/26m	9.5 ± 2.3	0.4 ± 2.5	150	170/189	0.95
5-2/56m	7.4 ± 2.3	1.5 ± 2.8	131	161/182	0.9
5-3/106m	5.2 ± 1.1	1.9 ± 1.3	116	51/52	1.0
6-1/26m	6.1 ± 3.6	-3.1 ± 1.6	241	273/121	1.5
6-2/56m	2.8 ± 1.8	-1.6 ± 1.1	234	105/59	1.3
6-3/75m	0.9 ± 1.1	-0.5 ± 1.1	223	63/45	1.2

Table 4.--Current meter statistics for Moorings #7, #8, and #9. Calculations are the same as in Table 2.

Meter	V(190T) (cm/s)	U(280T) (cm/s)	Dir (°T)	Variance (cm^2/s^2)	Ellipse
7-1/26m	23.0 ± 3.8	4.3 ± 1.5	201	369/116	1.8
7-2/56m	21.5 ± 3.9	5.0 ± 1.1	199	364/61	2.4
7-3/106m	11.3 ± 2.8	3.2 ± 0.7	199	233/33	2.7
7-4/185m	-0.4 ± 2.0	-1.6 ± 0.6	205	130/26	2.2
8-1/26m	21.1 ± 2.9	2.2 ± 1.7	186	241/163	1.2
8-2/56m	17.9 ± 2.8	1.4 ± 1.6	191	191/123	1.3
8-3/121m	8.6 ± 2.0	0.3 ± 0.9	204	142/53	1.6
8-4/205m	-1.2 ± 1.8	-3.0 ± 1.3	219	137/58	1.5
9-1/26m	6.2 ± 2.9	5.7 ± 1.2	181	278/70	2.0
9-2/56m	5.5 ± 2.5	3.2 ± 1.1	181	220/57	2.0
9-3/121m	3.6 ± 1.9	-0.1 ± 0.7	189	173/31	2.4
9-4/168m	-2.6 ± 1.0	1.9 ± 0.6	180	81/15	2.3

Table 5.--Statistics for the Geostrophic Winds, Integrated Transport and Bottom Pressure Gauges. All calculations are done as in Table 2.

WIND STATISTICS

Location	V(225T) (m/s)	U(315T) (m/s)	Variance (m^2/s^2)	Ellipse
Barren Islands	2.8 ± 0.6	0.9 ± 1.3	21/63	0.6
Shelikof Strait	2.3 ± 0.7	1.2 ± 1.3	21/66	0.6
Semidi Islands North	-0.2 ± 0.8	1.3 ± 1.1	28/52	0.7
Semidi Islands South	-0.5 ± 0.8	0.9 ± 1.2	32/55	0.8

TRANSPORT STATISTICS

Section	Mean TR (SV)	Standard Deviation (SV)	Time Scale (Hours)	Variance $(SV)^2$
1 surface	0.53 ± 0.06	0.32	136.1	0.105
1 bottom	0.29 ± 0.04	0.22	110.9	0.104
2 surface	0.24 ± 0.03	0.17	113.9	0.030
2 bottom	0.02 ± 0.01	0.03	89.1	0.001
3 surface	0.51 ± 0.07	0.32	144.3	0.103
3 bottom	0.17 ± 0.06	0.35	88.7	0.124

BOTTOM PRESSURE GAUGE STATISTICS

MOORING	Depth (m)	P(Mean) ($*10^4$mb)	Standard Deviation (mb)	Variance (mb^2)	Time Scale (hours)
PG 1	255	2.62	5.87	34.4	116.3
PG 3	190	1.98	5.46	29.8	153.2
PG 4	60	0.85	7.50	56.2	136.7
PG 6	90	1.05	6.76	45.7	130.1
PG 7	195	2.11	5.55	30.8	169.9
PG 9	183	1.97	4.20	17.6	289.0

Table 6.--Correlation matrix for current meter records on Section #1. The coefficient is followed by the lag in parentheses (in hours) with column lagging the row. If there is no number, the correlation was not significant at the 95% confidence level.

Record	1-1	1-2	1-3	1-4	1-5	2-2	2-3	2-4	2-5	3-1	3-2	3-3	3-4	3-5	T
1-1/26	1.0	.95	.72	.31	--	--	--	--	--	-.24	--	--	--	--	62.93
1-2/56		1.0	.83	.36	--	-.27	--	--	--	-.25	--	--	--	--	56.00
1-3/106			1.0	.45	.24	-.24(6)	-.21(6)	--	--	--	--	--	--	--	52.86
1-4/165				1.0	.57	--	--	--	--	-.27	-.28	-.25	-.26(24)	--	52.58
1-5/240					1.0	-.30(24)	-.27(24)	--	--	-.22	-.27(12)	-.24(12)	--	--	52.43
2-2/56						1.0	.96	.80	.48	--	--	--	--	--	155.62
2-3/106							1.0	.87	.55	--	--	--	--	--	174.29
2-4/165								1.0	.73	--	--	--	--	--	184.57
2-5/220									1.0	--	--	--	--	*	94.55
3-1/26										1.0	.94	.73	--	--	104.55
3-2/56											1.0	.86	--	--	104.11
3-3/106												1.0	--	--	103.45
3-4/165													1.0	.83	41.82
3-5/220														1.0	44.97

Table 7.--Correlation matrix for current meter records on Section #2. The coefficient is followed by the lag in parentheses (in hours) with column lagging the row. If there is no number, the correlation was not significant at the 95% confidence level.

Record	4-1	4-2	5-1	5-2	5-3	6-1	6-2	6-3	T
4-1/26	1.0	.67	--	--	.25(6)	--	--	--	56.55
4-2/56		1.0	--	--	.32(6)	--	--	--	63.69
5-1/26			1.0	.78	.39	--	--	.25	86.82
5-2/56				1.0	.44	--	--	--	110.55
5-3/106					1.0	--	--	--	89.45
6-1/26						1.0	.89	.77	111.95
6-2/56							1.0	.87	88.72
6-3/75								1.0	62.82

Table 8.--Correlation matrix for current meter records on Section #2. The coefficient is followed by the lag in parentheses (in hours) with column lagging the row. If there is no number, the correlation was not significant at the 95% confidence level.

Record	7-1	7-2	7-3	7-4	8-1	8-2	8-3	8-4	9-1	9-2	9-3	9-4	T
7-1/26	1.0	.93	.75	.50	--	--	--	.53	-.28(19)	-.26(30)	--	--	133.25
7-2/56		1.0	.85	.60	--	.37(30)	.38(6)	.56	-.33(30)	-.33(30)	--	.21	138.06
7-3/106			1.0	.73	+.45(30)	.47	.56	.62(6)	-.38(30)	-.45(30)	--	.20	117.70
7-4/185				1.0	.34(24)	.48	.56(6)	.61(12)	--	--	--	.34	100.38
8-1/26					1.0	.87	.54	.26	--	--	--	--	80.03
8-2/56						1.0	.72	.37	--	--	--	--	95.22
8-3/121							1.0	.51	--	--	--	--	80.68
8-4/205								1.0	-.34(30)	-.35(30)	--	.21	93.49
9-1/26									1.0	.89	.57	.23	89.74
9-2/56										1.0	.69	.37	88.20
9-3/121											1.0	.63	74.74
9-4/168												1.0	39.35

Table 9.--Correlation matrix for the relationship of the integrated transport sections with each other. The lag is in parentheses after the correlation coefficient and is expressed in hours.

	Surface 1	Bottom 1	Total 1	Surface 2	Bottom 2	Total 2	Surface 3	Bottom 3	Total 3
Surface 1	1.0								
Bottom 1	0.67	1.0							
Total 1	0.91	0.91	1.0						
Surface 2	0.39	0.42	0.44	1.0					
Bottom 2	*	0.35	0.33	0.56	1.0				
Total 2	0.39	0.44	0.45	0.99	0.66	1.0			
Surface 3	0.67	0.65	0.72	*	0.30	*	1.0		
Bottom 3	0.52(6)	0.56(12)	0.59(6)	*	0.29(30)	*	0.65	1.0	
Total 3	0.65	0.65	0.71	*	0.30	*	0.90	0.92	1.0

Table 10.--Correlation matrix for the along channel currents vs. Barren Island winds resolved along axis of maximum correlation.

Section 1					Section 2					Section 3				
Mooring	Instr.	r	lag (hrs.)	DIR (r_{max})	Mooring	Instr.	r	lag (hrs.)	DIR (r_{max})	Mooring	Instr.	r	lag (hrs.)	DIR (r_{max})
1	-1	.44	12	285°	4	-1	.27	6	225°/245°	7	-1	.41	18	265°
	-2	.44	18	285°		-2	.29	6	245°		-2	.48	12	265°
	-3	.39	24	285°							-3	.53	18	265°
	-4	.24	24	325°							-4	.62	12	285°
	-5	-.23	0	225°										
2	-2	.33	18	265°	5	-1	*	*	*	8	-1	.34	18	265°/285°
	-3	.33	18	265°		-2	*	*	*		-2	.48	12	285°
	-4	.38	18	265°		-3	*	*	*		-3	.60	18	285°
	-5	.49	18	265°/285°							-4	.63	18	265°
3	-1	-.34	24	345°	6	-1	.36	6	245°	9	-1	*	*	*
	-2	-.30	24	345°		-2	.44	6	245°		-2	*	0	345°
	-3	*	*	*		-3	.41	6	245°		-3	*	0	305°
	-4	.38	12	345°							-4	.33	0	265°/285°
	-5	.33	12	345°										

* Not significant at 95% level.

Table 11.--Correlation matrix for the integrated transport sections and bottom pressure series vs. the surface winds.

	Section 1		Section 2		Section 3	
Surface	0.44(18)	245°	0.36(12)	225°/245°	0.48(12)	285°
Bottom	0.52(18)	285°	0.26(18)	245°	0.70(12)	285°
Total	0.49(18)	265°	0.36(12)	225°/245°	0.64(12)	265°

Coefficients for 245° to 285° vary by <0.1.

Bottom pressure as a function of Barren Island wind direction.

PG 1	0.43(-6)	265°	PG 4	0.54(6)	265°	PG 7	0.40	245°/265°
PG 3	0.38(-6)	265°	PG 6	0.53(6)	265°	PG 9	*	

Table 12.--Correlation matrix for pressure differences vs. Section #1 current meters.

Δp Cross Stream Bottom Pressure Difference vs. Section 1 Currents

Record	1-1	1-2	1-3	1-4	1-5	2-2	2-3	2-4	2-5	3-1	3-2	3-3	3-4	3-5
Δp1-3	.28(6)	.30(6)	.24	.27	.33	--	--	--	.34(6)	--	--	--	.27	.26
Δp4-6	.25	.26	.26	.24	--	.36(30)	.35(18)	--	.40	--	--	--	--	--
Δp7-9	.38	.35	.32(18)	.26(42)	--	--	--	.45	.52	--	--	--	--	--
Δp6-9	.39	.40	.39(18)	.33(42)	--	.46(12)	.45(6)	.53(6)	.56	--	--	--	--	--

Δp Down Stream Bottom Pressure Difference vs. Section 1 Currents

Record	1-1	1-2	1-3	1-4	1-5	2-2	2-3	2-4	2-5	3-1	3-2	3-3	3-4	3-5
Δp1-4	--	--	-.26	-.30(30)	--	-.54	-.53	-.51	-.40	--	--	--	--	--
Δp1-6	--	--	-.22	--	--	-.54	-.51	-.48	-.33	--	--	--	--	--
Δp1-7	--	--	--	--	--	-.37	-.33	-.27	--	--	--	--	--	--
Δp3-9	--	--	--	--	--	--	--	--	.38(18)	--	--	--	--	--

Table 13.--Correlation matrix for pressure differences vs. Section #2 current meters.

Δp Cross Stream Bottom Pressure Difference vs. Section 2 Currents

Record	4-1	4-2	5-1	5-2	5-3	6-1	6-2	6-3
Δp1-3	--	--	--	--	--	--	--	--
Δp4-6	.23	.27	.45	.54	.43	.51	.54	.53
Δp7-9	--	.24	--	--	.31(30)	--	.39	.42
Δp6-9	--	.20	--	--	--	.51	.59	.56

Δp Down Stream Bottom Pressure Difference vs. Section 2 Currents

Record	4-1	4-2	5-1	5-2	5-3	6-1	6-2	6-3
Δp1-4	--	--	-.36(30)	-.41(42)	--	-.56	-.60	-.52
Δp1-6	--	--	--	-.34(42)	--	-.48	-.51	-.42
Δp1-7	--	--	--	--	--	--	--	--
Δp3-9	--	--	--	--	--	--	.36	.34

Table 14.--Correlation matrix for pressure differences vs. Section #3 current meters.

Δp Cross Stream Bottom Pressure Difference vs. Section 3 Currents

	7-1	7-2	7-3	7-4	8-1	8-2	8-3	8-4	9-1	9-2	9-3	9-4
Δp1-3	--	--	.31(30)	.32(24)	--	--	.20(18)	.27	--	--	--	.35(18)
Δp4-6	--	--	--	.22	--	.35(6)	.31(12)	--	--	--	--	--
Δp7-9	.54	.62	.75	.81	.40(12)	.57	.67	.79(6)	--	--	--	.42
Δp6-9	.63	.71	.78	.71	.54(18)	.70	.73	.54	--	--	--	.26

Δp Down Stream Bottom Pressure Difference vs. Section 3 Currents

	7-1	7-2	7-3	7-4	8-1	8-2	8-3	8-4	9-1	9-2	9-3	9-4
Δp1-4	-.51	-.51	-.54	-.44	-.44	-.58	-.56	--	--	--	--	--
Δp1-6	-.50	-.52	-.56	-.44	-.45	-.56	-.56	--	--	--	--	--
Δp1-7	--	--	-.21	-.23	-.17	-.18	-.24	-.25	--	-.21(18)	--	.34(18)
Δp3-9	.41(12)	.47(6)	.55(6)	.58(12)	.32(18)	.43(12)	.42(12)	.51(18)	--	--	--	.37

Table 15.--Correlation matrix for relations between down shelf and cross shelf pressure differences.

Cross Stream vs. Down Stream/Bottom Pressure Difference

	Δp1-3	Δp4-6	Δp7-9	Δp6-9	Δp1-4	Δp1-6	Δp1-7	Δp3-9
Δp1-3	1.0	--	.21	.23(18)	.35	.43	.58	-.20
Δp4-6		1.0	--	.51(12)	-.65(6)	-.48(12)	--	--
Δp7-9			1.0	.83	-.48(6)	-.48(6)	-.33(12)	.65
Δp6-9				1.0	-.80(6)	-.77(6)	-.28(12)	.66
Δp1-4					1.0	.96	.54	--
Δp1-6						1.0	.66	--
Δp1-7							1.0	.23(12)
Δp3-9								1.0

Table 16.--Correlation matrix for integrated transport vs. down and cross shelf pressure differences.

	1 Surface	1 Bottom	2 Surface	2 Bottom	3 Surface	3 Bottom
Wpg1-4	-.61	-.49(54)	-.50(6)	-.37(6)	-.60(12)	-.55(12)
Δpg1-6	-.59(6)	-.47(54)	-.37(12)	*	-.61(12)	-.57(12)
Δpg1-7	-.38(12)	-.31(54)	-.21(60)	-.17(12)	-.30(18)	-.38(12)
Δpg3-9	*	*	*	*	*	.53
Δpg1-3	-.21(70)	0.29	-0.24(10)	*	-0.22	*
Δpg4-6	0.38	0.41	0.69	0.55	0.35	0.32
Δpg7-9	0.47	0.50	*	0.32	0.49	0.86
Δpg6-9	0.58	0.55	*	*	0.66	0.80

Table 17.--Bands used in the description of the frequency distribution of the records (Figures 60 to 62). Also, the distance between pressure gauges (in kilometers) is given to show the separation in the pressure difference series.

Target Band	Period Days	Frequency Cycles/Day	Spectral Band Period/Frequency
Semi-Diurnal	0.50-0.54	1.859-2.005	0.492-0.551/ (1.815-2.033)
Diurnal	0.96-1.12	0.893-1.039	0.917-1.145/ (0.873-1.091)
Two to six days	2.00-5.99	0.50-0.167	1.96-6.73/ (0.149-0.511)
Six to thirteen days	6.00-12.99	0.167-0.077	6.73-13.14/ (0.149-0.076)
Greater than thirteen days	12.99	<0.077	13.14 (<0.076)

DISTANCE BETWEEN PRESSURE GAUGES (IN KM)

Down-Shelf Differences		Cross-Shelf Differences	
PG 1 - PG 4	176.8	PG 1 - PG 3	36.8
PG 1 - PG 6	186.2	PG 4 - PG 6	20.5
PG 1 - PG 7	214.7	PG 7 - PG 9	29.8
PG 3 - PG 9	198.5	PG 6 - PG 9	58.8